CRAZE INITIATION

IN

HETEROGENEOUS POLYMERS

by

MARY CUNNINGHAM BOYCE

B.S. Virginia Polytechnic Institute and State University
1981

Submitted to the Department of
Mechanical Engineering
in Partial Fulfillment of the
Requirement for the Degree of

MASTER OF SCIENCE IN MECHANICAL ENGINEERING

at the

MASSACHUSETTS INSTITUTE OF TECHNOLOGY

February, 1984

Signature of Author Mary Cunningham Boyce
Department of Mechanical Engineering
December 22, 1983

Certified by Ain S. Argon
Thesis Supervisor

Accepted by W M Rohsenow
Chairman, Departmental Graduate Committee

CRAZE INITIATION
IN
HETEROGENEOUS POLYMERS

by

MARY CUNNINGHAM BOYCE

Submitted to the Department of Mechanical Engineering on December 22, 1983 in partial fulfillment of the requirements for the Degree of Master of Science in Mechanical Engineering

ABSTRACT

The computational modelling of initiation of crazes in a matrix of polystyrene containing composite particles of varying morphology and material composition is discussed. The importance of each step in the stress history of the material is quantitatively determined. The stress history begins with the development of residual stresses due to the thermal mismatch between the matrix and the particle. These stresses are subsequently partly relaxed due to the non-linear creep behavior of the matrix. Finally, a tensile stress is applied producing a further stress concentration at the matrix/particle interface. A craze initiation criterion (Argon-Hannoosh) is used to determine whether the above sequence will result in the initiation of crazes. This analysis is conducted on four multiphase inclusions to determine which is the optimum craze initiator. The results give trends that are found to compare favorably with experiments.

Thesis Supervisor: Ali S. Argon
Title: Quentin Berg Professor of Mechanical Engineering

ACKNOWLEDGEMENTS

To Professors Ali S. Argon and David M. Parks, I express my sincerest appreciation for their invaluable guidance. I also extend my thanks to Professor Robert Cohen, Dr. Osman Gebizlioglu, and Dr. Chris Schwier for their help through numerous discussions.

The work described herein was supported by NSF/MRL under Grant No. DMR 78-24185, through the Center for Materials Science and Engineering at M.I.T.

TABLE OF CONTENTS

	Page
LIST OF FIGURES	6
LIST OF TABLES	10
1. INTRODUCTION	11
1.1. Background	11
1.2. Material Description	17
1.3. Stress History Description	26
2. THERMAL RESIDUAL STRESSES	28
2.1. Problem Description	28
2.2. Problem Solution	28
1. Isotropic Particles	28
2. Concentric Shell Particles	33
2.3. Results	33
1. Isotropic Particles	33
2. Concentric Shell Particles	38
3. RELAXATION OF RESIDUAL STRESSES	44
3.1. Description of Creep Behavior in Polystyrene Matrix	44
3.2. Solution	46
1. Isotropic Particles	46
2. Concentric Shell Particles	50
3.3. Results	52
1. Isotropic Particles	52
2. Concentric Shell Particles	55

4. UNIFORM APPLIED TENSILE STRESS 63

4.1. Problem Description 63
4.2. Solution 63
1. Isotropic Particles in an Infinite Matrix 63
2. Concentric Shell Particles in an Infinite Matrix 65
3. Particle in a Finite Matrix 65
4.3. Results 65
1. Infinite Matrix 65
2. Finite Matrix 76

5. INITIATION OF CRAZES 90

5.1. Theory 90
5.2. Application of the Craze Initiation Criterion to Specific Stress Histories 93
5.3. Results 96

6. DISCUSSION 102

APPENDICES 107

1. Computation of Homogenized Material Properties 108

2. Relaxation of Thermal Residual Stresses due to Creep of Polystyrene Matrix 111

3. Computation of Stress Relaxation and Porosity Development 120

4. Stress Field Surrounding a Spherical Particle due to a Uniform Tensile Stress at Infinity 127

5. Finite Element Analysis 130

LIST OF FIGURES

		Page Number
1.	Diagram of a Craze.	12
2.	Kawagoe and Kitagawa experimental results (from Kawagoe and Kitagawa; courtesy of J. Wiley and Sons, 1982).	16
3.	HIPS Particle.	18
4.	Homogenized Particle.	20
5.	CS PB/PS Particle.	22
6.	CS LMWPB/PS Particle.	23
7.	Idealized PB Particle Schematic.	25
8.	Spherical Particle Terminology.	25
9.	Concentric spheres of radius a and b; isotropic particle in isotropic matrix idealization.	29
10.	Concentric spheres of radius a and b; composite particle in isotropic matrix idealization.	29
11.	Geometry and boundary conditions to be modelled with finite elements for thermal expansion problem.	29
12.	Effect of particle concentration on the magnitude of the thermal residual stresses induced by the homogeneous PB particle.	36
13.	Effect of particle concentration on the magnitude of the thermal residual stresses induced by the Homogenized particle.	37

14. Negative pressure distribution in the PB shells of the CS PB/PS particle induced by the thermal mismatch and cooling from T_g (95°C) to room temperature. 39

15. Negative pressure distribution in the PB shells of the CS LMWPB/PS particle induced by the thermal mismatch and cooling from T_g (95°C) to room temperature. 40

16. Effect of particle concentration on the magnitude of the thermal residual stresses at the particle border, induced by the CS PB/PS particle. 42

17. Effect of particle concentration on the magnitude of the thermal residual stresses induced by the CS LMWPB/PS particle. 43

18. Relaxation of thermal stresses due to the PB particle in a PS matrix with c=0.20; comparison of creep solution with finite element creep analysis solution. 51

19. Relaxation of thermal residual stresses due to a PB particle in an infinite PS matrix. 53

20. Relaxation of thermal residual stresses due to Homogenized particle in an infinite PS matrix. 54

21. Relaxation of thermal residual stresses due to Homogenized particle in a PS matrix with c=0.20. 56

22. Relaxation of thermal residual stresses due to CS PB/PS particle in an infinite matrix. 57

23. Relaxation of thermal residual stresses due to CS LMWPB/PS particle in an infinite matrix. 58

24. Relaxation of residual stresses due to CS PB/PS particle in an infinite PS matrix. Comparison of using CS PB/PS particle properties and Homogenized particle properties in relaxation analysis with the same initial stress state. 60

25. Relaxation of thermal residual stresses due to CS PB/PS particle in a matrix of PS with c=0.20. 62

26. Schematic of particle in an infinite matrix subjected to a uniform tensile stress at infinity. 64

27. Geometry and boundary conditions to be modelled with finite elements for the problem of a particle in an infinite matrix subjected to uniform tension at infinity. 66

28. Geometry and boundary conditions to be modelled with finite elements for the problem of a particle in a finite matrix subjected to a uniform tensile load. 67

29. Displacement of the Homogenized particle and immediately surrounding PS matrix when subjected to a uniform tensile load at infinity. 69,70

30. Displacement of the CS PB/PS particle and immediately surrounding PS matrix when subjected to a uniform tensile load at infinity. 71,72

31. Displacement of the CS LMWPB/PS particle and immediately surrounding PS matrix when subjected to a uniform tensile load at infinity. 73,74

32. Mises equivalent stress contour in the PS matrix surrounding the PB particle in an infinite matrix subject to a tensile stress at infinity. 78

33. Mean normal stress contour in the PS matrix surrounding the PB particle in an infinite matrix subject to a tensile stress at infinity. 79

34. Mises equivalent stress contour in the PS matrix surrounding the Homogenized particle in an infinite matrix subject to a tensile stress at infinity. 80

35. Mean normal stress contour in the PS matrix surrounding the Homogenized particle in an infinite matrix subject to a tensile stress at infinity. 81

36. Mises equivalent stress contour in the PS matrix surrounding the CS PB/PS particle in an infinite matrix subject to a tensile stress at infinity. 82

37. Mean normal stress contour in the PS matrix surrounding the CS PB/PS particle in an infinite matrix subject to a tensile stress at infinity. 83

38. Mises equivalent stress contour in the PS matrix surrounding the CS LMWPB/PS particle in an infinite matrix subject to a tensile stress at infinity. 84

39. Mean normal stress contour in the PS matrix surrounding the CS LMWPB/PS particle in an infinite matrix subject to a tensile stress at infinity. 85

40. Broutman and Panizza Results: Particle Volume Percent Effect on Equatorial and Polar Interfacial Stresses. 87

41. Formation of micro-shear nucleus under deviatoric stress, s. 91

42. Locus of pore expansion under a combination of negative pressure, σ , and equivalent stress, σ_e. 91

LIST OF TABLES

		Page Number
1.	MATERIAL PROPERTIES	21
2.	THERMAL RESIDUAL STRESSES FOR PARTICLES IN AN INFINITE MEDIUM	35
3.	EQUATORIAL STRESS STATE DUE TO APPLIED TENSION	75
4.	POLAR STRESS STATE DUE TO APPLIED TENSION	77
5.	FINITE MATRIX (c=0.21) EFFECTS ON STRESS CONCENTRATIONS	88
6.	POROSITY LEVEL IN MATRIX AT EQUATORIAL PARTICLE/MATRIX INTERFACE	97
7.	COMPLETE EQUATORIAL STRESS STATE IN MATRIX AT PARTICLE/MATRIX INTERFACE	99
8.	CRAZE INITIATION CRITERION APPLICATION RESULTS	101

1. INTRODUCTION

1.1. Background

The incorporation of a rubber phase into a brittle polymer matrix has long been recognized to significantly toughen the material. The first patent on this type of processing was in 1927. Although the rubber phase was known to act as a stress raiser and to toughen the polymer, it was not understood why. Maxwell and Rahm were the first to note that crazes (to be described below) extended from these high stress regions. In 1965, Bucknall and Smith identified these crazes to be the actual source of toughness in the material. Here it must be noted that crazes are a source of toughness only when their initiation and growth is controlled. When a small percentage of a rubber phase is introduced into the polymer, the craze sites are known and controllable, and, therefore, the polymer will be toughened. Otherwise, crazes will act as a precursor to fracture as in the case of surface defects and surface crazing. In these cases, a crack may develop within the craze and propagate through the material to result in fracture. Thus, crazes can play a vital role as either an ingredient of toughness or as sites for fracture initiation.

A craze is a narrow band of voids connected by drawn polymer fibrils (Figure 1). It grows perpendicular to the highest tensile stress and can carry up to the yield stress of the material. Thus, a craze is not a crack either in form or behavior. This is because a craze preserves the continuity of the material as a whole through its load-carrying fibrils. Crazing can be thought of as a form of dilational plasticity. This process absorbs much

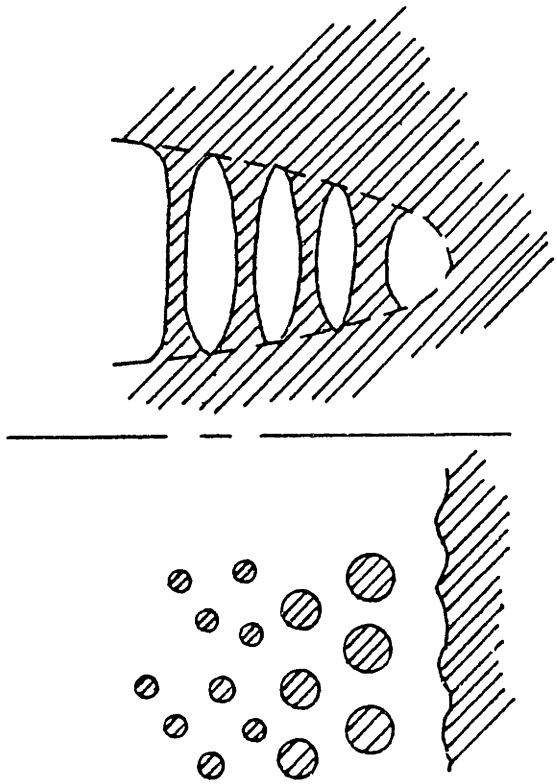

FIGURE 1. Diagram of a Craze.

energy, therefore becoming the major source of toughness in many polymers.

Although the structure of a craze as well as its important role in polymer toughening are known, the exact mechanism responsible for initiating a craze is still under debate. Many researchers have attempted to develop an initiation criterion, however to develop one which will encompass all of the apparent craze dependent factors -- dilational stress, distortional stress, temperature, time -- is a difficult task. Sternstein and Ongchin (1969) were the first to propose a multi-axial criterion for craze initiation based on their biaxial experiments with polymethymethacrylate (PMMA). According to this criterion crazes initiate when,

$$\sigma_b \equiv |\sigma_1 - \sigma_2| = A(T) + B(T)/(\sigma_1 + \sigma_2) \quad , \quad (1\text{-}1)$$

where σ_1 and σ_2 are the nonzero principal stresses, σ_b is the stress bias, A(T) and B(T) are temerature dependent material parameters. The criterion states that once the stress bias reaches a certain level which is dependent on the negative pressure, the material will craze. This criterion did predict their experimental results, however it fails to account for a triaxial state of stress because of the basic ambiguity in the definition of the stress bias. Oxborough and Bowden (1974) have presented a somewhat modified version of the above criterion which does encompass a triaxial stress state, and is:

$$E\epsilon_{11} \equiv \sigma_1 - \nu(\sigma_2 + \sigma_3) = C(t,T) - D(t,T)/(\sigma_1 + \sigma_2 + \sigma_3) \, . \quad (1\text{-}2)$$

This is a critical strain criterion which states that once the major principal strain, ϵ_{11}, reaches a certain level which decreases as the negative pressure increases, the material will craze. The above two criteria are based upon

a constant stress state.

A third criterion was proposed by Argon and Hannoosh (1977) which considers craze initiation to be a sequential process (Section 5). The first stage involves the formation of pores due to a localized microshear process. The porosity level which will develop in the material due to the presence of a local deviatoric stress, s, is:

$$\beta = \int_0^t \dot{\beta}_0 \exp\left[\Delta G(s)/\kappa T\right] dt \quad , \qquad (1-3)$$

where $\Delta G(s)$ is the free energy required to form a pore (expanded upon in Section 5). The second stage requires a combination of negative pressure (i.e. a positive mean stress) and a deviatoric shear stress to plastically expand the pores, which states that:

$$\sigma = \frac{2\gamma}{3}\left[\ln(1/\beta)\right]\left[Q(s/\gamma, \beta)\right] \quad . \qquad (1-4)$$

This criterion is discussed in detail in Section 5. For now, it is only important to notice that it states that craze initiation is a two stage process with the first stage involving the formation of pores, and the second involving the subsequent plastic expansion of these pores. A fourth criterion has been suggested by Kawagoe and Kitagawa (K-K, 1981) based on the Cottrell mechanism of microcrack formation in crystalline solids. Here it is suggested that a wedge-shaped microcrack is formed by intersecting slip bands which subsequently expand elastically into a cylindrical cavity under a negative pressure. By minimizing the work of the system with respect to the crack length, Kawagoe and Kitagawa were able to obtain the stable and unstable craze nucleus length and therefore an initiation criterion, that is:

$$\sigma(s - s_i + M\sigma) = 4\mu\gamma/L\left\{1 + \left[3(1-2\nu)/2(1-\nu^2)\right]^2\right\}^{1/2} \quad , \quad (1-5)$$

where σ and s are the dilational and deviatoric stress, μ and ν are the shear modulus and Poissons ratio as previously defined. The new parameters are S_i, the friction stress resulting from kink or void formation; M, a material constant; L, the length of the slip band; and γ, the surface energy of microcrack. Both the K-K and Argon-Hannoosh criteria have pointed out that the micromechanism for craze initiation involves a shearing of a region followed by a dilation of that region, however, only Argon presents a sequential process.

For comparative purposes, the K-K experimental data with the four corresponding criteria predictions are shown in Figure 2. All four criteria reasonably predict the results of the experiments in air however, only the Argon-Hannoosh and K-K criteria predict the results of experiments in kerosene. It is only the Argon-Hannoosh and K-K criteria which are based on a micromechanism for craze initiation; the S-O and the O-B criteria are empirical criteria developed on the basis of experiments in air. This may be why they fail to predict the experiments in a crazing agent.

A single criterion has not yet been widely recognized as representing the mechanism for craze initiation. However, since the Argon and Hannoosh criterion has been shown to predict the experimental results of various materials under different stress states as well as provide an explanation of the micromechanism responsible for craze initiation, it will be the criterion used in this thesis. Also, this thesis will deal with a material undergoing a stress history, and

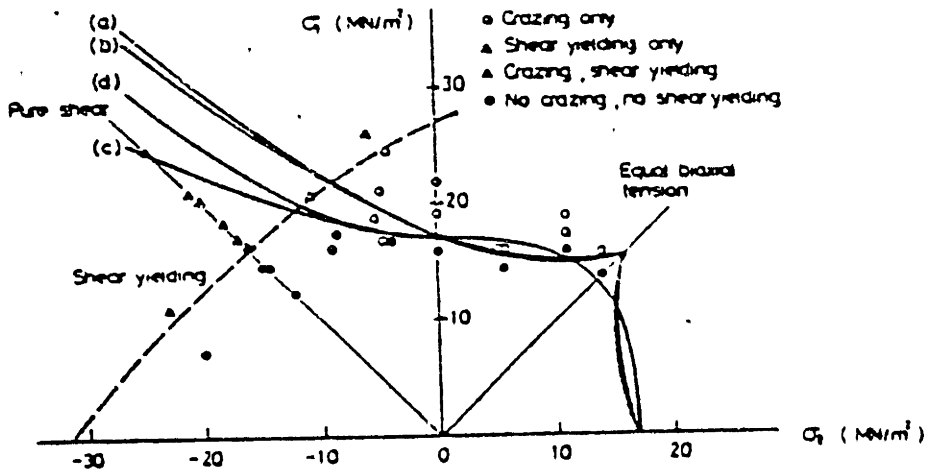

i) Crazing in air with theoretical predictions of (a) Sternstein-Ongchin, (b) Oxborough-Bowden, (c) Argon-Hannoosh, (d) Kawagoe-Kitagawa;

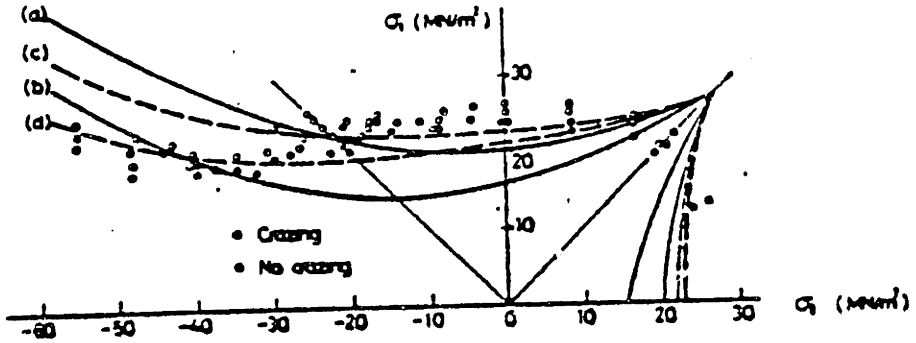

ii) Environmental crazing with (a) and (b) S-O predictions using two different sets of material constants, (c) and (d) O-B predictions using two different sets of material constants.

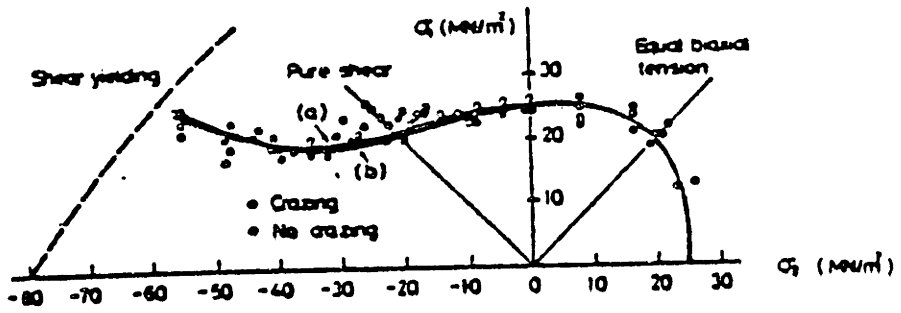

iii) Kerosene crazing with (a) A-H prediction, and (b) K-K prediction.

FIGURE 2. Kawagoe and Kitagawa experimental results (from Kawagoe and Kitagawa; courtesy of J. Wiley and Sons, 1982).

therefore a sequential craze initiation criterion is needed.

This thesis will examine the stress history in a polystyrene matrix containing composite particles of polybutadiene/polystyrene of various morphologies synthesized by Cohen, Argon, and their coworkers. The stress histories will be linked to the initiation of crazes as discussed in the above paragraphs. This is because the craze initiation step often controls the toughening of a polymer containing composite particles. It will be pointed out that not only is the stiffness mismatch between the particle and the matrix important in the initiation process, but the thermal expansion mismatch also plays an important role. This ability to initiate a craze will identify an optimum polybutadiene/polystyrene morphology, and will be compared with the experimental results of Gebizlioglu, et al (1983).

1.2. Material Description

Composite particles containing rubbery phases have been known to increase the toughness of polymers for some time. The most widely used particle morphology is that found in High Impact Polystyrene (HIPS). This particle is, essentially, a collection of occluded polystyrene (PS) spheres in a topologically continuous matrix of polybutadiene (PB) as shown in Figure 3. HIPS is a high energy absorbing material giving strains up to 40% before fracture. This material will not be further discussed in this thesis but will be used as a standard for comparison. Instead, other heterogeneous polymers synthesized at M.I.T., some with fracture strains far greater than those of HIPS, will be discussed. Some of these have strains to fracture in excess of 100%. Four materials will be

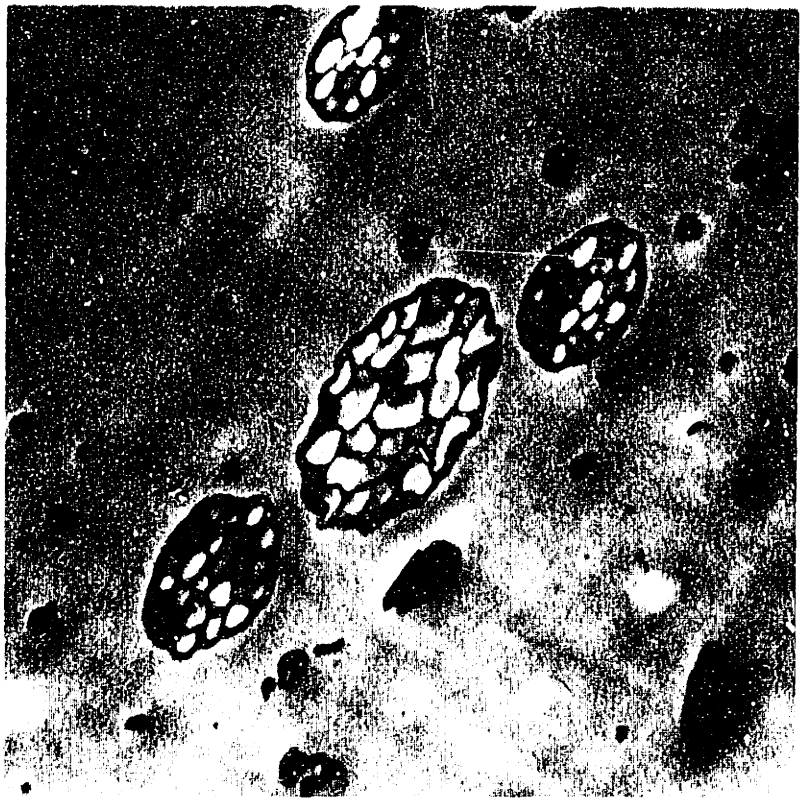

(a) micrograph,

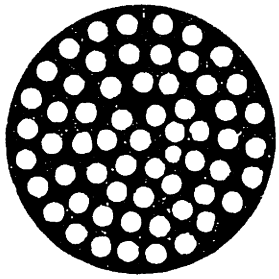

(b) schematic.

FIGURE 3. HIPS Particle.

analyzed: three contain particles of various morphologies made up of PB/PS and the fourth contains an idealized homogeneous PB particle; all are within a PS matrix. All particles are spherical and are in practice, larger than 1 μm in diameter. Particles much smaller than this have been observed to be poor craze initiators.

The first morphology to be discussed will be referred to as the Homogenized particle. It is in practice a collection of randomly wavy rods of PB in a block copolymer with PS, making up a spherical particle in a majority phase of PS as shown in Figure 4. Since the PB is randomly oriented it can be considered to behave isotropically. It will be analyzed as an equivalent homogeneous, isotropic inclusion possessing material properties which are a combination of those of PB and PS (thus the name Homogenized). The properties are listed in Table 1 and were determined with Chow's (1978) method discussed in Appendix 1.

The second particle consists of Concentric Spheres of PB and PS (CS PB/PS) shown in Figure 5. It is composed of a collection of alternating layers of PB and PS block copolymer domains (properties listed in Table 1). The volume ratio of PB to PS is 1/3 and is given by the molecular weight ratio of PB to PS in the block copolymer. This, of course, is a composite microstructure and is analyzed as such.

The third particle also consists of Concentric Spheres of PB and PS but incorporating additional Low Molecular Weight PB (CS LMWPB/PS),as shown in Figure 6. It is much like the second one; however, it contains additional low molecular weight PB dispersed in the PB spherical shells, resulting in a smaller volume fraction of

(a) micrograph,

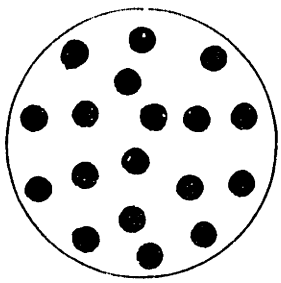

(b) schematic for modelling purposes.

FIGURE 4. Homogenized Particle.

TABLE 1. MATERIAL PROPERTIES

MATERIAL	BULK MODULUS (MPa)	SHEAR MODULUS (MPa)	VOLUMETRIC COEFFICIENT THERMAL EXPANSION ($^{\circ}C^{-1}$)
PS	$3.265(10^3)$	$1.25(10^3)$	$2.0(10^{-4})$
PB	$1.938(10^3)$	0.62	$7.5(10^{-4})$
LMWPB	$1.938(10^3)$	0.31	$7.5(10^{-4})$
HOMOGENIZED	$2.880(10^3)$	$0.88(10^3)$	$3.07(10^{-4})$
H2	$2.849(10^3)$	$0.86(10^3)$	$3.17(10^{-4})$

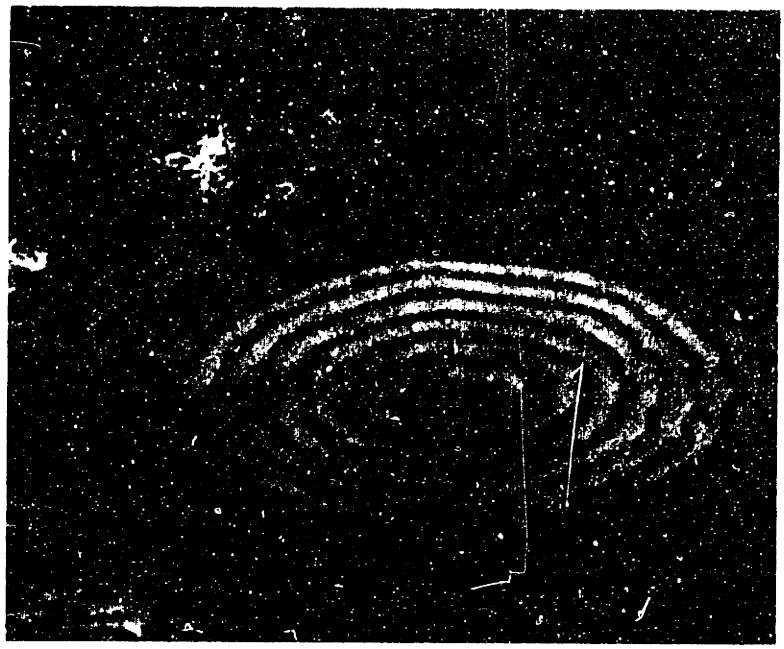

(a) micrograph,

(b) schematic for modelling purposes.

FIGURE 5. CS PB/PS Particle.

(a) micrograph,

(b) schematic for modelling purposes.

FIGURE 6. CS LMWPB/PS Particle.

PS, and giving a volume ratio of PB to PS of 2/3 among the concentric spherical shells. It is also analyzed as a composite.

The fourth particle is an idealized, homogeneous particle of PB. It is a completely homogeneous, isotropic particle composed of 100% PB. It is pictured in Figure 7.

All of the above particles are assumed to have a perfect bond between themselves and the matrix. This is a valid assumption for the first three particles because they are composed of block copolymers and therefore there does exist a high concentration of chemical bonds between the two phases of polybutadiene and polystyrene. For the PB particle, if it were to exist, the lack of a primary chemical bond across the interface would be its greatest disadvantage. This is because a weakly bonded particle will readily decohere from the matrix, creating a cavity from which it is more probable that a crack will propagate than a craze. When a strong bond exists between the particle and the matrix, the particle will be able to support some of the load because of its high bulk modulus. Since the pure PB particle is an idealized one, an assumption of perfect bonding will also be applied for comparative purposes. The assumption of a perfect bond makes the analysis specific. Other assumptions such as transmission of only normal tractions across the interface are also possible but have no basis in experimental facts.

All of these particles are contained in a matrix of polystyrene. The matrix will primarily exhibit elastic behavior, however it will also creep under sustained load. This creep behavior will be further discussed in Section 3.

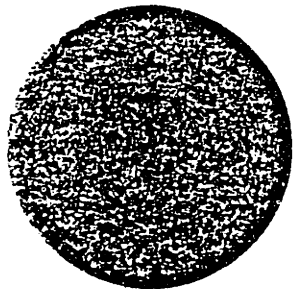

FIGURE 7. Idealized PB Particle schematic.

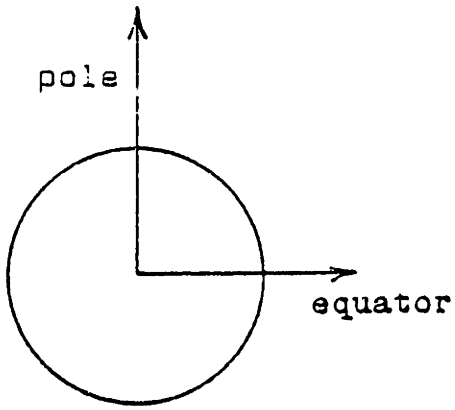

FIGURE 8. Spherical Particle Terminology

1.3. Stress History Description

As mentioned above, each particle introduces a thermal expansion and a stiffness mismatch to the matrix. The magnitude of the mismatches differ with each particle because the morphology and/or the material composition of each differs. These mismatches induce stresses in the material which in turn will contribute to the initiation of crazes.

The thermal expansion mismatch is introduced during the processing of the material. At the glass transition temperature of PS (95°C) both the PS and the PB should be fully relaxed and free of internal stress. All material is given an excursion to this temperature to remove unknown internal stresses due to the previous processing steps consisting of solvent casting and differential removal of solvent by evaporation. The material is cooled from T_g of PS to room temperature at 20°C. The two components of the particles, i.e. PB and PS, have very different coefficients of thermal expansion in the temperature range below 95°C where PS acts as a stiff solid while PB acts as a rubber (captured liquid). This different behavior thus induces a thermal stress between the inclusion and the matrix in order to assure compatibility.

Subsequently, this stress is partially relaxed because of the creep behavior of the PS matrix. It will be shown that, for lengths of time of interest, this stress relaxation can sometimes be significant.

The mechanical mismatch is introduced when an external stress is imposed on the material. In most cases the stress of interest is an applied far field tensile stress. The

mismatch occurs because each component material, PB and PS, possess different elastic properties causing a nonuniform distribution of the stress in the matrix. The end result is a stress concentration around the particle, and particularly at the equatorial plane as shown in Figure 8.

2. THERMAL RESIDUAL STRESSES

2.1. Problem Description

Thermal residual stresses develop in both the matrix and the particle when there is a temperature change below T_g of PS. Because of the different free thermal expansion characteristics of the particle and the matrix, each responds differently to a temperature change. However, since continuity between the particle and the matrix must always be maintained, stresses will develop because of the differential thermal expansions.

2.2. Solution

2.2.1. Isotropic Particle

To determine the magnitude of these stresses, first consider two concentric spheres of radius a and radius b (Figure 9). The inner sphere of radius a represents the isotropic particle, and the material from radius a to b represents the average amount of isotropic matrix allocated per particle. Now, separate the two materials and subject each to the same temperature differential, ΔT. The expansion that each undergoes at radius r=a is:

$$u_{r_p} = \alpha_p \Delta T\, a \quad ; \quad u_{r_m} = \alpha_m \Delta T\, a,$$

where the subscript p indicates particle, and the subscript m indicates matrix. (This notation will be used throughout the thesis.)

A radial stress σ must be exerted along r=a on both

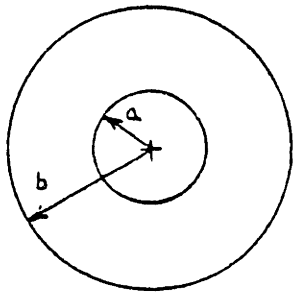

FIGURE 9. Concentric spheres of radius a and b; isotropic particle in isotropic matrix idealization.

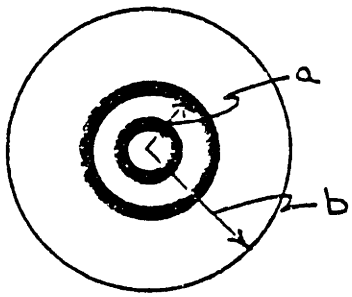

FIGURE 10. Concentric spheres of radius a and b; composite particle in isotropic matrix idealization.

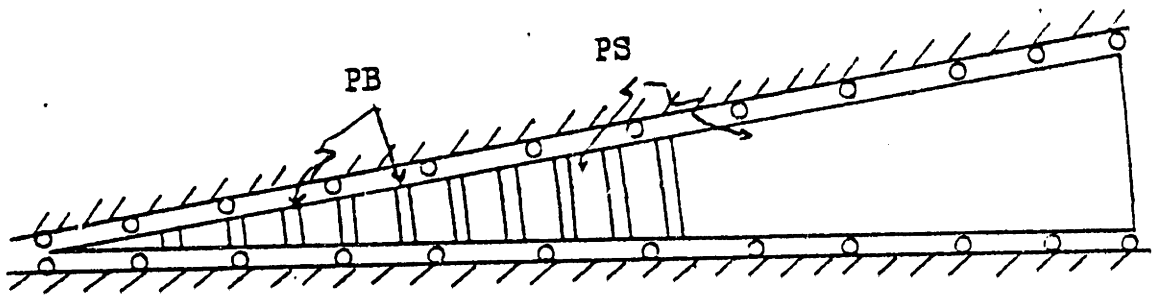

FIGURE 11. Geometry and boundary conditions to be modelled with finite elements for thermal expansion problem. The rollers represent zero displacement normal to the line and therefore induce spherically symmetric displacements.

the particle and the matrix in order to place the particle of altered size back within the matrix. The problem description is now complete: There exist two concentric spheres of different isotropic materials of radius a and radius b with a uniform stress at r=a and zero stress at r=b. Determine the stress distribution throughout both materials.

To begin with the inner sphere, the solution is straight forward. Note that it is simply a solid sphere subjected to a uniform external pressure, σ, therefore:

$$\sigma_{r_p} = \sigma_{\theta_p} = \sigma_{\phi_p} = \sigma \quad .$$

Using the stress-strain relation for bulk behavior of the particle,

$$\epsilon_{r_p} = \sigma / 3K_p \quad ,$$

and the strain-displacement relation

$$u_{r_p} = (\sigma / 3K_p) \, a \quad ,$$

the total displacement of the inner sphere at radius r=a is:

$$u_{r_p} = (\sigma / 3K_p) \, a + \alpha_p \Delta T \, a \quad . \qquad (2\text{-}1)$$

To obtain the solution for the outer shell of material from a to b, note that it is simply a hollow sphere subjected to internal pressure σ. The governing equilibrium equation for a spherically symmetric problem is:

$$d\sigma_r / dr + 2 (\sigma_r - \sigma_\theta) / r = 0 \quad .$$

Then stress-strain and strain-displacement relations yield:

$$d^2 u/ dr^2 + (2/r)\, du/dr - (2/r^2)\, u = 0 .$$

The solution of which for the single radial displacement u is:

$$u = C_1 / r^2 + C_2 r , \qquad (2\text{-}2)$$

where C_1 and C_2 are constants determined by applying boundary conditions. Using strain-displacement and stress-strain relations, equation (2-2) yields:

$$\epsilon_\theta = C_1 / r^3 + C_2 ; \qquad (a)$$

$$\epsilon_r = -2\, C_1 / r^3 + C_2 ; \qquad (b)$$

$$\sigma_r = -2\, E\, C_1 / [(1+\nu) r^3] + E\, C_2 / (1-2\nu); \qquad (c) \qquad (2\text{-}3)$$

$$\sigma_\theta = E\, C_1 / [(1+\nu)\, r^3] + E\, C_2 / (1-2\nu) . \qquad (d)$$

The constants C_1 and C_2 are found using the following boundary conditions:

1. @ r=a, $\sigma_r = \sigma$;

2. @ r=b, $\sigma_r = 0$.

The result:

$$C_1 = -\{ (1+\nu_m) a / [2E_m(1-c)] \} , \qquad (a)$$

$$C = = \{ (1-2\nu_m)\, c / [E_m(1-c)] \} , \qquad (b) \qquad (2\text{-}4)$$

where $c=(a/b)^3$. Substituting equations (2-4) into equations (2-2) and adding the thermal expansion term gives the total displacement in the matrix at r=a:

$$u_m=\frac{-\sigma}{2E_m}\frac{a}{1-c}\left[(1+\nu_m)+2(1-2\nu_m)c\right]+\alpha_m\Delta T a \quad . \qquad (2\text{-}5)$$

Since a perfect bond between matrix and particle is assumed, the radial displacements at r=a must be continuous:

$$u_m(a) = u_p(a) \quad . \qquad (2\text{-}6)$$

This relationship yields a solution for σ :

$$\sigma = \frac{K_p(\gamma_m-\gamma_p)\Delta T}{1+\frac{1}{1-c}\frac{K_p}{K_m}\left[\frac{1+\nu_m}{2(1-2\nu_m)}+c\right]} \quad , \qquad (2\text{-}7)$$

where $\gamma=3\alpha$ is the volumetric coefficient of thermal expansion. Therefore, the stress distribution in the particle and matrix are:

$$\text{Particle:}\quad \sigma_r=\sigma_\theta=\sigma_\phi=\sigma \quad ; \quad (a)$$

$$\text{Matrix:}\quad \sigma_r=\left(\frac{a^3}{r^3}-c\right)\frac{\sigma}{1-c} \quad ; \quad (b) \qquad (2\text{-}8)$$

$$\sigma_\theta=\left(\frac{1}{2}\frac{a^3}{r^3}+c\right)\frac{\sigma}{1-c} \quad . \quad (c)$$

2.2.2. Solution -- Concentric Spherical Shell Particles

Consider a particle of radius a in a matrix extending from radius a to radius b. The particle is not isotropic but is itself composed of concentric spheres of two alternating materials as shown in Figure 10. A closed form solution for the stresses developed due to the thermal mismatch between the materials is possible but tedious to obtain because of the complex internal structure of the particle and the thermal mismatch between the layers within the particle. However, a very good solution can easily be obtained with a finite element analysis. Both the geometry and the loading of the problem are spherically symmetric; therefore, only a small section of the problem must be modelled. This section, with appropriate boundary conditions, is pictured in Figure 11. The finite element code ABAQUS was used in the analysis. The stress distribution within the particle as well as in the matrix was obtained. The accuracy of the solution was determined by conducting a finite element analysis on an isotropic particle and comparing the results with the elasticity solution. The error was less than 1%. For a more detailed explanation of the finite element modelling, analysis and accuracy see Appendix 5.

2.3. Results of Thermal Residual Stress Analysis

2.3.1. Isotropic Particles

The solution for the case of an isotropic particle in an isotropic matrix will yield the results for the Homogenized and the homogeneous PB particles. The stress within the particle and the stress distribution in the

matrix will be obtained. Also, the effect of concentration of particles on both of these stress states will be discussed.

The stress within an isotropic particle, such as the Homogenized and homogeneous PB particles, due to a thermal mismatch is a uniform hydrostatic stress as shown by equation (2-8). The results for each particle in an infinite matrix are shown in Table 2. One can see that the homogeneous PB particle carries a much higher stress than the Homogenized particle. This is due to its greater thermal mismatch with its surroundings as is clear from Table 1. The Homogenized particle contains 77% PS making it more compatible with the PS matrix than the 100% PB particle, and hence, has a much smaller internal negative pressure.

The stress state in the matrix at the particle/matrix interface, also shown in Table 2, is seen to be purely deviatoric for the case of an infinite matrix. This is clearly seen by equations (2-8 b,c); by substituting a concentration of c=0, the equations become $\sigma_r = \sigma$ and . Since $\sigma_\theta = -\sigma/2$, one obtains a mean normal stress of zero leaving a purely deviatoric stress state outside the particle.

Including the concentration of particles in the solution alters the stress state in both the particle and the matrix. The stress state in the particle remains purely hydrostatic although it decreases slightly in magnitude with increasing concentration (Figures 12 and 13). The concentration effect is more significant on both the form and the magnitude of the stress state in the matrix. The state changes from a purely deviatoric state to one of both deviatoric and hydrostatic. The radial stress

TABLE 2.

THERMAL RESIDUAL STRESSES FOR PARTICLES IN AN INFINITE MEDIUM

PARTICLE	PARTICLE STRESS	MATRIX STRESS AT PARTICLE BORDER	
	σ_r(MPa)	σ_r(MPa)	σ_θ(MPa)
PB	34.5	34.5	-17.8
HOMOGENIZED	7.95	7.95	-3.97
CS PB/PS	---	9.68	-4.84
CS LMWPB/PS	---	14.9	-7.45
H2	8.64	8.64	-4.32

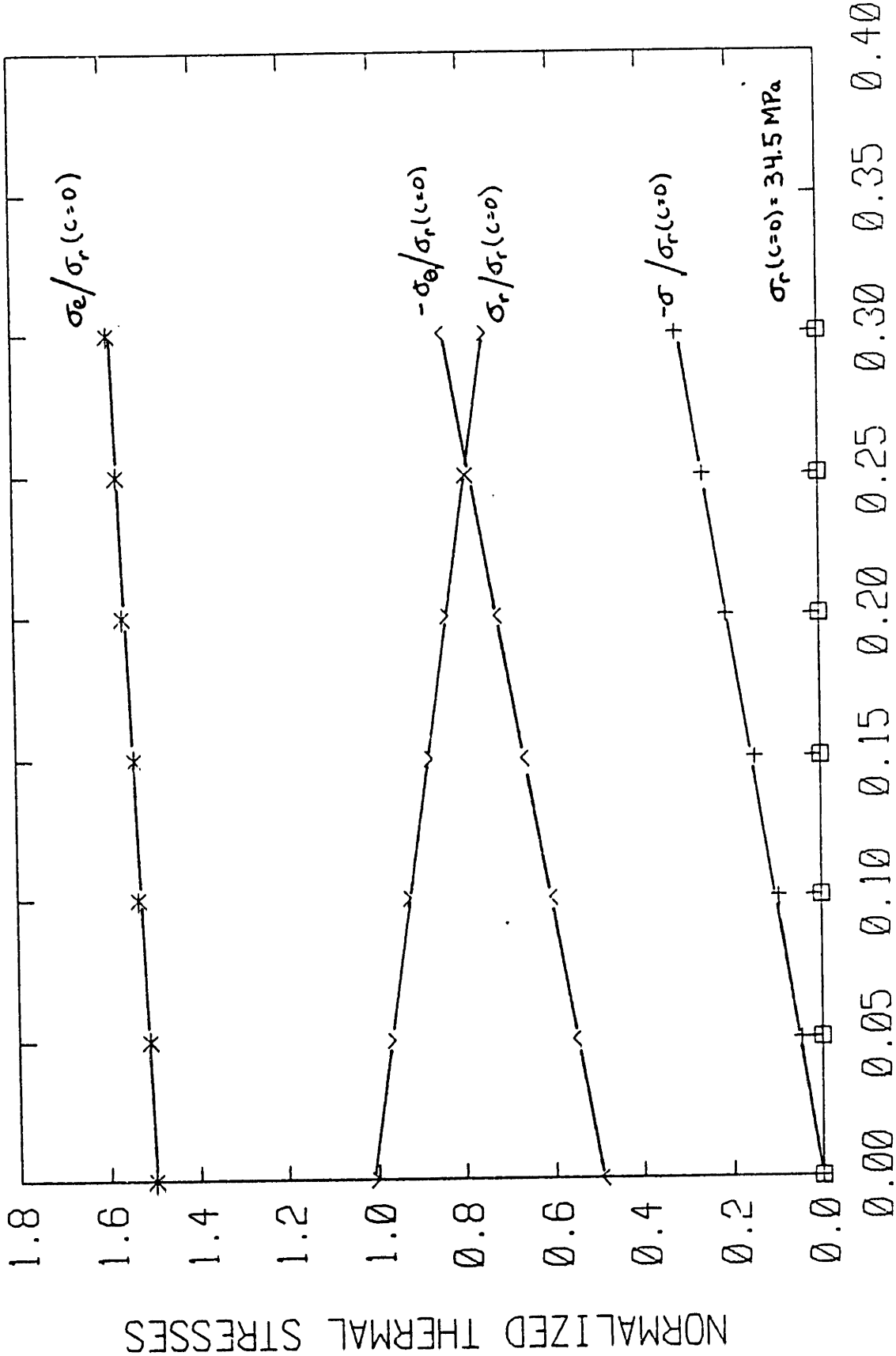

FIGURE 12. Effect of particle concentration on the magnitude of the thermal residual stresses induced by the homogeneous PB particle.

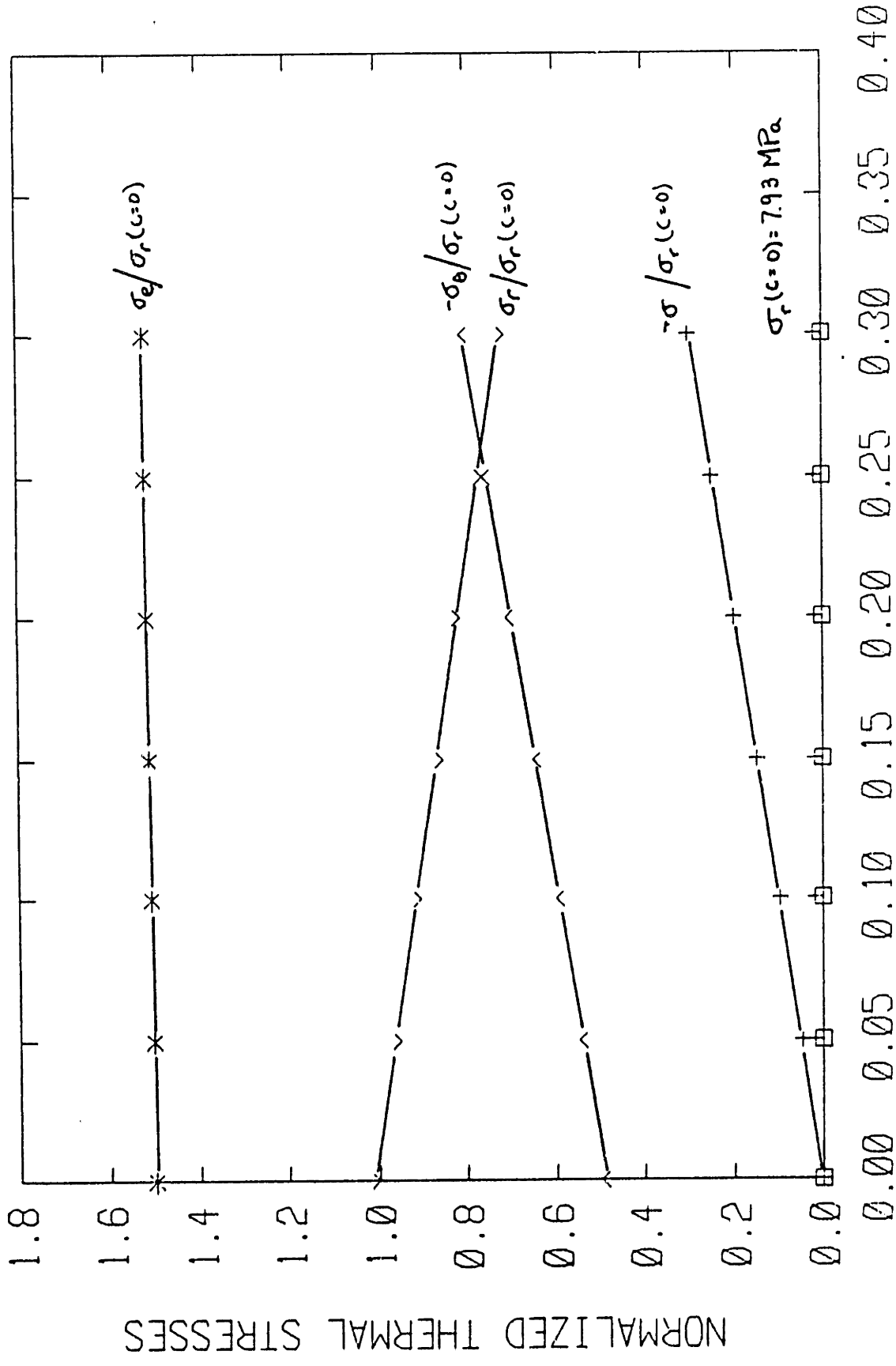

FIGURE 13. Effect of particle concentration on the magnitude of the thermal residual stresses induced by the Homogenized particle.

decreases slightly with increasing concentration, and the tangential stresses increase greatly in magnitude (remaining compressive) with increasing concentration (Figures 12 and 13). This results in a compressive mean stress (previously zero) and a slightly greater equivalent stress in the matrix at the interface (Figures 12 and 13).

2.3.2. Concentric Spherical Shell Particles

As described in Section 2.3, a finite element analysis was used to obtain the thermal mismatch solution when considering a composite particle. The stress distribution within the particle as well as that within the matrix was obtained. Also, by changing the location of the outer radius, concentration effects were determined.

The stress state within the two composite particles, without, and with additional low $\bar{M}_w$ PB, CS PB/PS and CS LMWPB/PS, due to the compounded thermal mismatch is very complex. Figures 14 and 15 show the increasing negative pressure (i.e. mean normal stress) carried by the PB layers as the particle center is approached. Since the shear modulus of PB is three orders of magnitude less than that of PS (Table 1), the PB layers do not support any significant deviatoric stress. The PS layers carry both a deviatoric and a mean stress, also increasing as the particle center is approached. In the LMWPB/PS particle, the negative pressure of the innermost layer of PB exceeds the cavitation strength of PB. The significance of this is not yet fully appreciated. However, it is very likely that the inner layer may indeed partially cavitate yet still be contained. It would therefore unload onto the surrounding material, eventually increasing the stress state in the matrix. This highly non-uniform stress distribution within

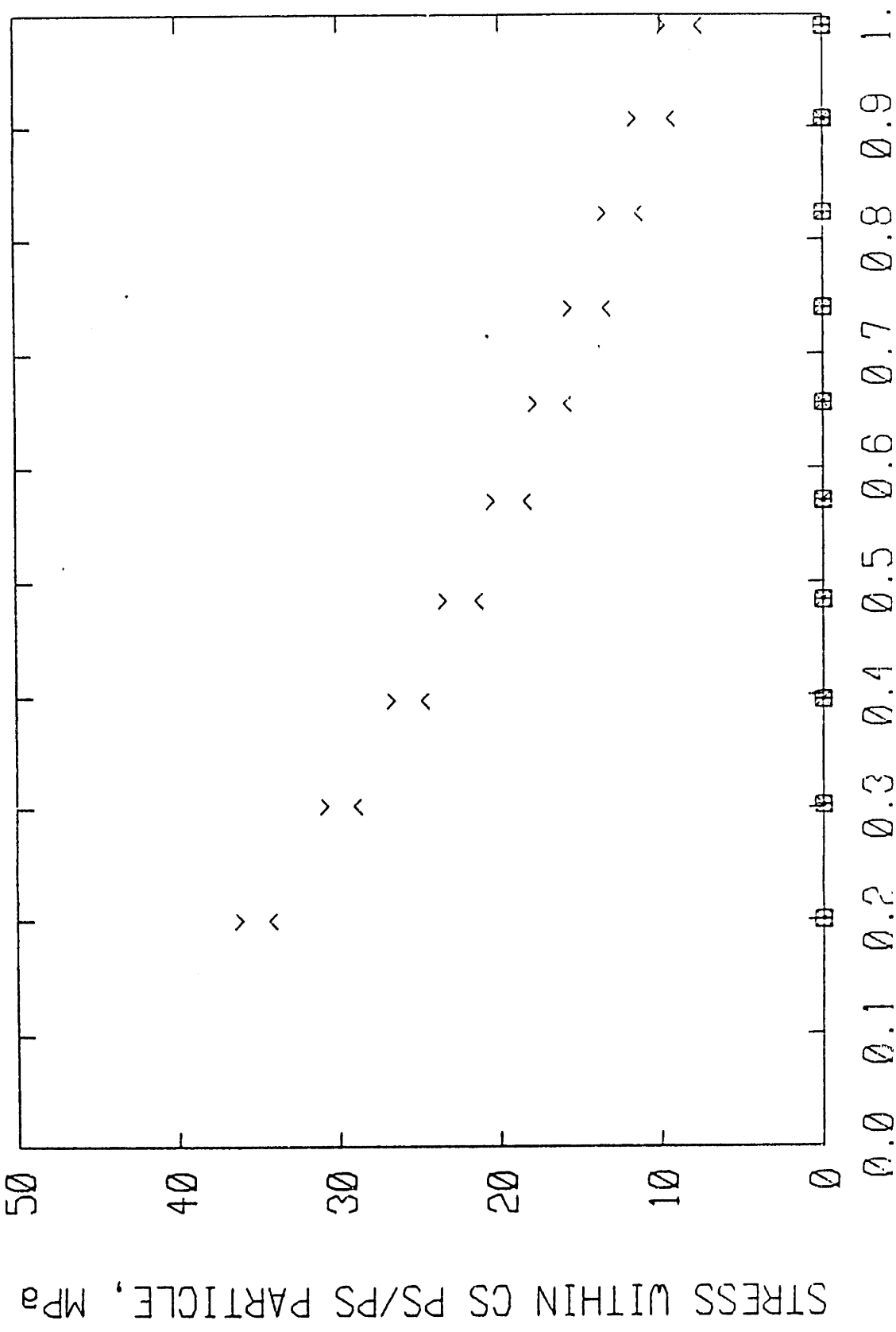

FIGURE 14. Negative pressure distribution in the PB shells of the CS PB/PS particle induced by the thermal mismatch and cooling from T_g (95°C) to room temperature.

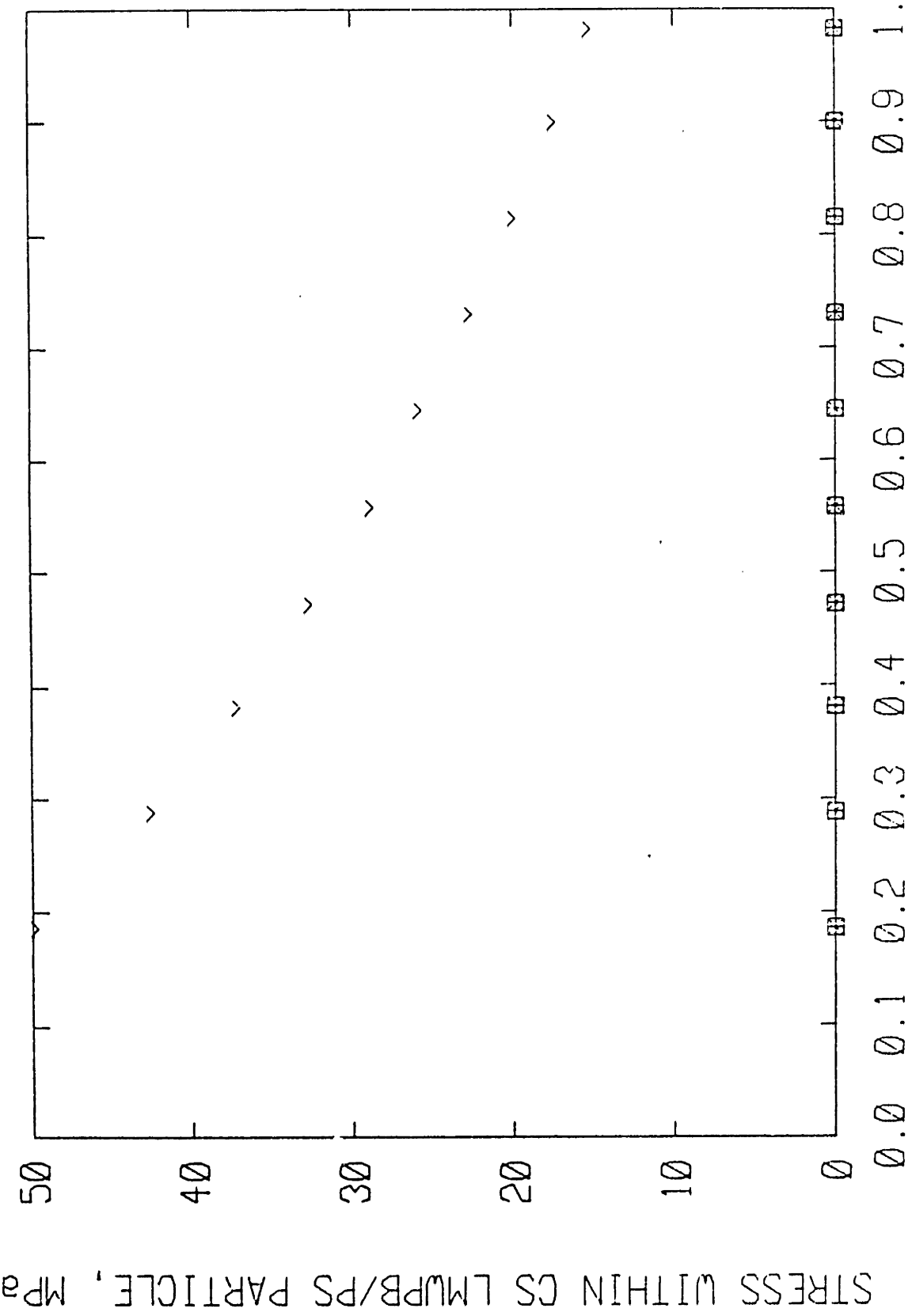

FIGURE 15. Negative pressure distribution in the PB shells of the CS LMWPB/PS particle induced by the thermal mismatch and cooling from T_g (95°C) to room temperature.

these particles is one of the most notable differences between the composite and isotropic particles.

In an infinite matrix, the stress state in the matrix at the particle/matrix interface is like that for an isotropic particle -- purely deviatoric. The actual magnitudes are shown in Table 2. One can see that the two composite particles fall between the Homogenized and the homogeneous PB particles in degree of mismatch by comparing the resulting stresses. The homogeneous PB particle, in essence, represents the highest degree of mismatch as it does not contain any PS. The CS LMWPB/PS particle contains twice the amount of PB by volume as the CS PB/PS particle, therefore producing a higher stress state. For comparative purposes a particle containing the same volume ratio of PB and PS as the CS PB/PS particle, but homogenized form (H2 particle in Table 1) was analyzed. The H2 stresses are lower than the CS PB/PS stresses, therefore the differing morphologies of the two particles must produce the differing degrees of mismatch.

The concentration of particles also alters the stress state for the material containing a composite particle. The stress distribution within the particle falls to a lower overall magnitude, but otherwise remains the same. The stress in the matrix at the interface changes as much as it did for that containing an isotropic particle. The tangential stresses increase in magnitude (remaining compressive) with increasing concentrations, while the radial stresses decrease in magnitude (Figures 16 and 17). These changes occur at approximately the same rates as those due to the isotropic particle. This results in a barely distinguishable change in the equivalent stress while still causing a rather noticable positive pressure in the matrix (Figures 16 and 17).

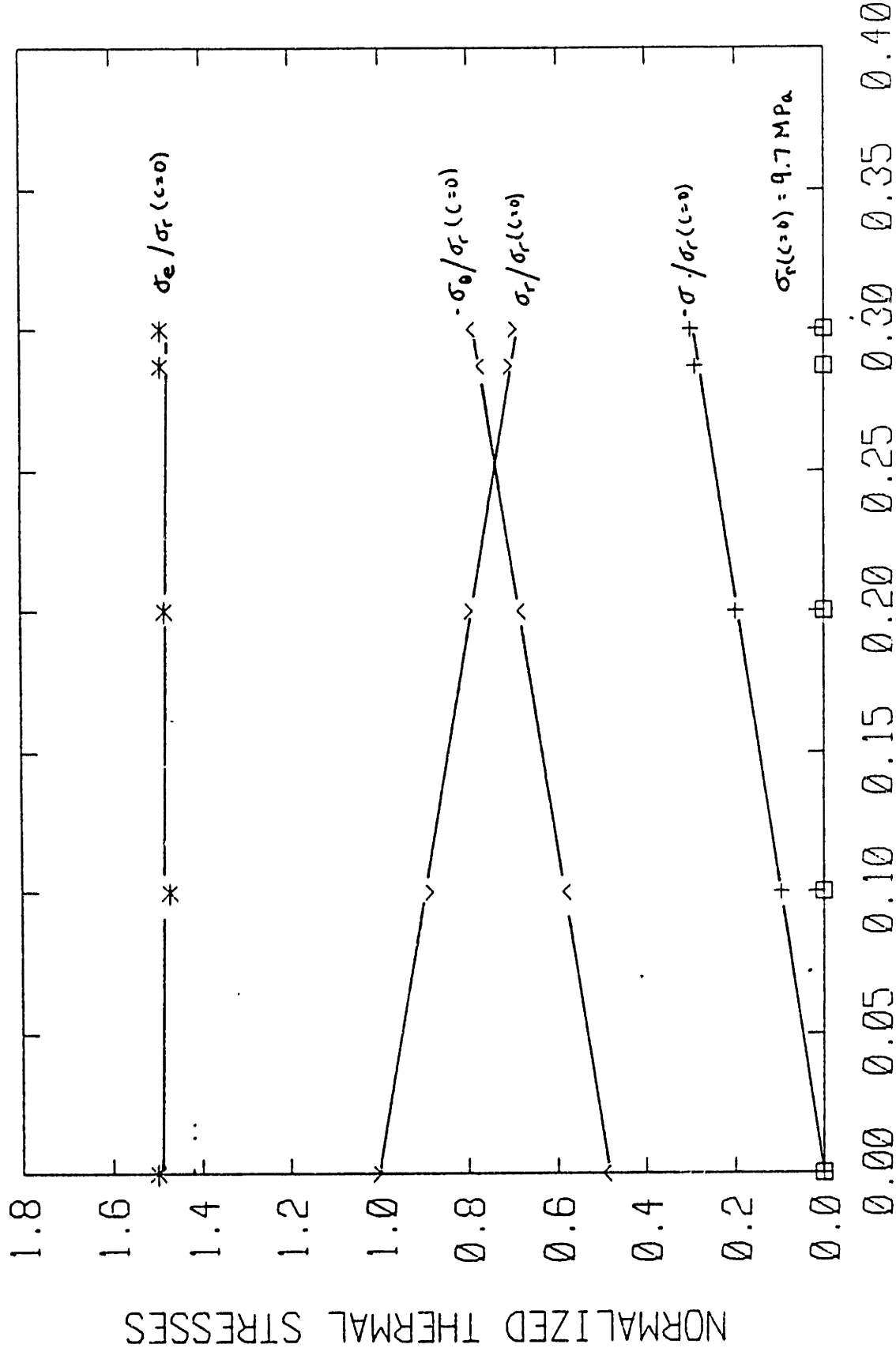

FIGURE 16. Effect of particle concentration on the magnitude of the thermal residual stresses at the particle border, induced by the CS PB/PS particle.

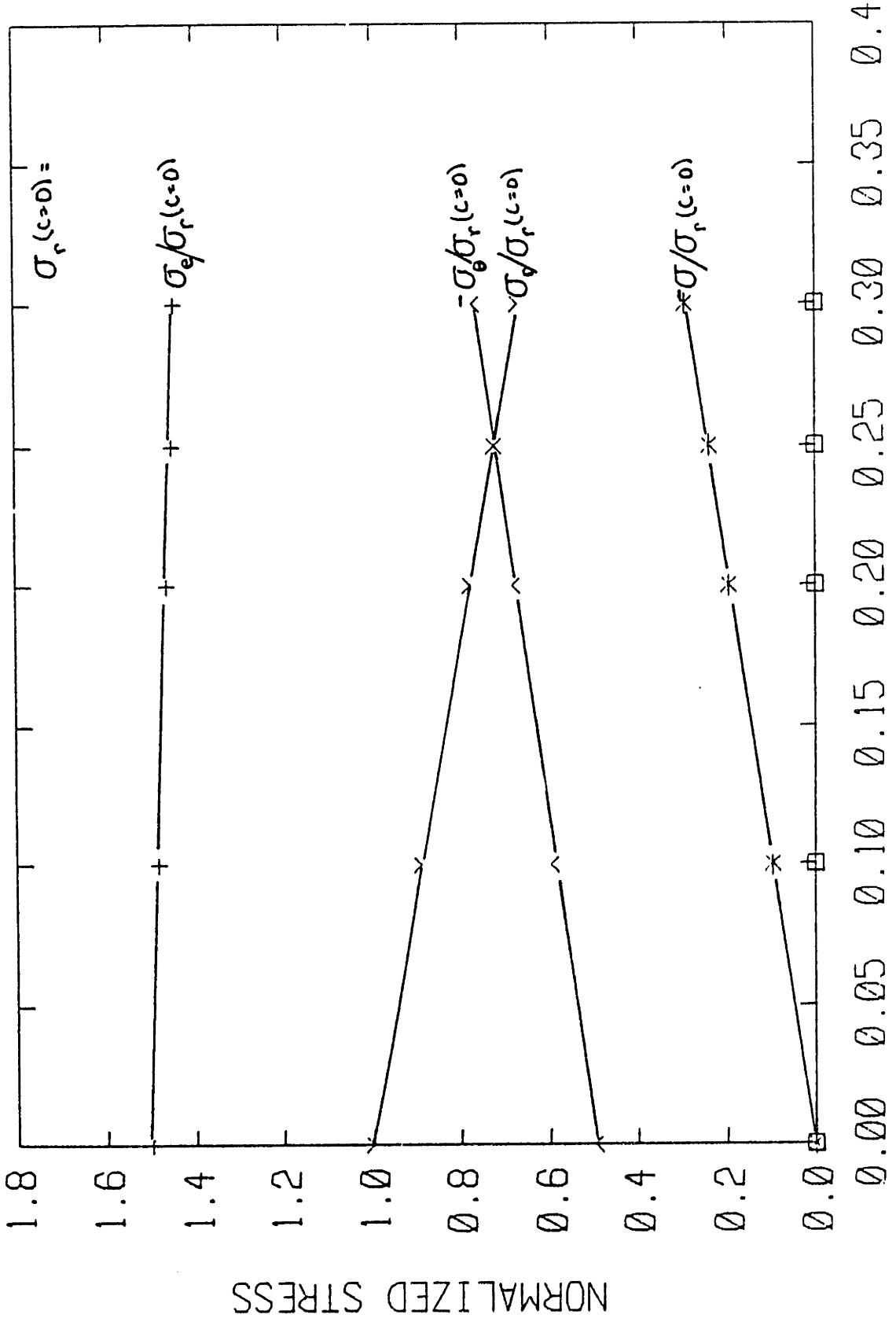

FIGURE 17. Effect of particle concentration on the magnitude of the thermal residual stresses induced by the CS LMWPB/PS particle.

3. RELAXATION OF RESIDUAL STRESSES

3.1. Description of Creep Behavior in Polystyrene Matrix

The PS matrix will creep when under a sustained residual stress such as that produced by the thermal expansion mismatch. At room temperature the linear viscoelastic stress relaxation should be quite small, but appreciable non-linear relaxation can occur at high local stress levels. This relaxation was described by Argon and Bessonov (1976) who have given strain rate-stress laws for the behavior. The inelastic shear strain rate may be written as:

$$\dot{\gamma} = \dot{\gamma}_0 \exp\left[-\Delta G^*/KT\right] \quad ,$$

where the activation free enthalpy ΔG^* is given as,

$$\Delta G^* = \frac{3\pi\mu\omega^2 a^3}{16(1-\nu)}\left[1 - 8.5(1-\nu)^{5/6}\left(\frac{s}{\mu}\right)^{5/6}\right] \quad .$$

The various terms in the above expression are defined as follows:

$\dot{\gamma}$ = net inelastic shear strain rate
$\dot{\gamma}$ = pre-exponential factor
ΔG^* = activation free enthalpy
μ = shear modulus
ω = net angle of rotation of a molecular segment between initial and activated configuration
a = mean molecular radius
ν = Poisson's ratio
s = deviatoric stress (shear)

The activation free enthalpy may be rewritten as

$$\Delta G^* = \left(1 - \left(\frac{s}{\hat{\tau}}\right)^{5/6}\right) \frac{3\pi\omega^2 a^3 \mu}{16(1-\nu)} \quad ,$$

where $\hat{\tau} = 0.077\mu/(1-\nu)$= the athermal shear strength. The above variables were measured in collective groups during controlled experiments by Argon and Bessonov. The following constant was obtained for PS:

$$\frac{16(1-\nu)}{3\pi\omega^2 a^3} = 7.46(10^{-2}) \ \frac{MPa}{^oK} \quad .$$

At room temperature, T = 295 °K, this gives

$$\frac{3\pi\omega^2 a^3}{16(1-\nu)} \frac{\mu}{KT} = 56.8 \quad .$$

The strain rate expression finally becomes

$$\dot{\epsilon} \equiv \frac{\dot{\gamma}}{\sqrt{3}} = \frac{\dot{\gamma}_o}{\sqrt{3}} \exp\left[-56.8\left(1-\left(\frac{\sigma_e}{\sqrt{3}\,\hat{\tau}}\right)^{5/6}\right]\right. \qquad (3\text{-}1)$$

where $\dot{\gamma}_o = 3(10^{13})$ sec , $\sqrt{3}\,\hat{\tau}$ = 238 MPa. This is the creep rate that PS exhibits under sustained "load", at room temperature (i.e. well below the glass transition temperature).

Since a sustained "load" exists in the form of the residual thermal stress state, the PS is creeping. The problem now is to determine how this creep behavior affects the residual stresses.

3.2. Solution

3.2.1. Isotropic Particles

To obtain a solution for the stresses as a function of time during the creep of the PS matrix, basic kinematics will first be considered. One can write the total strain as the sum of the elastic, thermal, and creep strains:

$$\epsilon_r = \epsilon_r^e + \epsilon_r^T + \epsilon_r^c$$
$$\epsilon_\theta = \epsilon_\theta^e + \epsilon_\theta^T + \epsilon_\theta^c$$
$$\epsilon_\phi = \epsilon_\theta .$$

where $\epsilon_i^c = \int_\tau \dot{\epsilon}_i^c \, dt$. The thermal strains are considered to be imposed initially by cooling from T_g to room temperature where they set up an initial thermal strain misfit which remains constant in time. Therefore, after the initial conditions are established, the total strain will be considered as the sum of the elastic and creep strains:

$$\epsilon_r = \epsilon_r^e + \epsilon_r^c$$
$$\epsilon_\theta = \epsilon_\theta^e + \epsilon_\theta^c \qquad (3\text{-}2)$$
$$\epsilon_\phi = \epsilon_\theta$$

Introducing the elastic stress-strain relation, the strains may be written as

$$\epsilon_r = \frac{1}{E}\left[\sigma_r - 2\nu\sigma_\theta\right] + \epsilon_r^c \,, \qquad (3\text{-}3\ a,b)$$
$$\epsilon_\theta = \frac{1}{E}\left[(1-\nu)\sigma_\theta - \nu\sigma_r\right] + \epsilon_\theta^c \,.$$

These can be rewritten to give expressions for the stresses as a function of the total strain and the creep strain:

$$\sigma_r = \frac{E}{(1-2\nu)(1+\nu)}\left[(1-\nu)(\epsilon_r - \epsilon_r^c) + 2\nu(\epsilon_\theta - \epsilon_\theta^c)\right] ;$$

$$\sigma_\theta = \frac{E}{(1-2\nu)(1+\nu)}\left[(\epsilon_\theta - \epsilon_\theta^c) + \nu(\epsilon_r - \epsilon_r^c)\right] . \qquad (3\text{-}4\ a,b)$$

Now, in order to obtain expressions for $\dot{\epsilon}_r^c$ and $\dot{\epsilon}_\theta^c$ in terms of $\dot{\epsilon}^c$, which has been defined in equation (3-1), the assumption of material incompressibility during creep flow is first introduced:

$$2\dot{\epsilon}_\theta^c + \dot{\epsilon}_r^c = 0 \quad ;$$
$$\dot{\epsilon}_r^c = -2\dot{\epsilon}_\theta^c . \qquad (3\text{-}5)$$

Then the definition of effective strain rate is used to relate the effective rate with the radial rate:

$$\dot{\epsilon}_c = \left[\frac{2}{3}\epsilon_{ij}\epsilon_{ij}\right]^{1/2} ;$$
$$\dot{\epsilon}^c = \pm\dot{\epsilon}_r^c = \mp 2\dot{\epsilon}_\theta^c .$$

The appropriate signs are determined by the deviatoric stress state. In this case, the initial radial deviatoric stress state is positive, and the initial tangential deviatoric stresses are negative. This results in:

$$\dot{\epsilon}^c = +\dot{\epsilon}_r^c = -2\dot{\epsilon}_\theta^c \qquad (3\text{-}6)$$

Writing equations (3-4) in rate form and substituting in equation (3-6), expressions in terms of total strain rates

and effective creep rates are obtained for the stress rates:

$$\dot{\sigma}_r = \frac{E}{(1-2\nu)(1+\nu)}\left[(1-\nu)\dot{\epsilon}_r + 2\nu\dot{\epsilon}_\theta - (1-2\nu)\dot{\epsilon}^c\right] \quad ;$$

$$\dot{\sigma}_\theta = \frac{E}{(1-2\nu)(1+\nu)}\left[\dot{\epsilon}_\theta + \nu\dot{\epsilon}_r + \frac{1}{2}(1-2\nu)\dot{\epsilon}^c\right] \quad . \qquad (3\text{-}7\ \text{a,b})$$

The total strain rates are still unknown, and are found from the equilibrium equations. This problem is spherically symmetric, therefore only one equilibrium equation needs to be satisfied:

$$\frac{d\dot{\sigma}_r}{dr} + \frac{2(\dot{\sigma}_r - \dot{\sigma}_\theta)}{r} = 0$$

This can be rewritten in terms of strain rates through the use of equations (3-5) and (3-7):

$$\frac{d}{dr}\left[r^4 \frac{d\dot{\epsilon}_\theta}{dr}\right] = \frac{(1-2\nu)}{(1-\nu)} \frac{d}{dr}\left[r^3 \dot{\epsilon}_c\right] . \qquad (3\text{-}8)$$

Integrating twice yields:

$$\dot{\epsilon}_\theta = \frac{1-2\nu}{1-\nu}\left[I(r) - \frac{A}{3}\left(1 - \frac{a^3}{r^3}\right)\right] - \frac{C_1}{r^3} + C_2 \quad ; \qquad (3\text{-}9)$$

where, $A = \dot{\epsilon}^c(a)$ = known;

$I(r) = \int_a^r \frac{1}{r}\dot{\epsilon}^c dr$ = known;

C_1, C_2 are unknown.

The two unknown constants C_1 and C_2 are determined by applying boundary conditions:

1. @ r = a, $\dot{\sigma}_r = \dot{\sigma}_p$, where $\dot{\sigma}_p$ = particle stress rate;

2. @ r = a, $\dot{u}_r = \dot{u}_p$, where $\dot{u}_p$ = particle border displacement rate;

3. @ r = b, $\dot{\sigma}_r = 0$. (3-10)

This yields complicated algebraic expressions for C_1 and C_2, that are symbolically,

$$C_1 = \hat{C}_1(E_m, E_p, \nu, c, \epsilon),$$
$$C_2 = \hat{C}_2(E_m, E_p, \nu, c, \epsilon) . \quad (3-11)$$

Substitution of equation (3-11) into equation (3-9) yields the complete solution for the total tangential strain rate. Because of the spherical symmetry of the problem, and expression for the radial strain rate may be determined from the tangential strain rate with the following relation (see Appendix 2):

$$\epsilon_r = \epsilon_\theta + r \frac{d\epsilon_\theta}{dr}$$

Subsequently, the stress rates may be determined from equations (3-7 a,b). A detailed solution up to and including this point is given in Appendix 2.

The resulting equations are solved with a scheme which progresses with time. For example,

$$^{t+\Delta t}\epsilon_\theta = {}^{t}\epsilon_\theta + {}^{t}\dot{\epsilon}_\theta \Delta t . \quad (3-12)$$

Each time increment, Δt, is determined at the end of each iteration by setting the total creep strain to be less than five percent of the elastic strain:

$$\Delta t \leq 0.05 \epsilon^e / \dot{\epsilon}^c \quad .$$

The computations are carried out with a short FORTRAN program which is explained and listed in Appendix 3. The end result gives the strains and stresses as a function of time.

3.2.2. Concentric Spherical Shell Particles

The solution for the stress state as a function of time for the isotropic particle was found to be quite lengthy. To obtain a solution for the concentric shell particle by a similar method would be even more so because not only must the creep behavior of the PS matrix be considered, but also that of the PS shells within the particle. Therefore, a finite element analysis was conducted to obtain the solution.

The same basic finite element mesh may be used for the creep problem as that used for the thermal stress problem because the geometry and behavior remain spherically symmetric. The modelling of the material, of course, differs because now the creep behavior of the PS must be incorporated. The details of the analysis are described in Appendix 5. The solution yields the stress, elastic strain and creep strain as a function of time. Again, accuracy was checked by conducting a finite element analysis on an isotropic particle and comparing the results with the solution obtained from the Section 3.2 method. The results were shown to be very accurate as depicted in Figure 18.

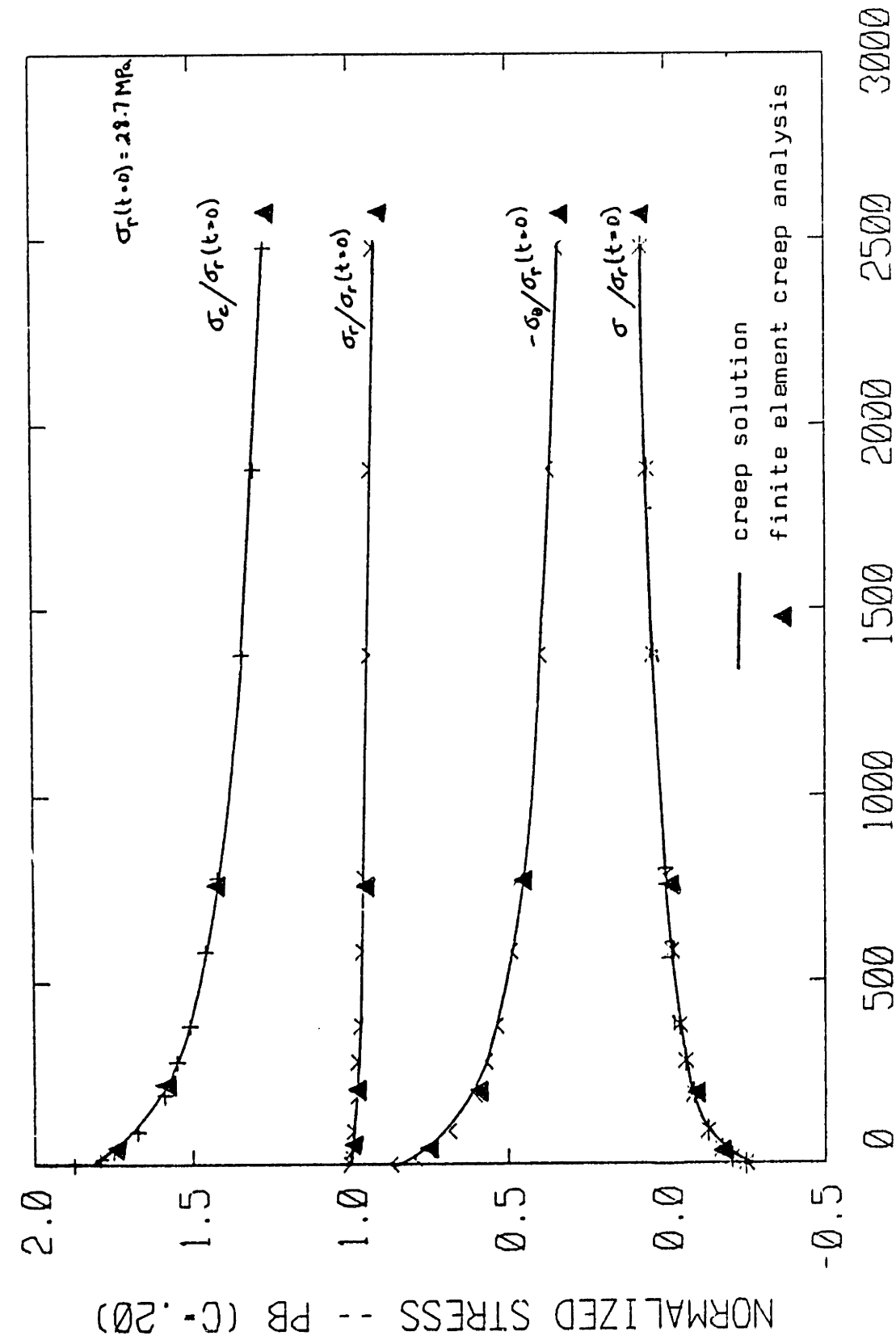

FIGURE 18. Relaxation of thermal stresses due to the PB particle in a PS matrix with c=0.20; comparison of creep solution with finite element creep analysis solution. Stresses are normalized with respect to σ_r (t=0)=28.7 MPa.

3.3. Results of Relaxation Analysis

3.3.1. Isotropic Particles

The solution for the isotropic particle shows that the strain rates and stress rates are dependent upon the material properties of both the matrix and the particle, but are primarily dependent upon the deviatoric stress state in the matrix. In other words, the higher the deviatoric stress state in the matrix, the greater the creep strain rate and subsequently the greater the relaxation of the stresses.

This is most clearly seen by comparing the relaxation around the fictitious PB particle with that around the Homogenized particle. The initial deviatoric stress due to the thermal mismatch is 51.8 MPa in the infinite matrix at the interface with the PB particle and 11.9 MPa at that with the Homogenized particle. Referring to Figures 19 and 20, one can see the dramatic effect this initial field has on the relaxation rate. [Note: the curves are normalized with respect to their own radial stress at time t=0.] Not only is the exponential decay more pronounced for the PB particle, but also the time scale is two orders of magnitude smaller. However, both particles do result in the same basic trend which is a large decrease in the magnitude of the compressive tangential stresses and a very small decrease in the radial stress. These two effects combine to yield the development of a negative pressure (initially, this is zero for the infinite matrix) and a decrease in the deviatoric stress state. The negative pressure in the matrix is given by in the figures. The development of a negative pressure is beneficial to the initiation of crazes because the presence

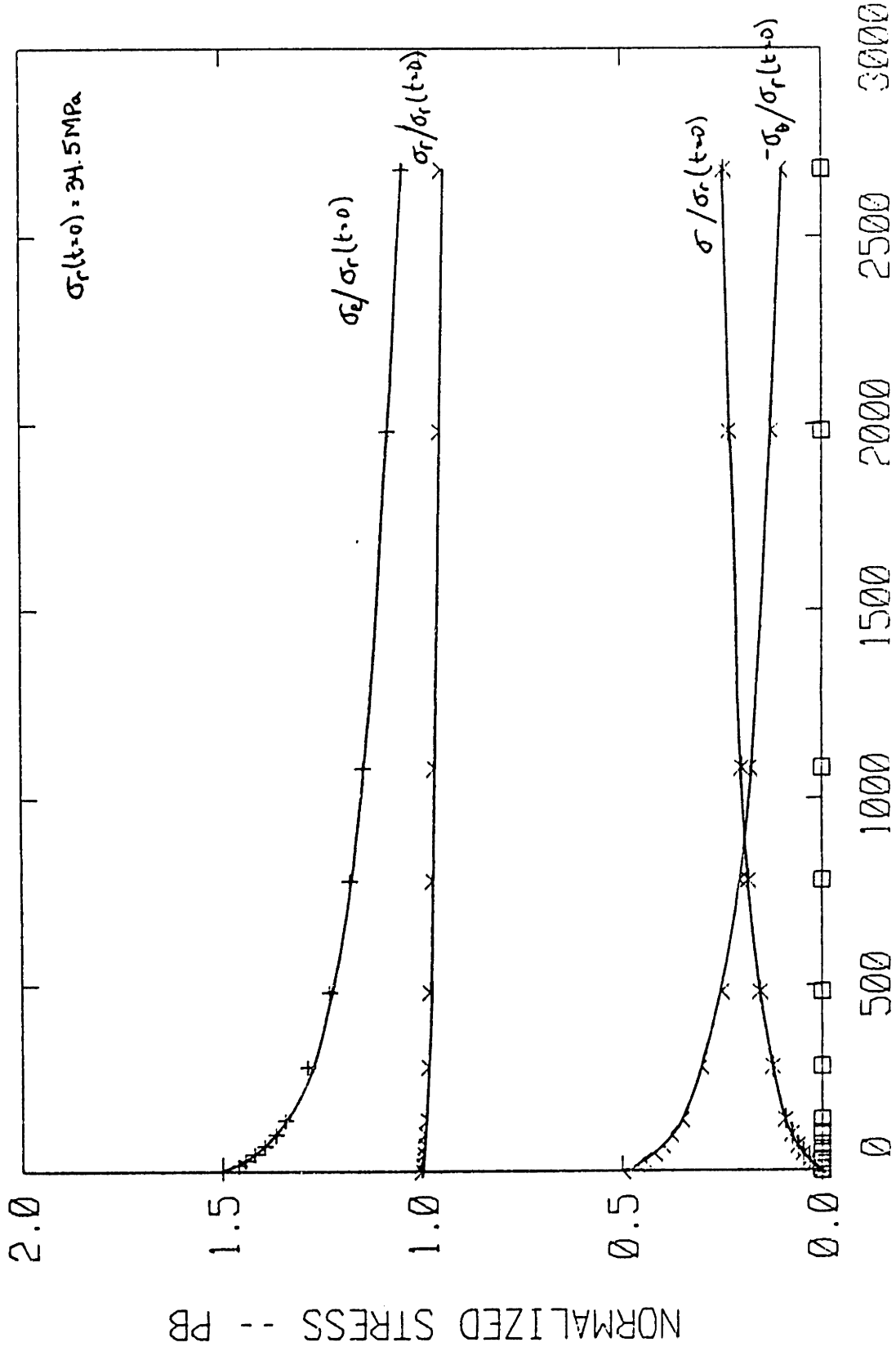

FIGURE 19. Relaxation of thermal residual stresses due to a PB particle in an infinite PS matrix. Stresses are normalized with respect to σ_r (t=0)=34.5 MPa.

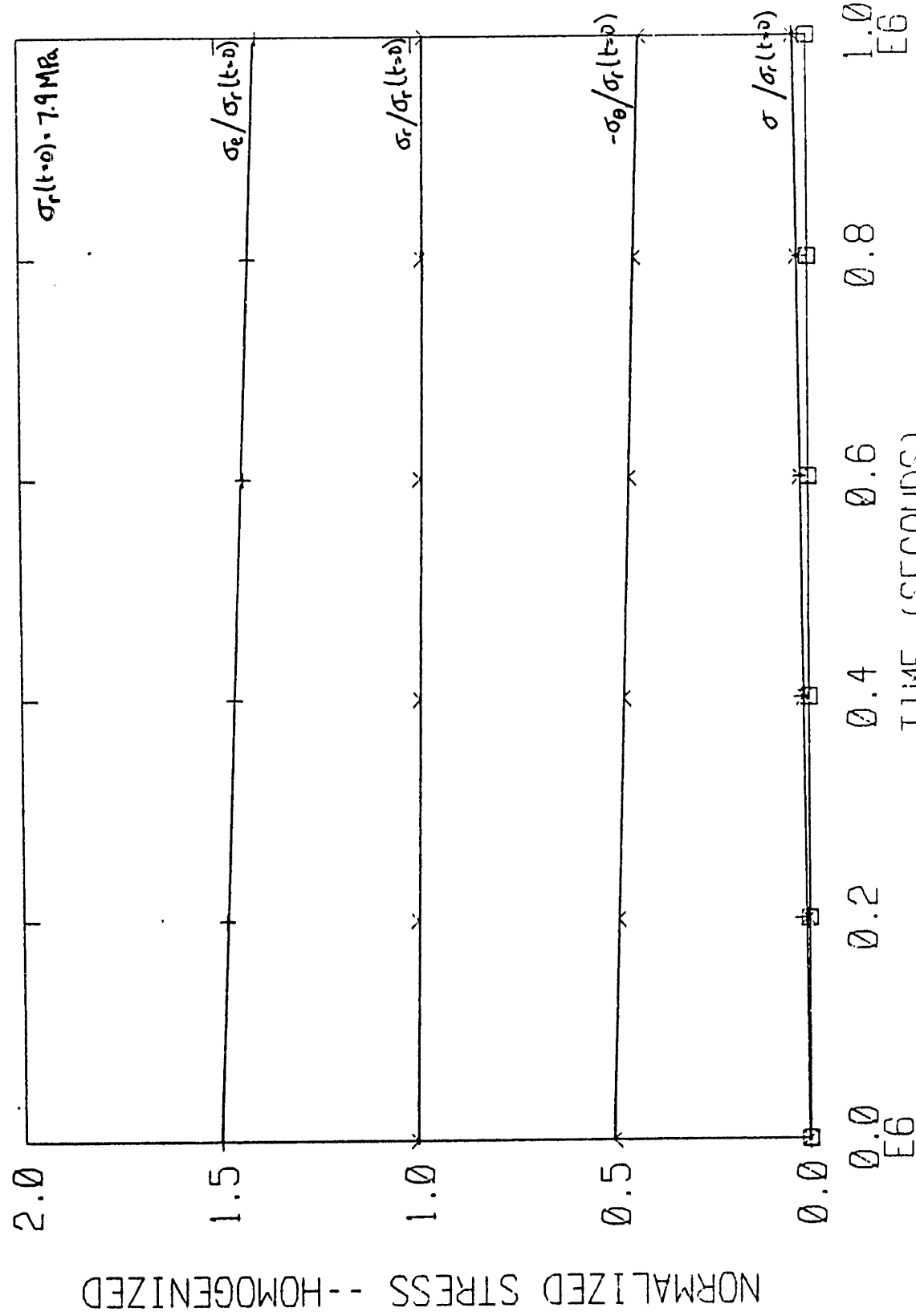

FIGURE 20. Relaxation of thermal residual stresses due to Homogenized particle in an infinite PS matrix. Stresses are normalized with respect to $\sigma_r(t=0)$=7.93 MPa.

of a negative pressure is required to plastically expand voids which are nucleated by the deviatoric stress. The development of a porosity level (voids) due to the presence of a deviatoric stress will be further discussed in Section 5.

The effect of the concentration of particles on the relaxation behavior is not great although there do exist some minor differences. The basic trend of a small decrease in the radial stress and a large decrease in the tangential stress magnitude remains the same. However, the presence of a larger deviatoric stress state does cause the creep rates to be slightly greater. Another difference is the initial presence of a positive pressure, σ , around the particles. As the stresses relax, this positive pressure decreases in magnitude and with time becomes a negative pressure. However, it is only for the idealized PB particle, which possesses very high initial stresses, that the rates are high enough for the positive pressure to develop into a negative pressure in reasonable lengths of time. The stress relaxation behavior for the PB and Homogenized particles in various finite matrices is depicted in Figures 18 and 21.

3.3.2. Concentric Spherical Shell Particles

The relaxation behavior of the stresses in the matrix at the interface with the Concentric Shell particles is very similar to that with the isotropic particles. The relaxation around the CS PB/PS particle and around the CS LMWPB/PS particle are highly dependent upon the initial level of deviatoric stress set up by the thermal mismatch (Figures 22 and 23). One may have thought that since the PS shells within the particle are relaxing as well as the

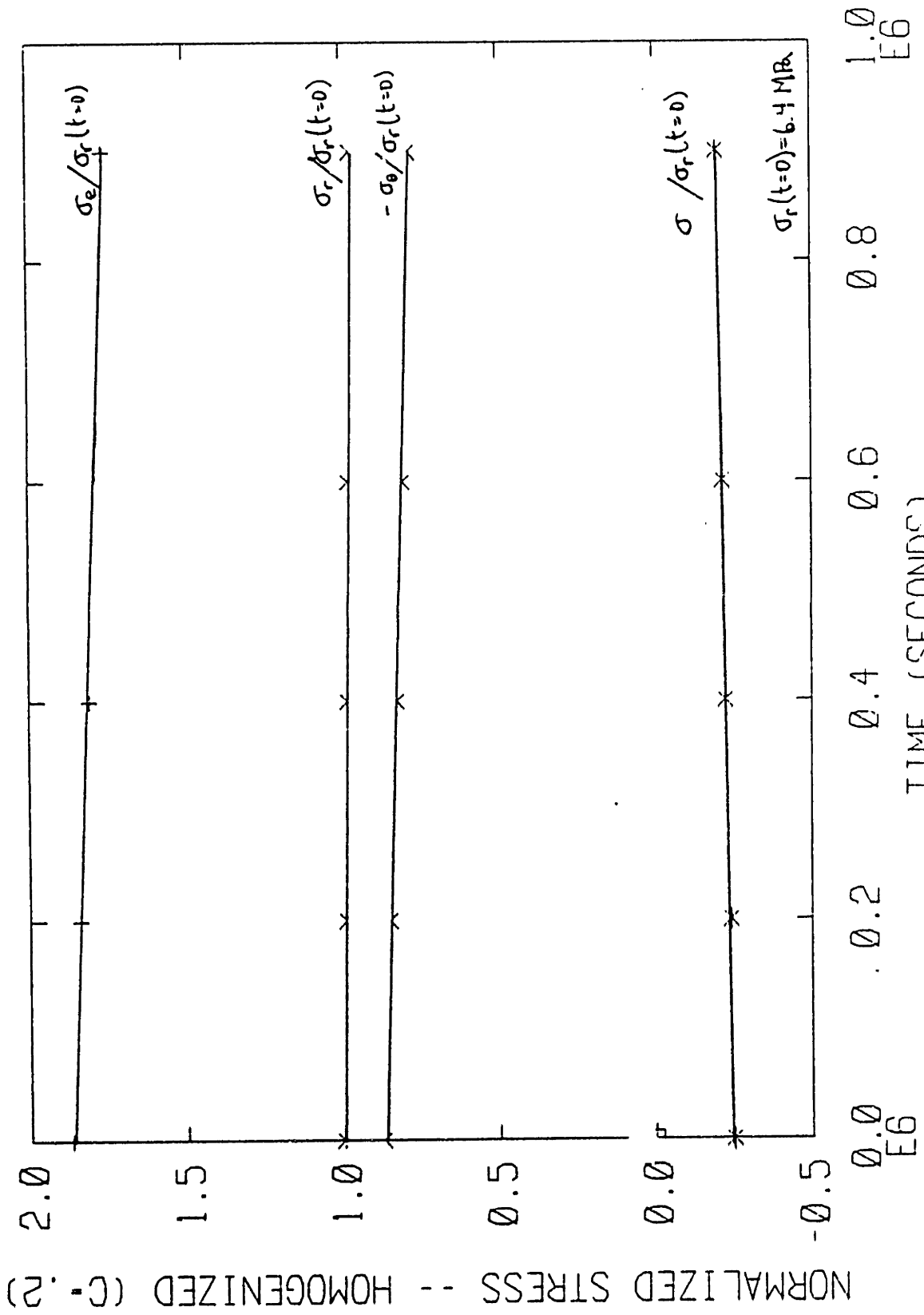

FIGURE 21. Relaxation of thermal residual stresses due to Homogenized particle in a PS matrix with c=0.20. Stresses are normalized with respect to $\sigma_r(t=0)=6.40$ MPa.

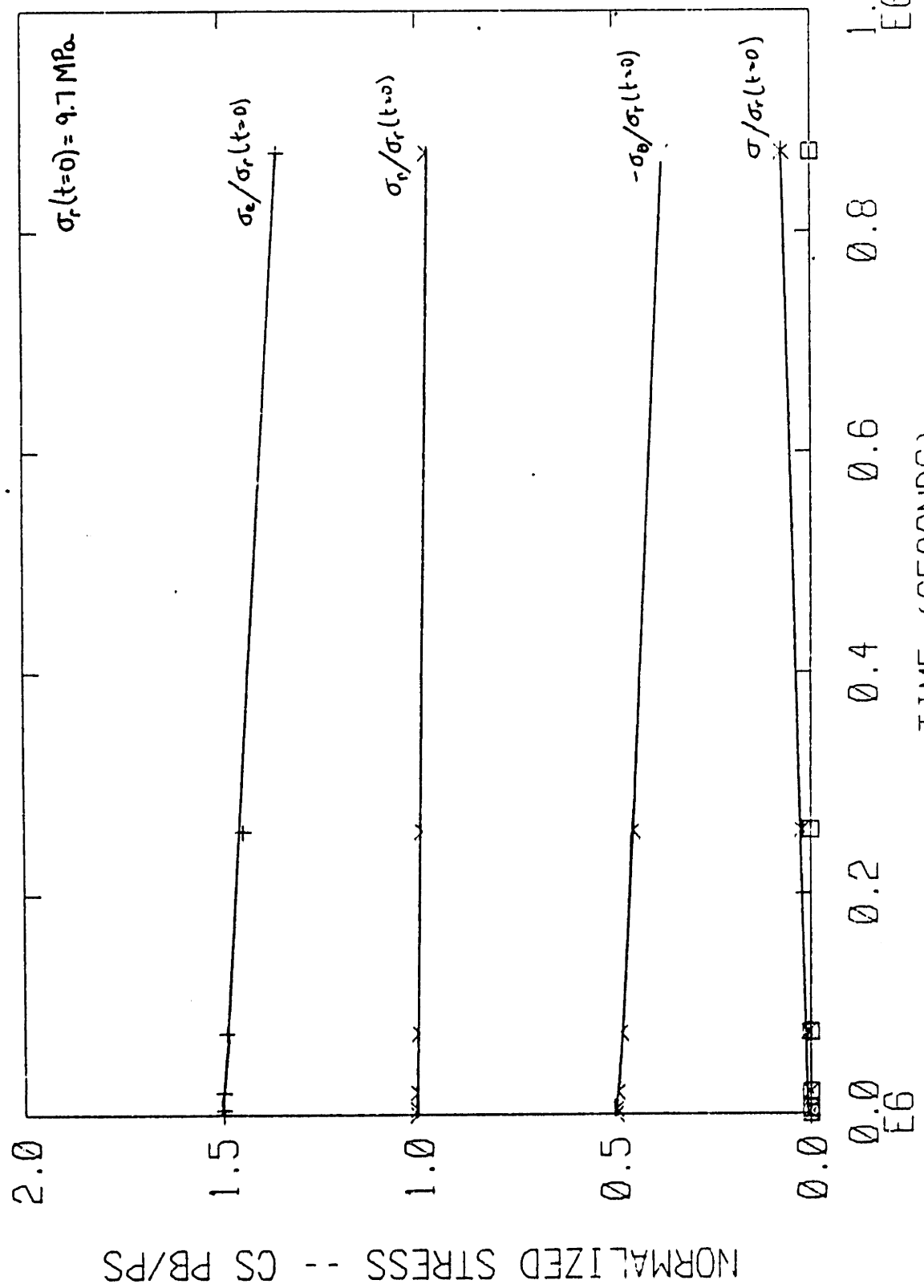

FIGURE 22. Relaxation of thermal residual stresses due to CS PB/PS particle in an infinite matrix. Stresses are normalized with respect to $\sigma_r(t=0)=9.7$ MPa.

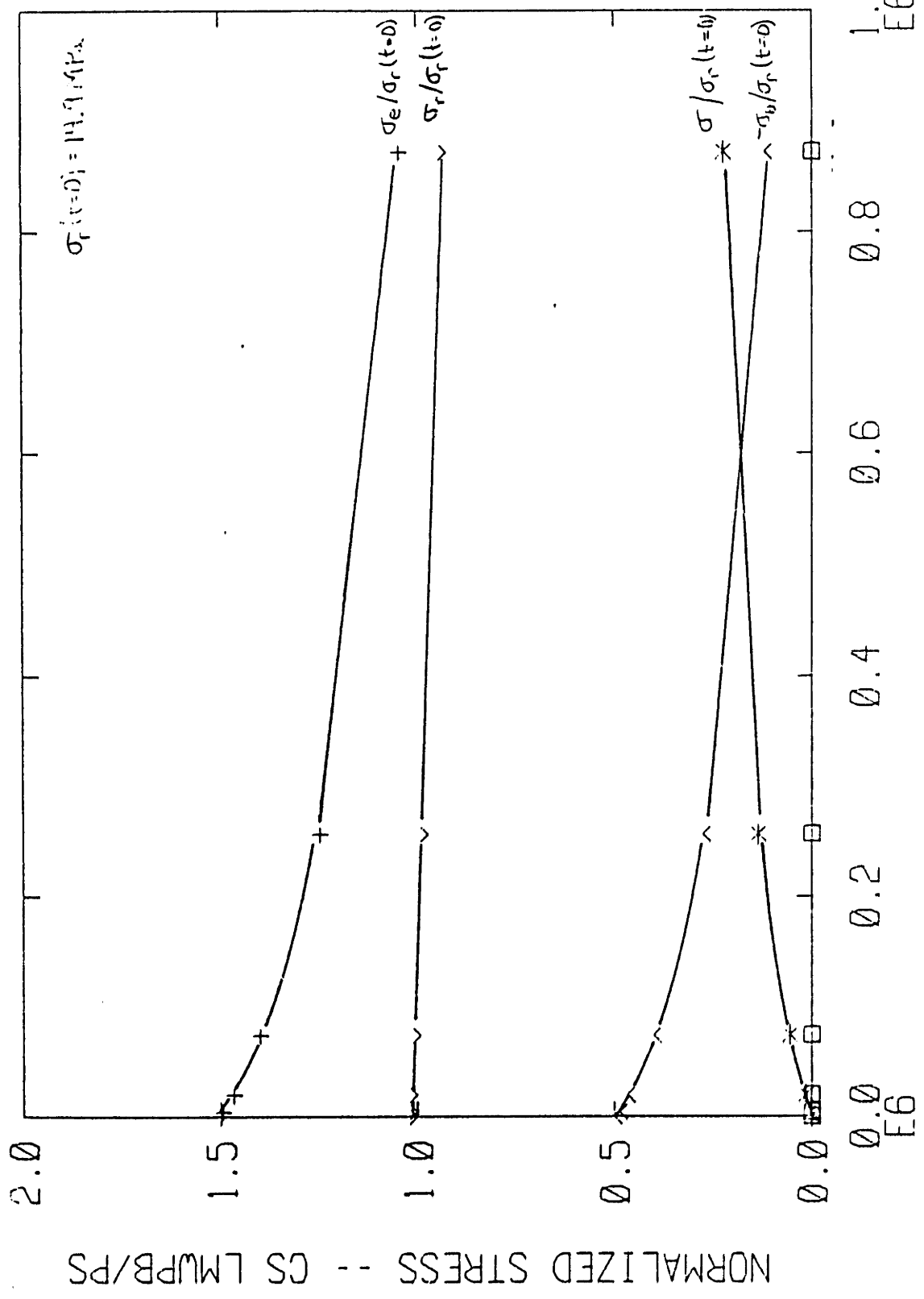

FIGURE 23. Relaxation of thermal residual stresses due to CS LMWPB/PS particle in an infinite matrix. Stresses are normalized with respect to $\sigma_r(t=0)=14.9$ MPa.

PS matrix, a faster overall relaxation of stresses would result, but this is not the case.

In order to show that the stress relaxation does indeed depend almost entirely on the deviatoric stress and very weakly on the particle properties, the same initial stresses were set up in the matrix surrounding two different particles -- one a Concentric Shell particle and the other an isotropic Homogenized particle -- and allowed to relax. Figure 24 shows that these two sets of relaxation curves are very close indicating a very strong dependence on the initial deviatoric stress and a very weak dependence on particle properties. Since the overall relaxation behavior depends almost solely on the deviatoric stress, and not on the relaxation or elastic properties of the particles themselves, the overall relaxation behavior around the composite particles is similar to that around the isotropic particles.

The CS LMWPB/PS particle contains a larger percentage of PB and therefore creates a larger thermal mismatch and, subsequently, a larger deviatoric stress than the CS PB/PS particle. This explains why the relaxation rate of the CS LMWPB/PS particle is much greater than that of the CS PB/PS particle. If the particle properties had been as crucial to relaxation as originally thought, one may have thought the CS PB/PS particle would cause a faster relaxation because of its greater percentage of PS. But, as shown, it is the initial mismatch which determines the relaxation behavior.

It is easy to conclude that the effect of particle concentration on the relaxation will also be similar to the isotropic particle results. The relaxation trends are the same as in the infinite matrix; a very slight decrease in

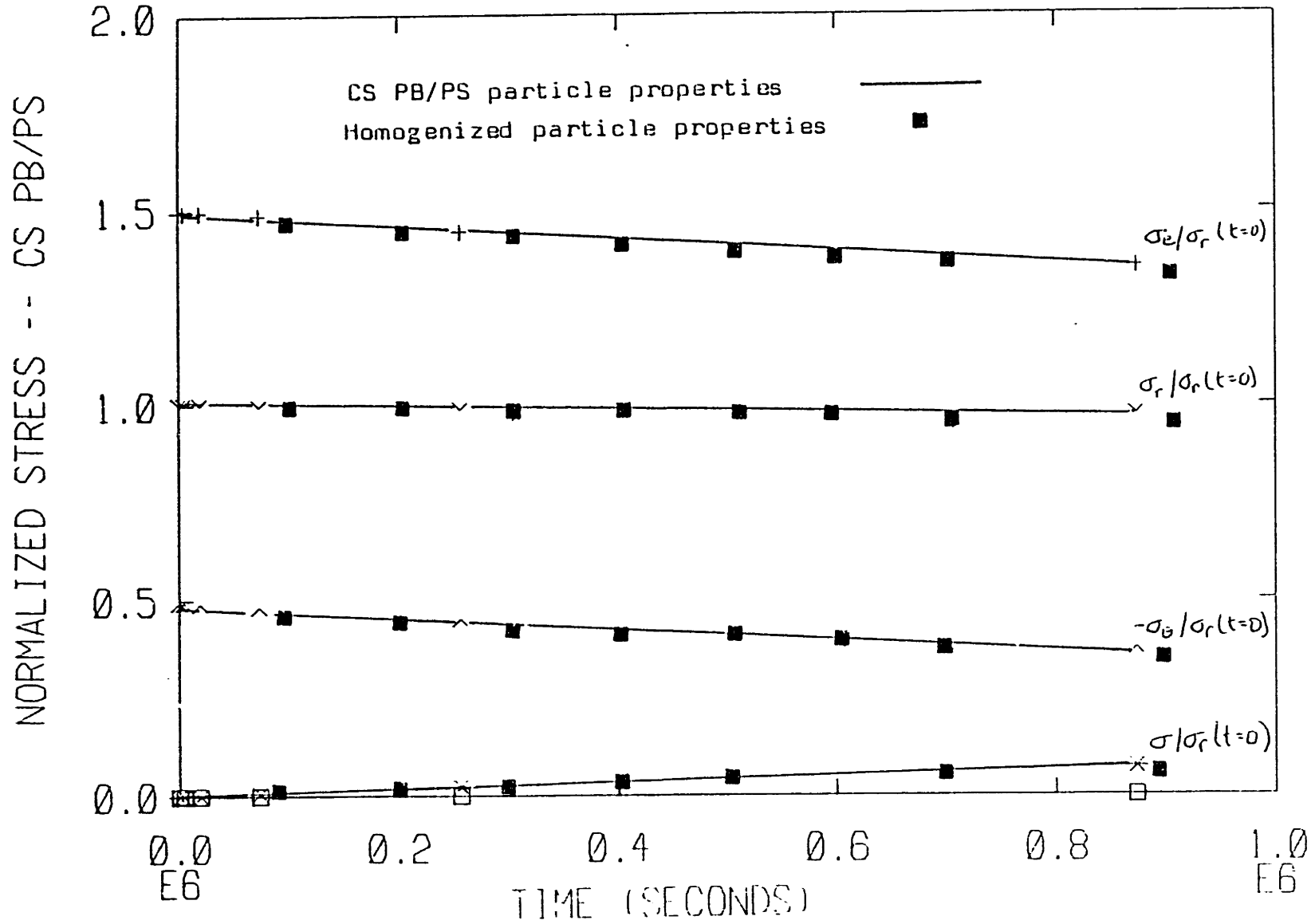

FIGURE 24. Relaxation of the residual stresses due to CS PB/PS particle in an infinite PS matrix. Comparison of using CS PB/PS particle properties and Homogenized particle properties in relaxation analysis with the same initial stress state.

the radial stress, and a somewhat greater decrease in the tangential stress as shown in Figure 25. A positive pressure does exist initially. Since the deviatoric stresses initially are not large enough to induce a high creep rate, the positive pressure will not reach the zero value in reasonable lengths of time. These are not surprising results.

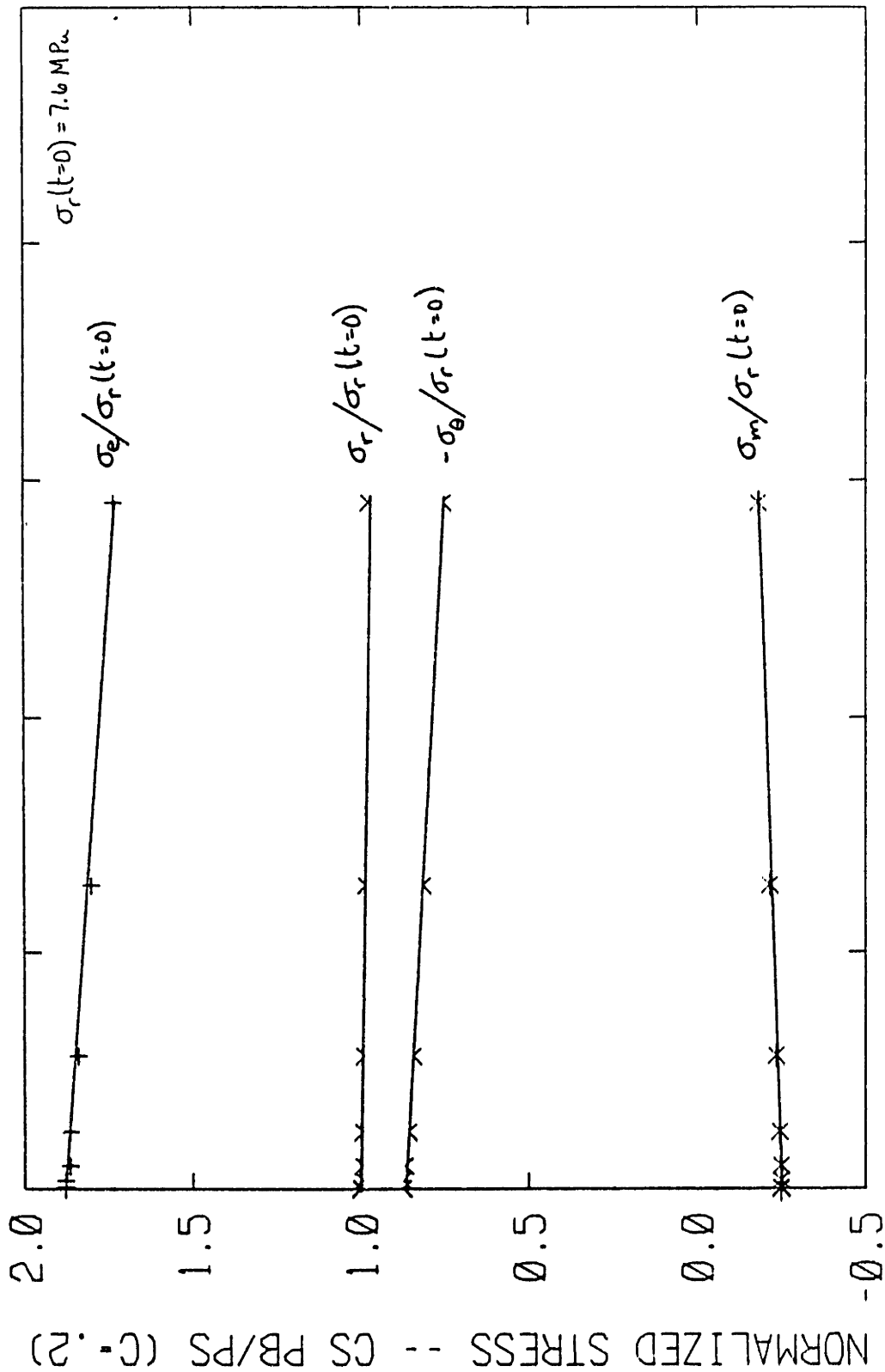

FIGURE 25. Relaxation of thermal residual stresses due to CS PB/PS particle in a matrix of PS with c=0.20. Stresses are normalized with respect to $\sigma_r(t=0)$=7.64 MPa.

4. UNIFORM APPLIED TENSILE STRESS

4.1. Problem Description

We are now interested in the effect of an applied tensile stress on the stress distribution around the particles. Figure 26 depicts the problem in idealized form. Stress concentrations will develop at the equatorial interface in the matrix because the particle has a lower shear modulus, and therefore the matrix must carry a greater percentage of the load. This is much like the problem of a cavity in a matrix. The stress concentration factor due to a spherical cavity is 2.05. The concentration factor caused by the particles will be lower than this because the particles are capable of carrying some of the load, primarily by their stiff bulk behavior.

4.2. Solution

4.2.1. Isotropic Particle

The stress distribution around a spherical elastic inclusion in an infinite elastic matrix with a uniform tensile stress applied at infinity has been determined by Goodier (1933). His solution assumes the matrix and the particle to be homogeneous and isotropic as well as perfectly bonded to one another. All of these are assumptions which have already been made concerning this material, and therefore the Goodier solution may be used. His solution is quite lengthy and is given in Appendix 4.

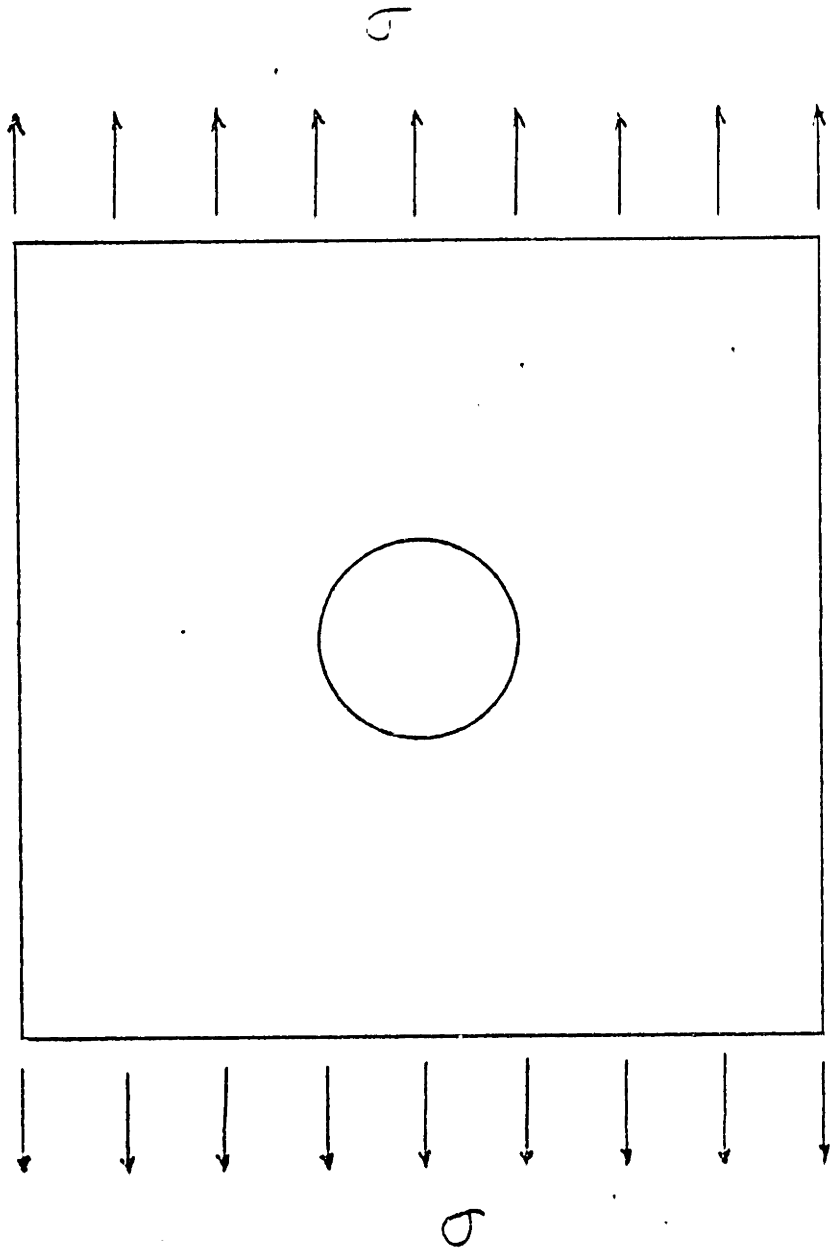

FIGURE 26. Schematic of particle in an infinite matrix subjected to a uniform tensile stress at infinity.

4.2.2. Solution -- Concentric Sphere Particle

A finite element analysis is conducted to determine the stress distribution around the Concentric Sphere particles due to a tensile stress applied at "infinity". The axial symmetry of the geometry and loading are taken advantage of in the finite element modelling (Figure 27). Details of the finite element analysis are given in Appendix 5. The accuracy of the solution is determined by conducting a finite element analysis on an isotropic particle and comparing it with Goodier's elasticity solution. The results indicated less than 3% error in the axial stress concentration factor.

4.2.3. Particle in a Finite Matrix

To obtain the solution with a finite boundary imposed on the problem, a finite element analysis was conducted. This was first done by Broutman and Panizza (1971). An analysis similar to the "method of images" of fluid mechanics is conducted by forcing the free side of the axisymmetric model to displace uniformly (Figure 28). This accounts for the concentration effects assuming the particles are uniformly distributed.

4.3. Results

4.3.1. Infinite Matrix

The mechanical mismatch between the particle and the matrix causes a nonuniform stress distribution in the region surrounding the particle (approximately 4 radii -- Goodier, 1933) in an otherwise uniform stress field. This

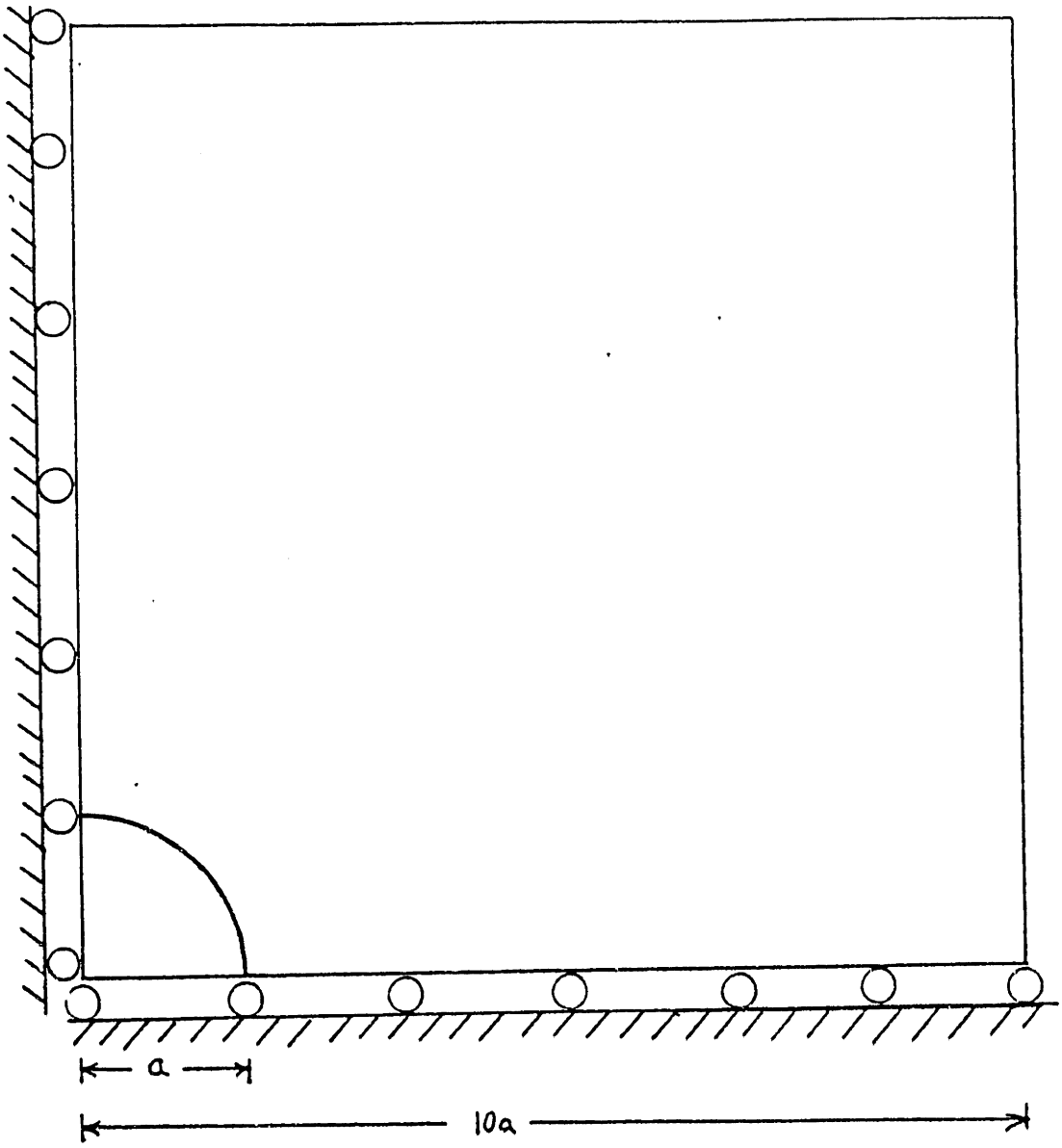

FIGURE 27. Geometry and boundary conditions to be modelled with finite elements for the problem of a particle in an infinite matrix subjected to uniform tension at infinity. The rollers represent zero displacement normal to the line and therefore induce the reflective symmetry.

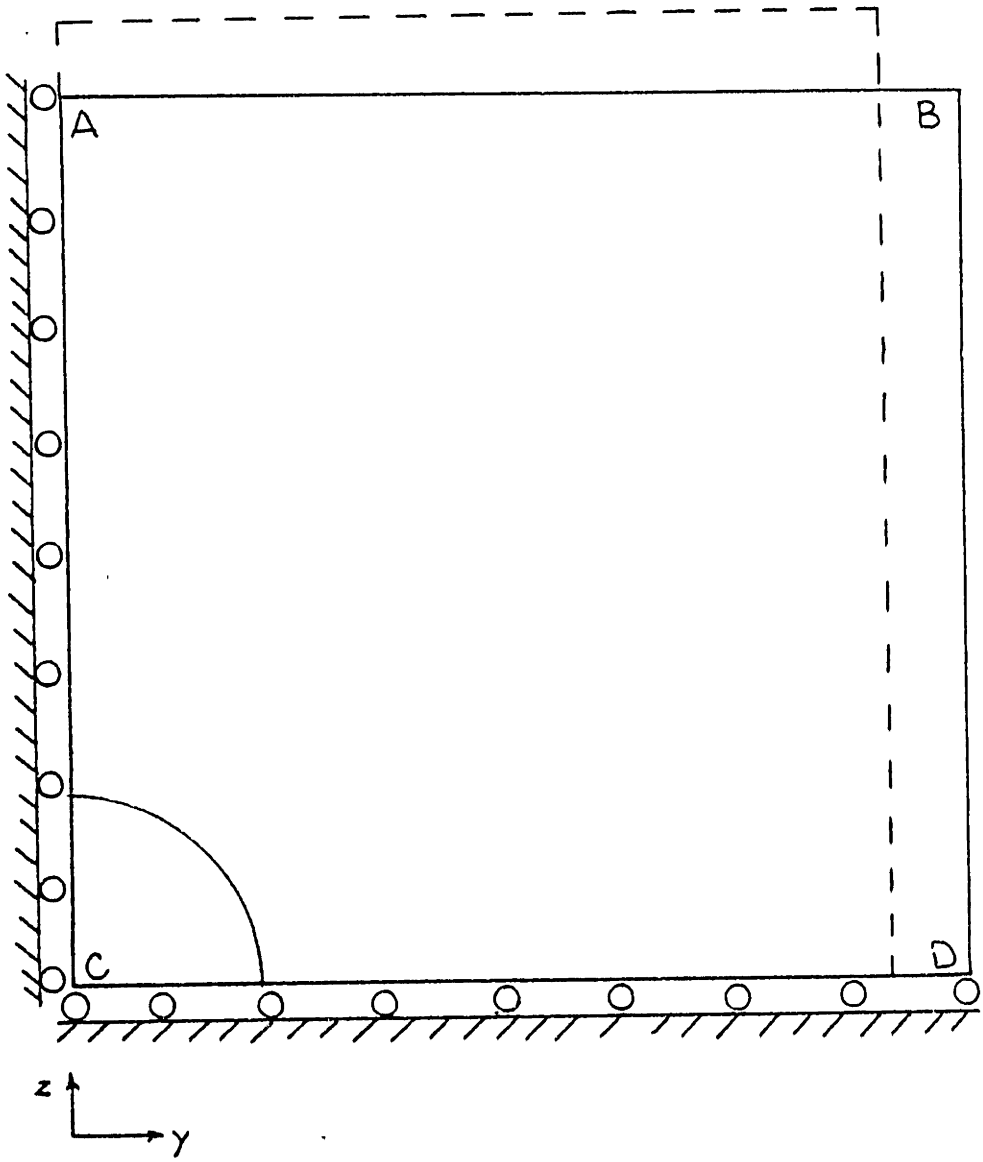

FIGURE 28. Geometry and boundary conditions to be modelled with finite elements for the problem of a particle in a finite matrix subjected to a uniform tensile load. Line AB is made to displace uniformly in the z direction; line BD is made to displace uniformly in the y direction.

mismatch is optimal when the particle is in fact a cavity. The tensile stress concentration for a spherical cavity is 2.05 as mentioned in the problem description. The solutions described in Sections 4.2 and 4.3 yield the stress concentration factors due to the four particles, as well as the stress fields surrounding the particles.

The stress concentration factors were found to increase as the particles ability to support shear decreased (Table 3). The PB particle which has the lowest shear modulus, 0.62 MPa, had the highest concentration factor, 1.88. The Homogenized particle (shear modulus -- $0.88(10^3)$ MPa) had the lowest concentration factor, 1.16. This, of course, is a sensible result because the particles with lower shear moduli cannot carry a significant portion of the load, and therefore the matrix must support more stress, raising the concentration factor. Figures 29, 30, and 31 show the displacements of the Homogenized, CS PB/PS, and CS LMWPB/PS particles and their surrounding matrices when a tensile stress is applied. These figures give a pictorial view of the extensive shearing (almost flowing) behavior of the PB layers of the concentric sphere particles. This shows the limited ability of these particles as compared with the Homogenized particle in supporting shear stresses; this makes their stress concentration factors much higher.

Although the concentration factor due to the Homogenized particle is lower than that due to the other particles, the actual stress due to its applied tension is higher. This is because the flow stress of the Homogenized particle's material is 30 MPa versus 10 MPa for the other three materials. The stress state due to uniform tension is listed in Table 3 for the equatorial interface of the four particles.

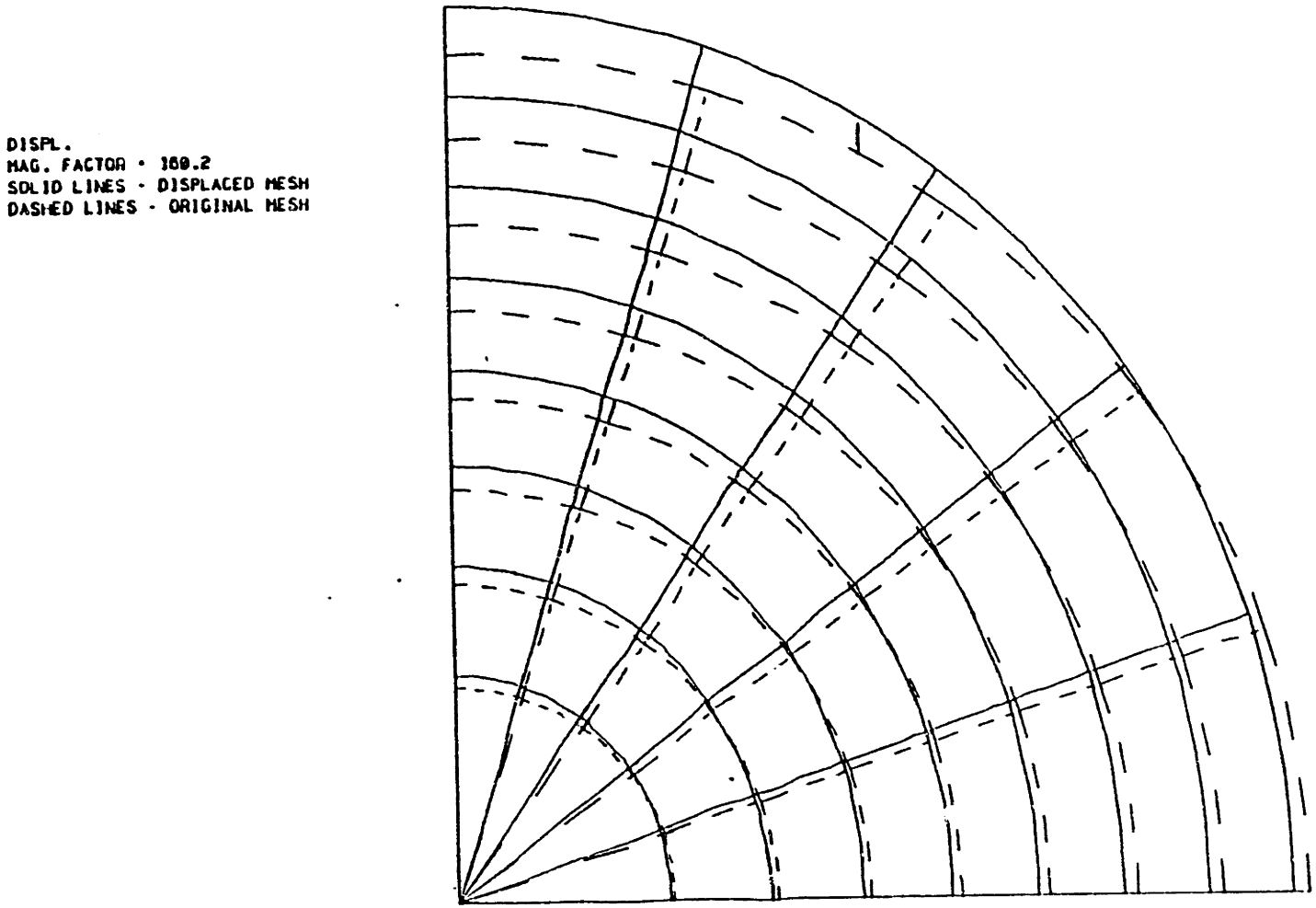

FIGURE 29a. Displacement of the Homogenized particle (inner 75%) in a PS matrix subjected to uniform tension at infinity.

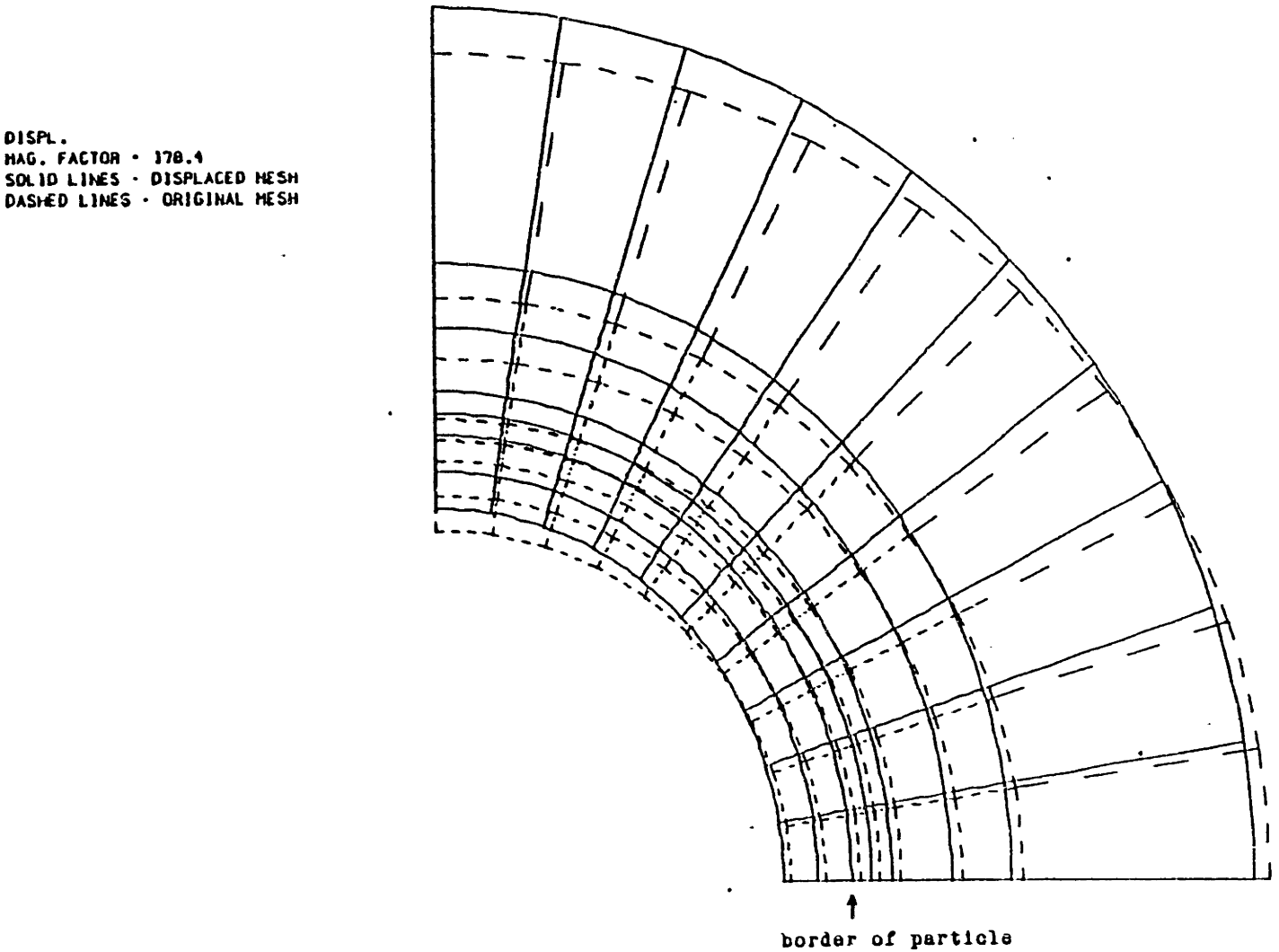

FIGURE 29b. Displacement of the Homogenized particle (outer portion) and immediately surrounding matrix when subjected to uniform tension at infinity.

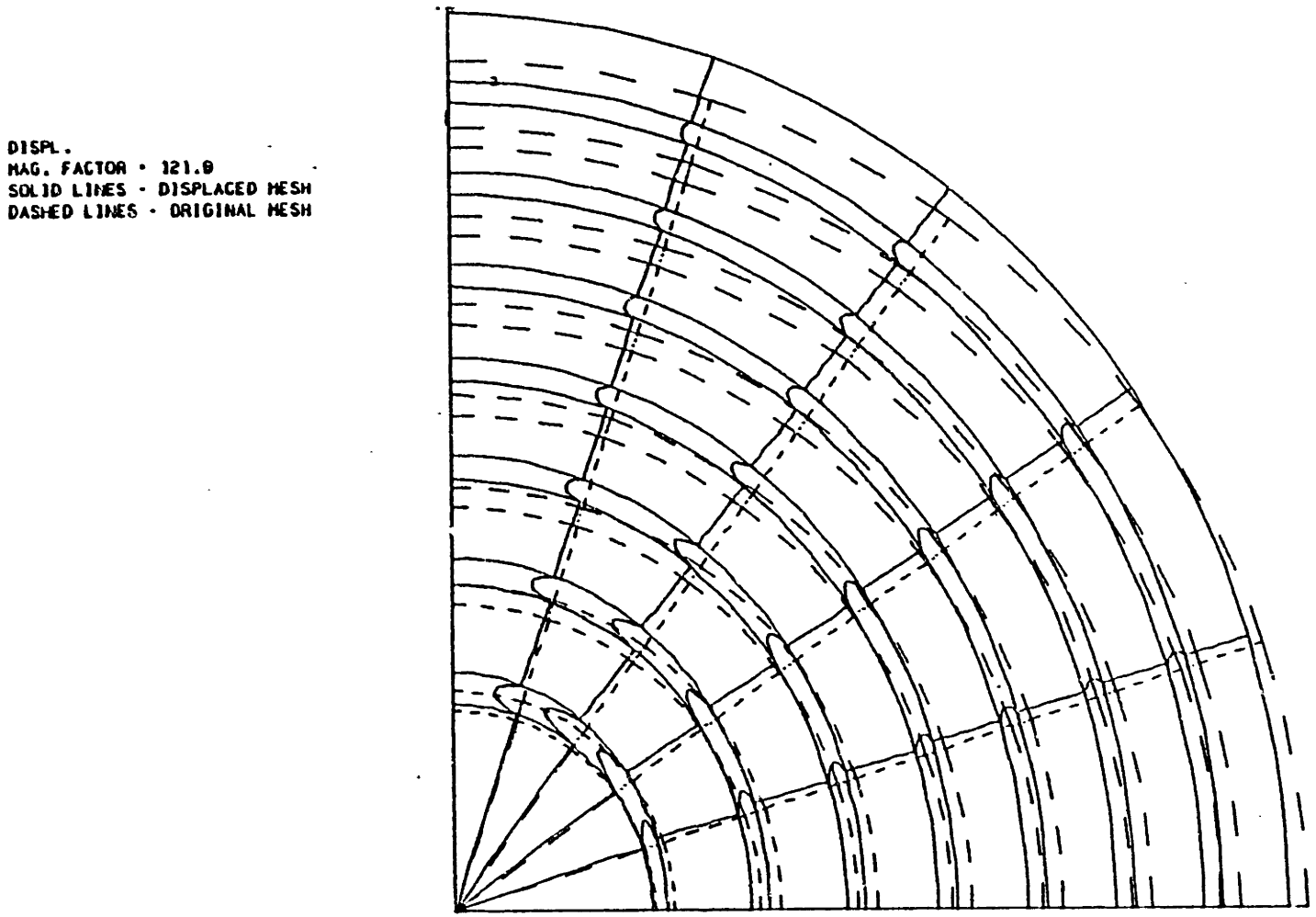

FIGURE 30a. Displacement of the CS PB/PS particle (inner 75%) in a PS matrix subjected to uniform tension at infinity.

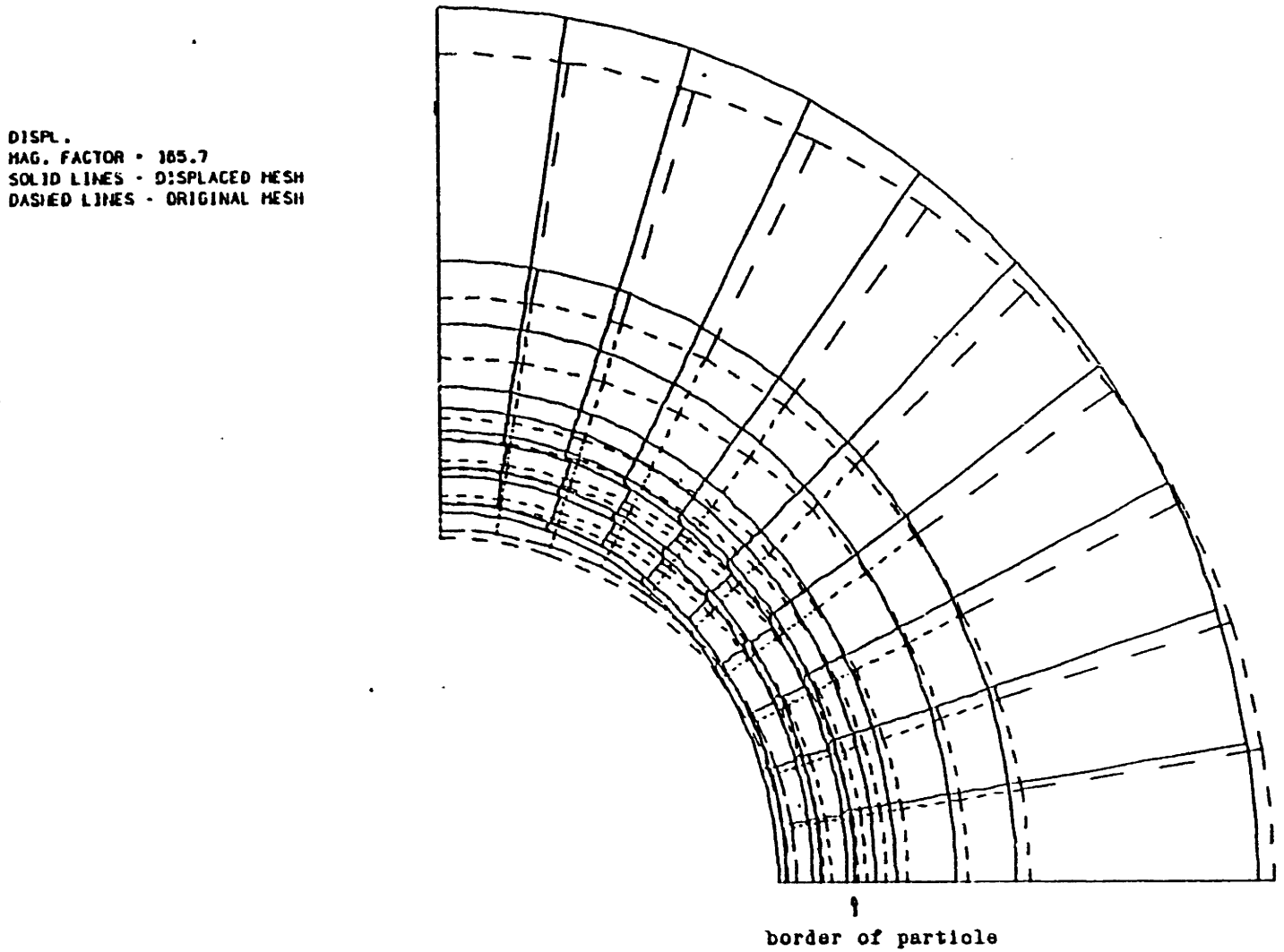

FIGURE 30b. Displacement of the CS PB/PS particle (outer portion) and immediately surrounding matrix when subjected to uniform tension at infinity.

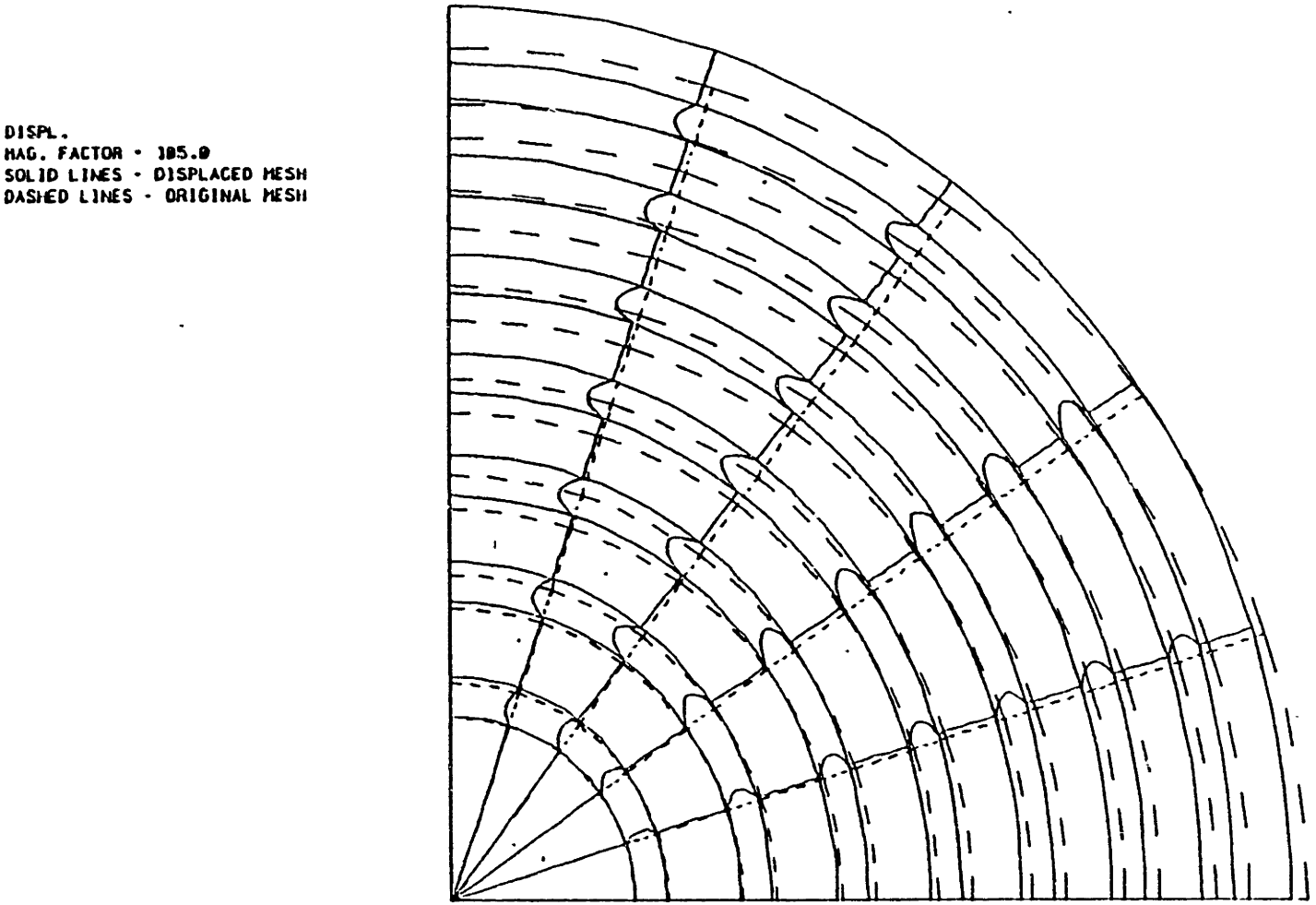

FIGURE 31a. Displacement of the CS LMWPB/PS particle (inner 75%) in a PS matrix subjected to uniform tension at infinity.

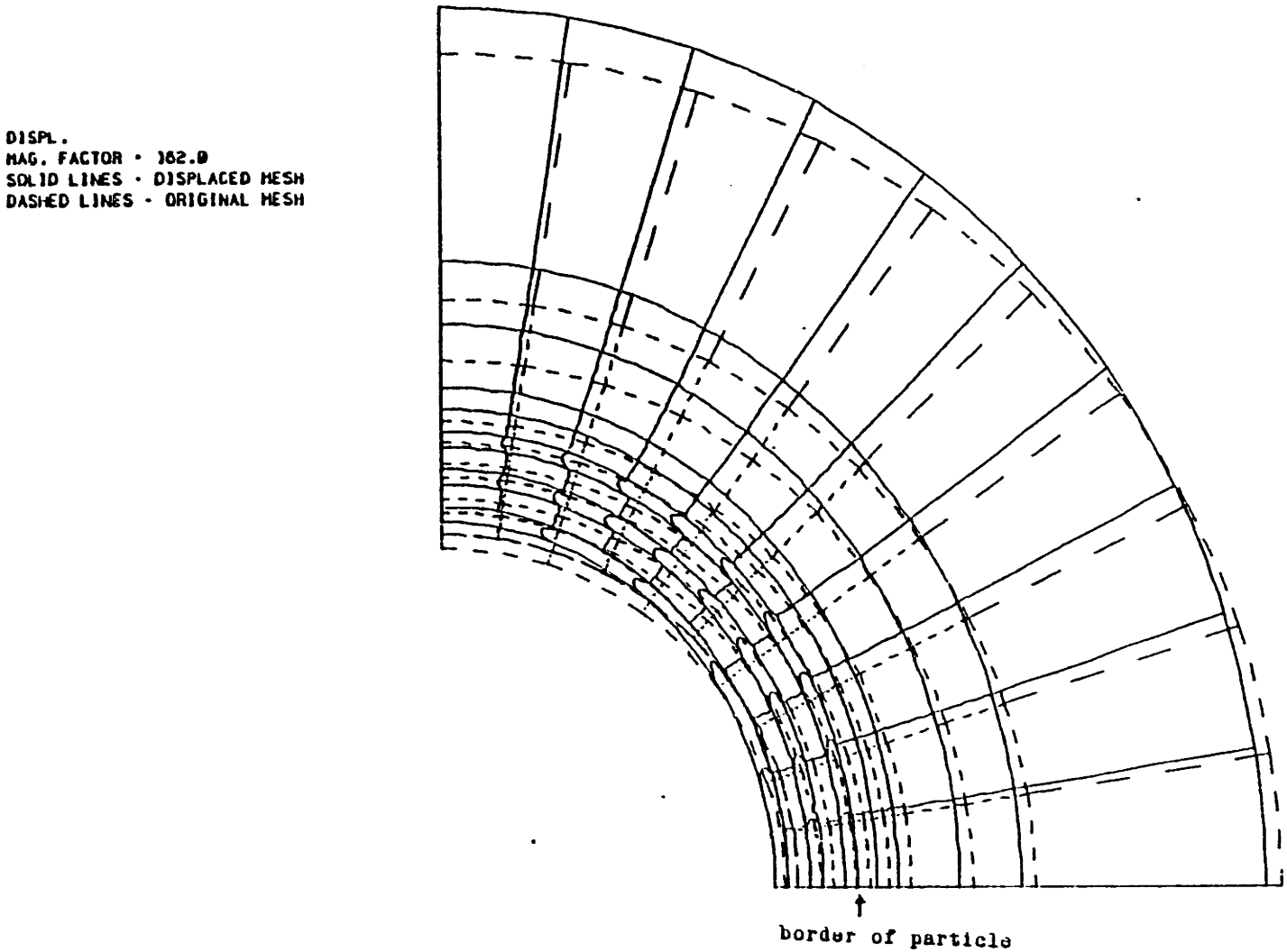

FIGURE 31b. Displacement of the CS LMWPB/PS particle (outer portion) and immediately surrounding matrix when subjected to uniform tension at infinity.

TABLE 3.

EQUATORIAL STRESS STATE DUE TO APPLIED TENSION

PARTICLE	PB	Homogenized	CS PB/PS	CS LMWPB/PS
Flow Stress (MPa)	10.	30.	10.	10.
Concentration Factor, k	1.88	1.16	1.69	1.76
Equatorial Stresses (MPa):				
σ_r	2.86	1.50	0.39	1.30
σ_θ	18.8	34.8	16.9	17.6
σ_ϕ	0.40	0.24	0.54	0.46
σ_e	17.3	33.9	16.4	16.7
σ	7.35	12.2	5.94	6.45

It is also of interest to observe the stress state at the polar interfaces. Here, the behavior of the concentric shell particles differ from the isotropic particles. At the poles of the concentric shell particles there exists a deviatoric stress concentration almost as high as that at the equator. This does not occur at the isotropic particle poles. The stress state at the polar interface for each of the particles is shown in Table 4. The equator, however, remains the optimal craze nucleation site because the tensile stress induces a negative pressure at the equator and a positive pressure at the poles.

In order to ascertain that another site between the equator and the pole is not a better craze nucleation site than the equator, it is necessary to examine the stress field surrounding each particle. Figures 32-39 show the contour lines of the negative pressure and the deviatoric stress for each particle. One can easily pick out the regions where the stress is concentrated. Since the stress state due to the thermal mismatch and subsequent relaxation is spherically symmetric, it is at these regions of stress concentration due to mechanical mismatch that crazes are most likely to initiate. Therefore, the contour maps are useful to quickly select those regions around the particle to be examined in the Initiation Criterion -- the equator and possibly the pole.

4.3.2. Finite Matrix

Accounting for the effect of a finite matrix increases the magnitude of each component of stress. Broutman and Panizza determined the effect of Rubber Particle Volume Percent on interfacial stresses. Their

TABLE 4.

POLAR STRESS STATE DUE TO APPLIED TENSION

PARTICLE	PB	Homogenized	CS PB/PS	CS LMWPB/PS
Flow Stress (MPa)	10.	30.	10.	10.
Polar Stresses (MPa)				
σ_r	2.48	25.7	7.83	6.37
σ_θ	-8.35	-4.50	-6.28	-7.92
σ_ϕ	-8.35	-4.50	-6.28	-7.92
σ_e	10.8	30.2	14.1	14.3
σ	-4.74	5.56	-1.58	-3.16

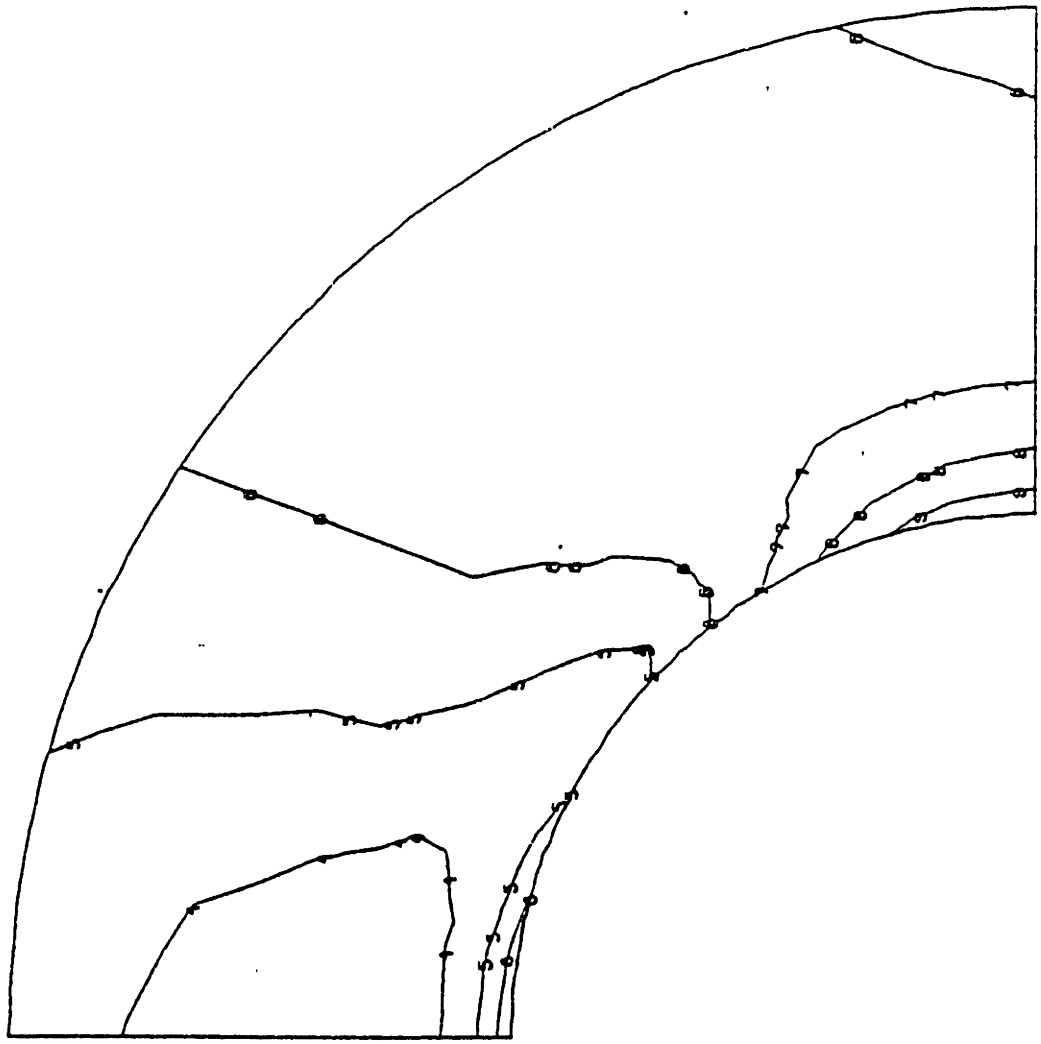

FIGURE 32. Mises equivalent stress contour in the PS matrix surrounding the PB particle in an infinite matrix subject to a tensile stress at infinity, in units of the applied tensile stress.

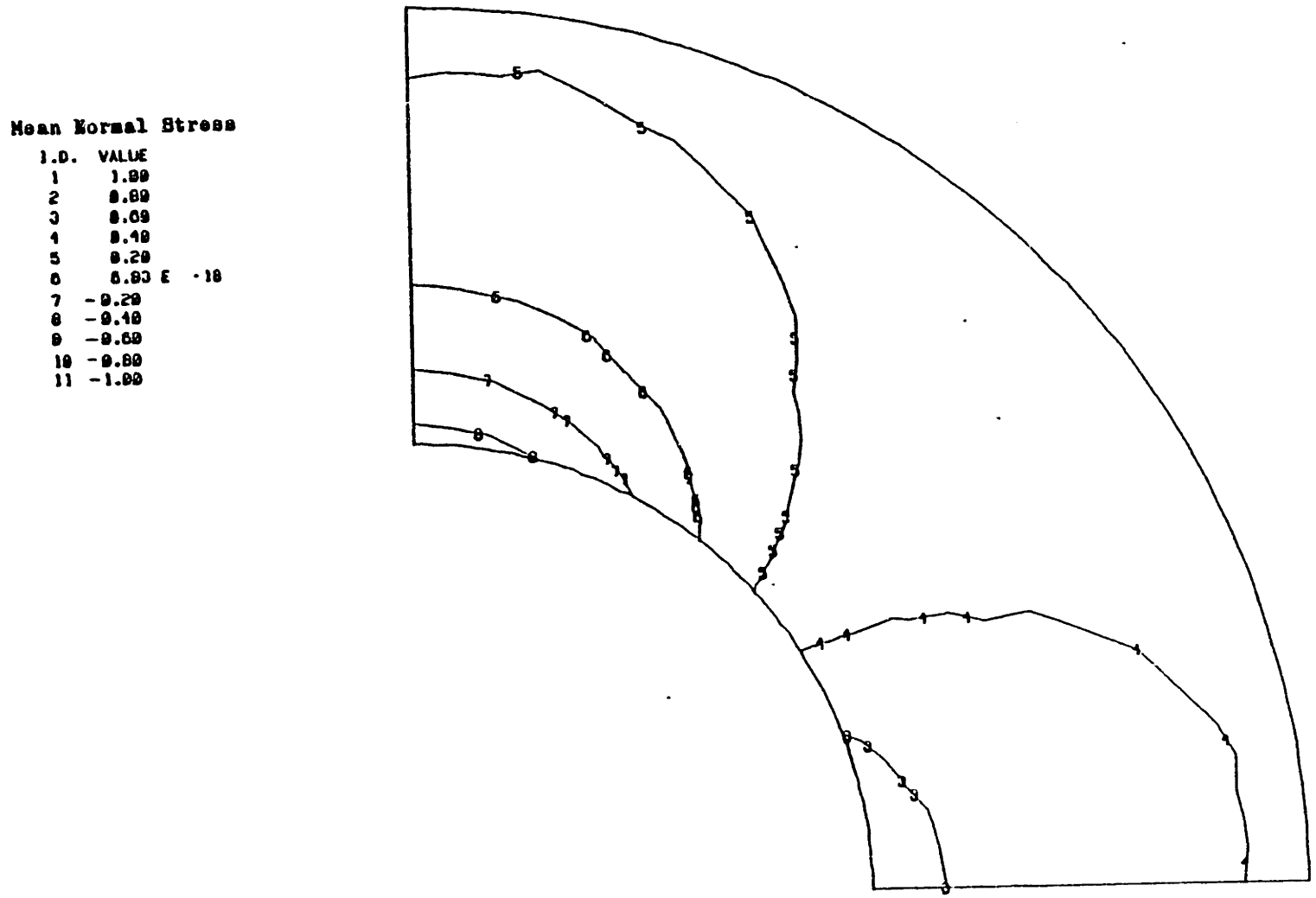

FIGURE 33. Mean normal stress contour in the PS matrix surrounding the PB particle in an infinite matrix subject to a tensile stress at infinity, in units of the applied tensile stress.

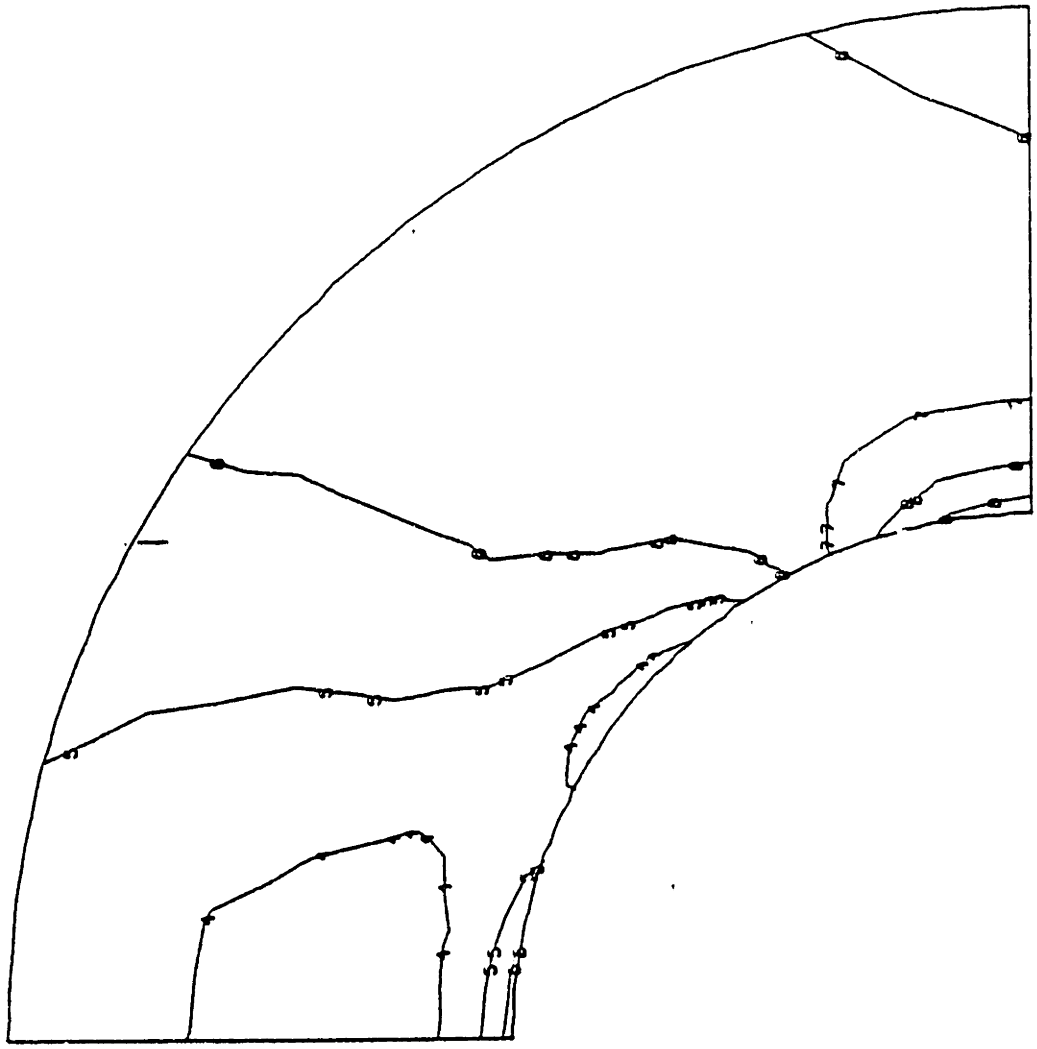

FIGURE 34. Mises equivalent stress contour in the PS matrix surrounding the Homogenized particle in an infinite matrix subject to a tensile stress at infinity, in units of the applied tensile stress.

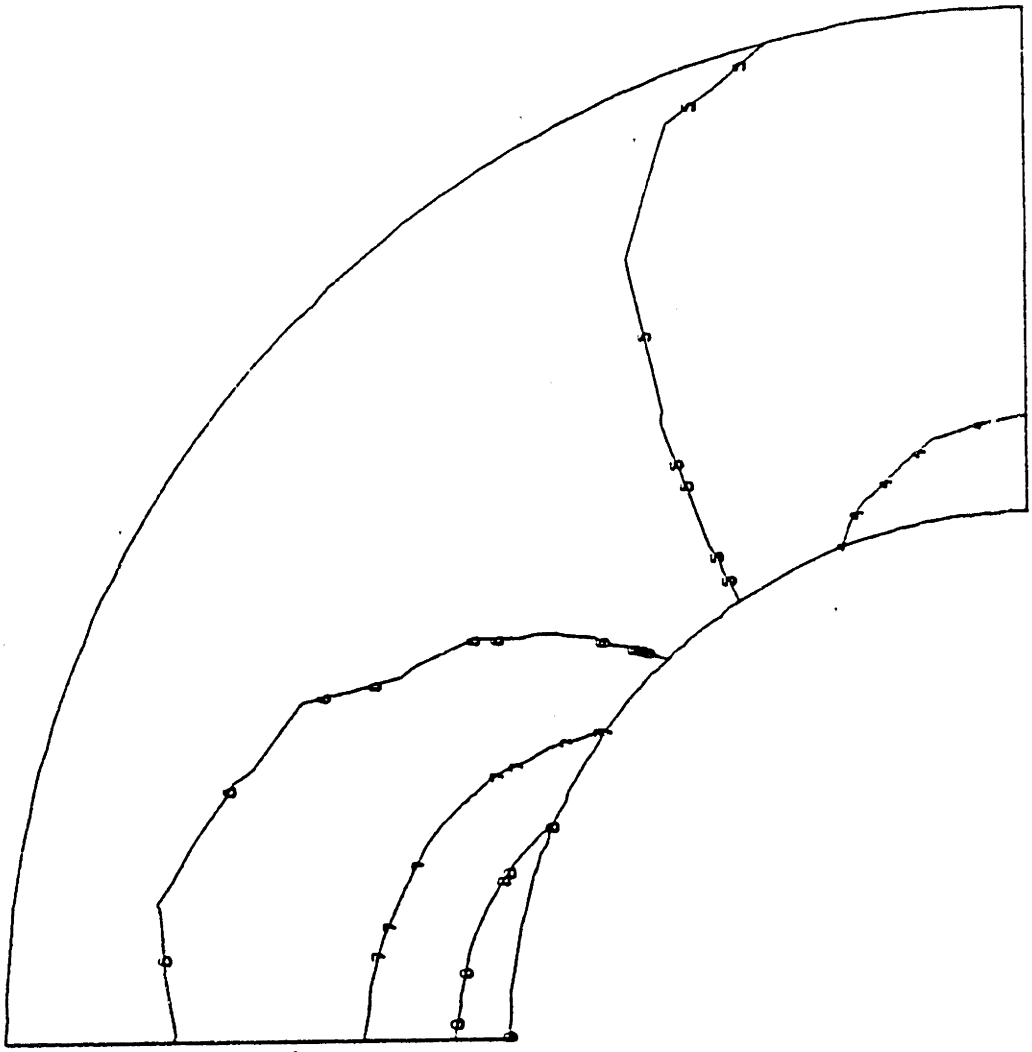

FIGURE 35. Mean normal stress contour in the PS matrix surrounding the Homogenized particle in an infinite matrix subject to a tensile stress at infinity, in units of the applied tensile stress.

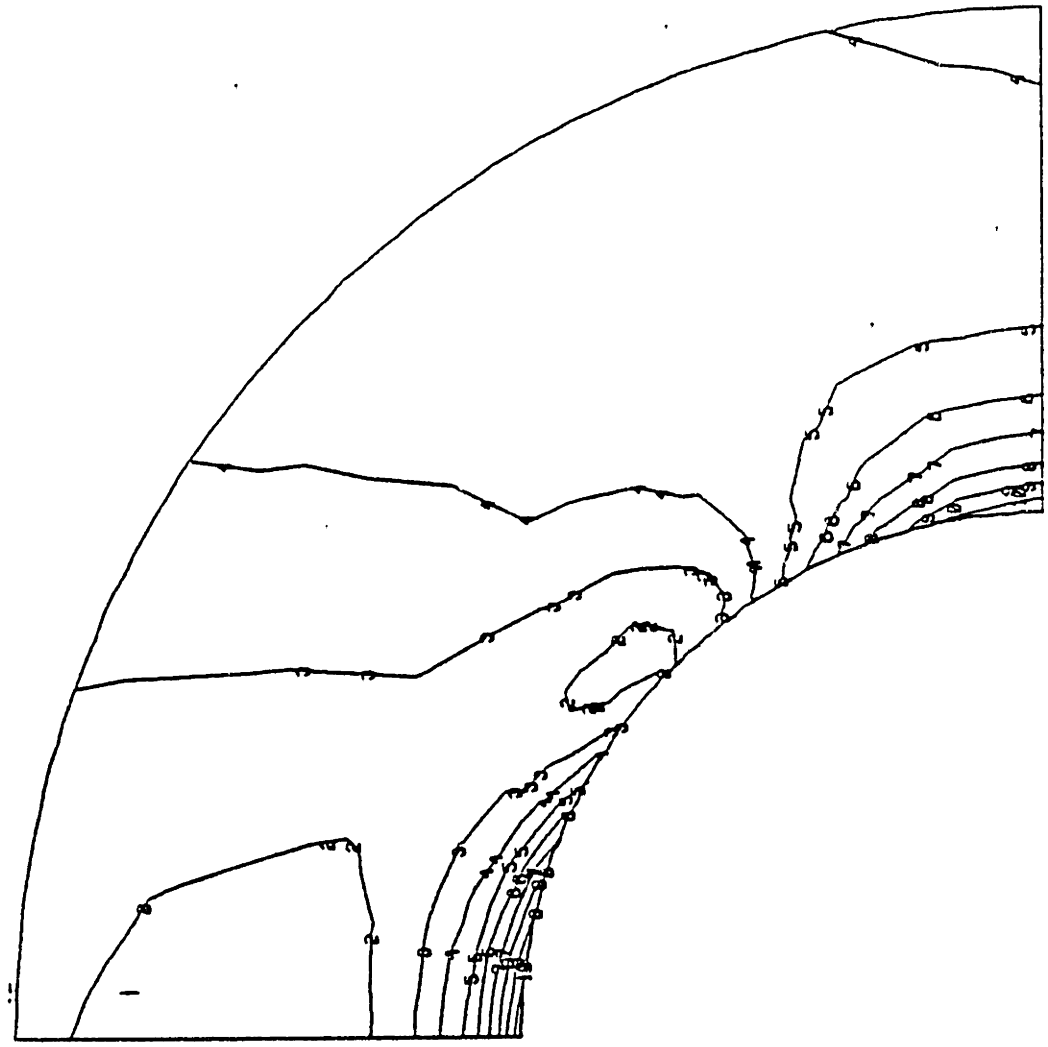

FIGURE 36. Mises equivalent stress contour in the PS matrix surrounding the CS PB/PS particle in an infinite matrix subject to a tensile stress at infinity, in units of the applied tensile stress.

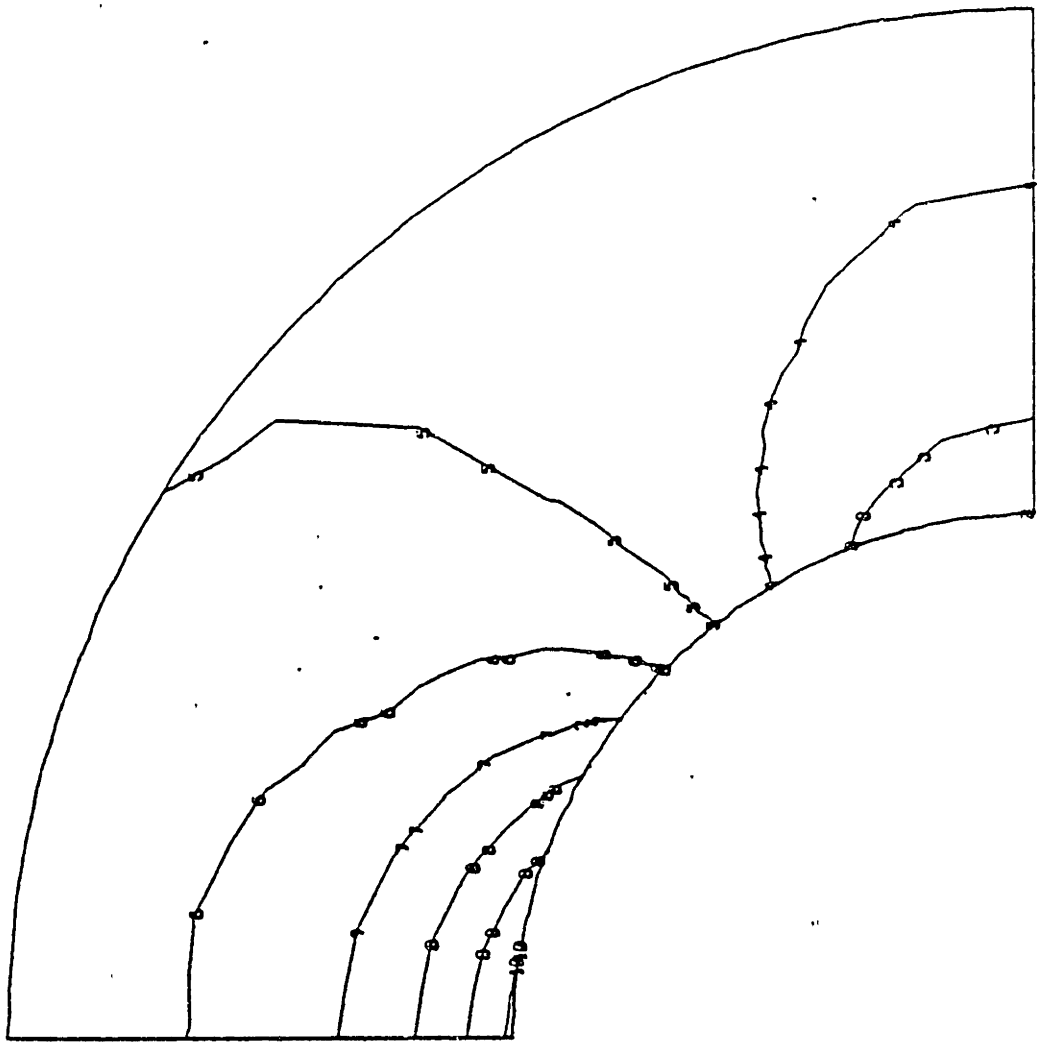

FIGURE 37. Mean normal stress contour in the PS matrix surrounding the CS PB/PS particle in an infinite matrix subject to a tensile stress at infinity, in units of the applied tensile stress.

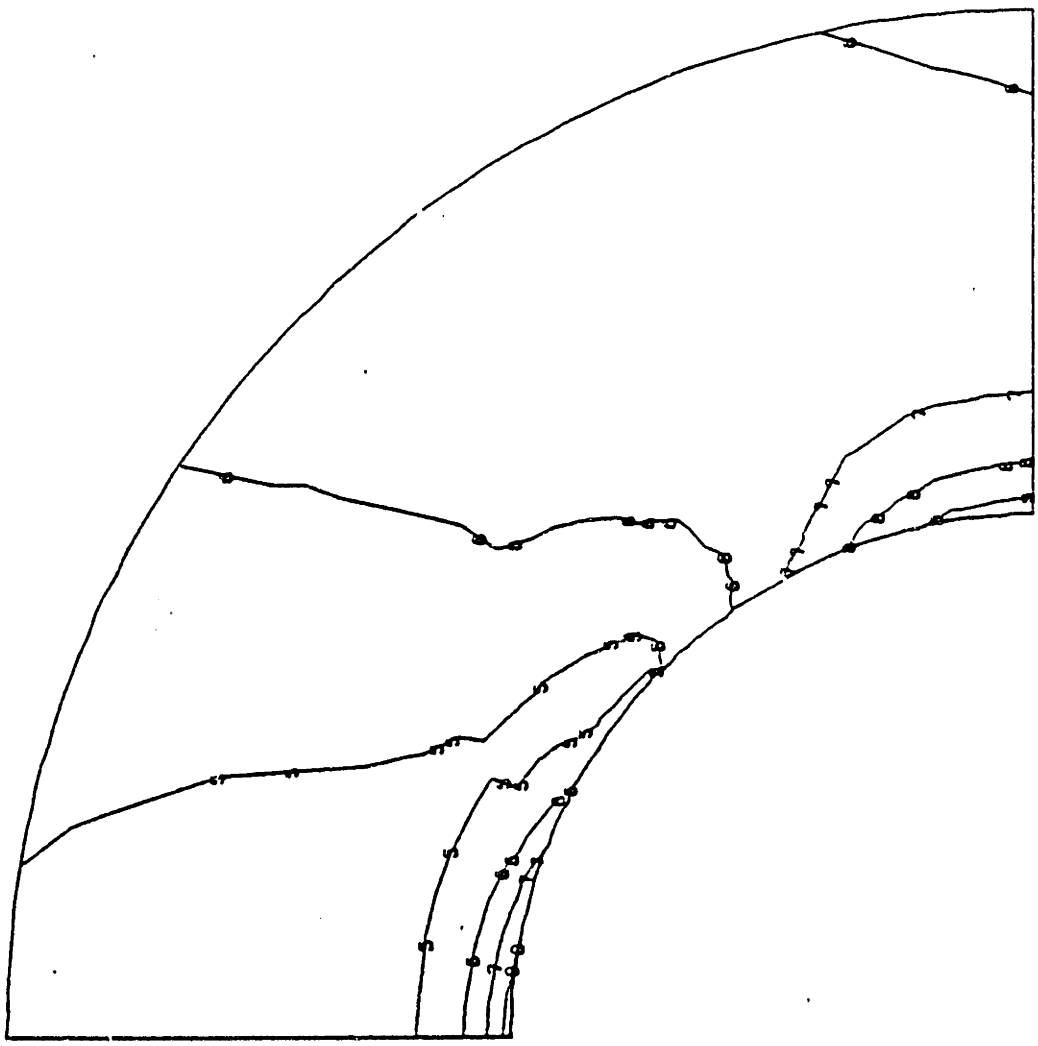

FIGURE 38. Mises equivalent stress contour in the PS matrix surrounding the CS LMWPB/PS particle in an infinite matrix subject to a tensile stress at infinity, in units of the applied tensile stress.

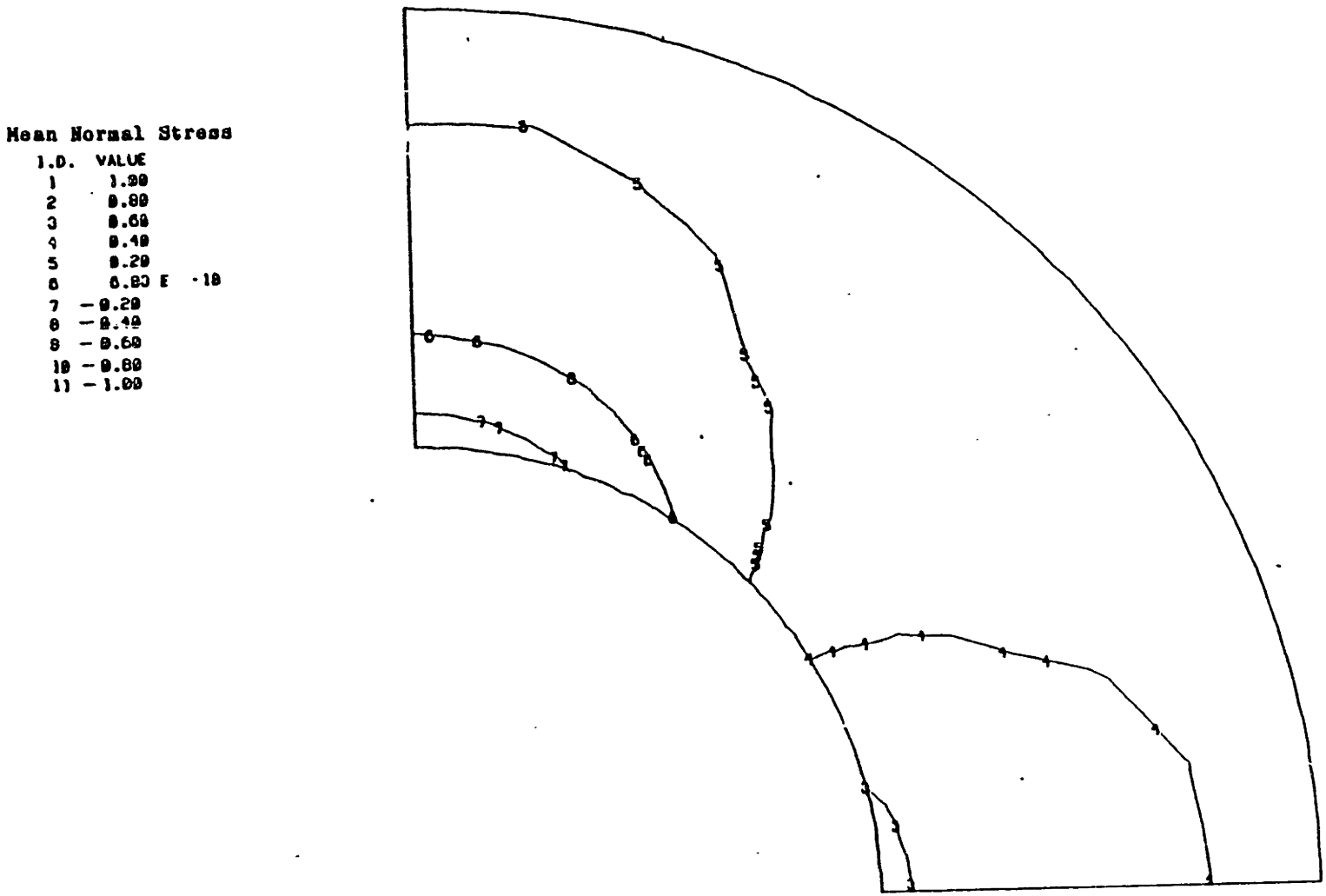

FIGURE 39. Mean normal stress contour in the PS matrix surrounding the CS LMWPB/PS particle in an infinite matrix subject to a tensile stress at infinity, in units of the applied tensile stress.

results for the equatorial and polar interfaces are shown in Figure 40. Analyses for a concentration of c=0.21 of PB particles and c=0.21 of CS LMWPB/PS particles was conducted as described in Section 4.4. These results are listed in Table 5. The results agree with the trend shown in the Broutman and Panizza curves. One can see there is a slight increase in magnitude of the stress states except for the PB polar tangential stresses which remain the same. The concentration effects on Applied Tension will not dramatically alter the complete stress history analysis unless concentrations greater than 0.30 are considered as shown on the Broutman and Panizza curves.

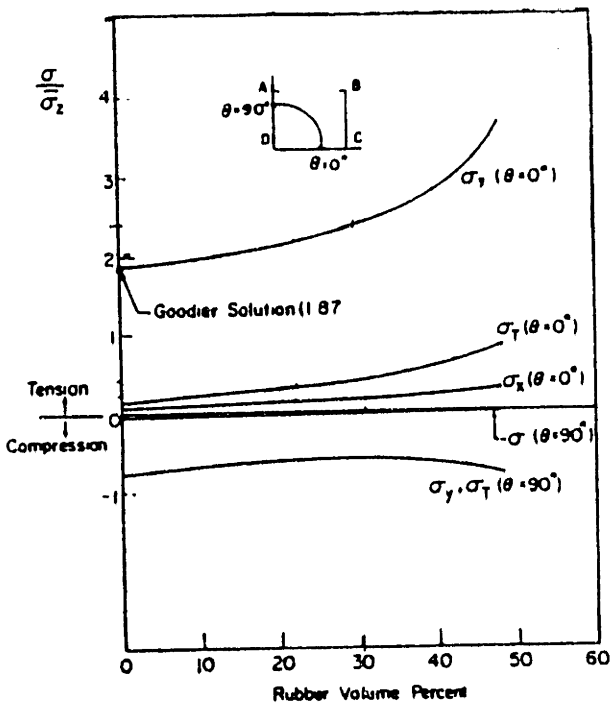

FIGURE 40. Broutman and Panizza Results: Particle Volume Percent Effect on Equatorial and Polar Interfacial Stresses.

TABLE 5.

FINITE MATRIX (c=0.21) EFFECTS ON STRESS CONCENTRATIONS

PARTICLE:	PB	CS LMWPB/PS
Flow Stress (MPa)	10.	10.
Equatorial Stresses:		
σ_r (MPa)	3.24	1.58
σ_θ (MPa)	20.3	18.8
σ_ϕ (MPa)	1.16	1.0
σ_e (MPa)	18.2	17.5
σ (MPa)	8.23	7.13
Polar Stresses:		
σ_r (MPa)	2.82	6.64
σ_θ (MPa)	-8.33	-8.13
σ_ϕ (MPa)	-8.33	-8.13
σ_e (MPa)	11.2	14.8
σ (MPa)	-4.61	-3.21

49 29

5. INITIATION OF CRAZES

5.1. Theory

The application of a tensile stress is the final step in a typical stress history. Now, it must be determined whether this stress history and final stress state will initiate a craze. As mentioned in the Introduction, the Argon-Hannoosh criterion will be used to determine craze initiation. This criterion is ideal for a stress history as it provides a sequential process which can follow a stress state that varies with time; whereas, the other criteria mentioned can only be applied to a stress state at any given instant in time. Before expanding on what exactly is meant by this, the Argon-Hannoosh theory on the mechanism resulting in craze initiation will be briefly reviewed.

As explained in the Introduction, the A-H criterion proposes that craze initiation is a two stage process: stage one involves pore formation on the scale of molecular aggregates; while stage two involves the plastic expansion of these pores. Argon (1975) suggested that the formation of pores is due to an arrested localized micro-shear process as depicted in Figure 41. The total free energy ΔG_{pore} required to form a micro-shear nucleus under a shear stress s that produces a flat microcrack and the energy required to make this flat microcrack a stable, round micro-cavity is:

$$\Delta G_{pore} = (0.15)^2 \pi (\mu/s)(\mu\phi^3) + \alpha L^3 \gamma \quad . \quad (5\text{-}1)$$

In this expression; μ is the shear modulus; s is the

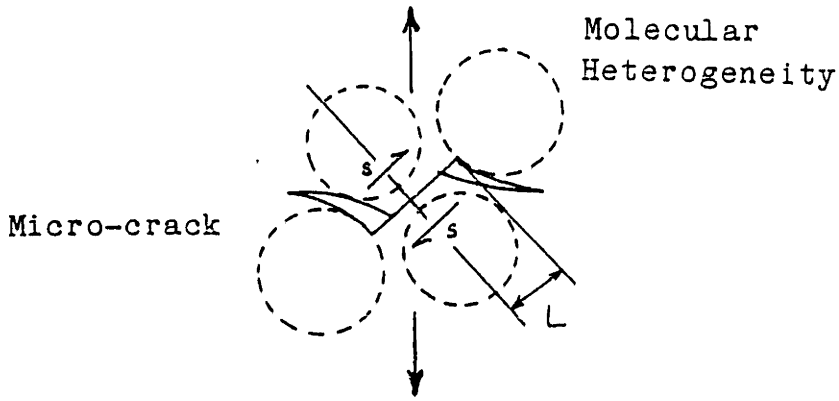

Figure 41. Formation of micro-shear nucleus under deviatoric shear stress, s.

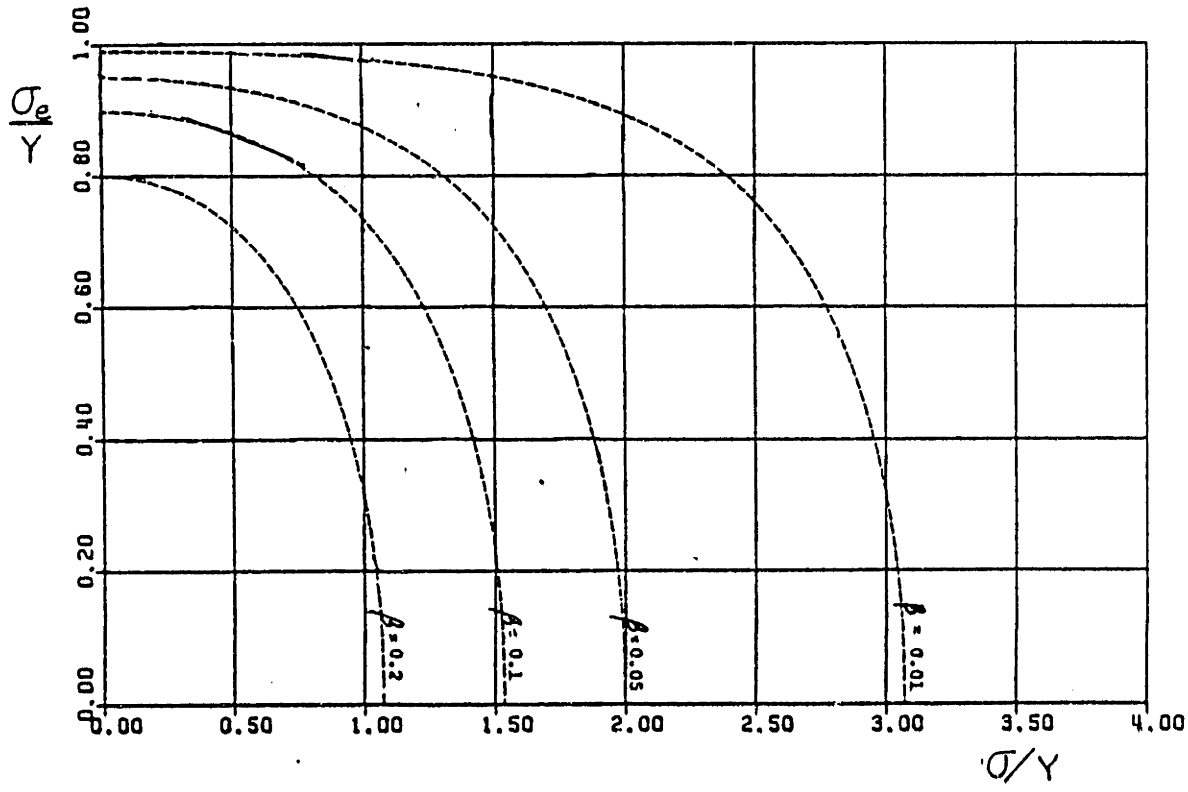

Figure 42. Locus of pore expansion under a combination of negative pressure, σ, and equivalent stress, σ_e; after McClintock and Stowers (1970).

deviatoric shear stress ($=(1/\sqrt{3})\sigma_e$, where σ_e is the equivalent tensile stress); ϕ is the relative displacement across the sheared region; α is a factor of order 0.10; L is a micro-shear patch length governed by the spacing of molecular heterogeneities; and Y is the tensile yield strength of the polymer. It can be assumed that the porosity develops with time according to a simple integral over time of the current stress dependent pore initiation rate which leads to the relation for porosity β:

$$\beta = \dot{\beta}_0 \int_0^t \exp\left[-\Delta G_{pore}(\sigma_e)/KT\right] dt \qquad (5\text{-}2)$$

where $\dot{\beta}_0$ is a characteristic frequency factor of the region, and where σ_e can in general be slowly varying in time.

It is now necessary to determine the stress required to expand the pores into craze nuclei. A plasticity analysis shows that the negative pressure σ required to plastically expand a porous region in which the surroundings of each pore are conceived as a thick wall sphere, is $\sigma = (2Y/3)\ \ln(\ 1/\beta\ )$. If the region is subjected in addition to a distant deviatoric stress σ_e along with the negative pressure σ, the negative pressure required to plastically expand the pores is reduced by a factor of Q:

$$\sigma = (2Y/3)\ \ln(\ 1/\beta\ )\ (\ Q(\sigma_e/Y, \beta)\ ). \qquad (5\text{-}3)$$

The reduction factor Q is dependent on the porosity level and the average deviatoric stress in the region. McClintock and Stowers (1970) and Gurson (1977) have given

loci for the generalized yield of porous plastic media, subjected to a combination of distant deviatoric shear τ_e and negative pressure σ for different porosity levels (see e.g., Figure 42). These loci determine the factor Q. The craze initiation criterion is now complete. To summarize, pore formation in stage 1 is characterized by the expression:

$$\beta = \dot{\beta}_0 \int_0^t \exp\left[-\Delta G(\sigma_e)/\kappa T\right] dt \quad ; \quad \sigma_e = \sigma_e(t) ;$$

giving the time dependent increase of micro-porosity under deviatoric shear stress σ_e. Pore expansion in stage 2 occurs when the local porosity reaches a level that satisfies the generalized "yield" condition for the porous solid under the local negative pressure and deviatoric stress σ_e, i.e.:

$$\sigma = (2Y/3) \ln (1/\beta) \; (\; Q(\sigma_e/Y) \;).$$

5.2. Application of the Craze Initiation Criterion to Specific Stress Histories

Applying the A-H criterion to the given stress history is straight-forward. The development of micro-porosity begins with the initial thermal mismatch and continues as these stresses relax up to and including the final application of a tensile stress. Since the stress is updated at particular instants in time with a numerical scheme and since the porosity rate is governed by the current deviatoric stress, the porosity level must then be obtained by numerical integration as a function of time. In other words, at any time, t, for a program of updating the local equivalent stress,

$$^{t+\Delta t}\sigma_e = {}^{t}\sigma_e + {}^{t}\dot{\sigma}_e \Delta t \,, \qquad (5\text{-}5a)$$

the current pore development rate,

$$^{t}\dot{\beta} = \dot{\beta}_0 \exp\left[-\Delta G_{pore}(\sigma_e)/KT\right] \;;\; {}^{o}\beta = 0 \,, \qquad (5\text{-}5b)$$

gives current levels of micro-porosity,

$$^{t+\Delta t}\beta = {}^{t}\beta + {}^{t}\dot{\beta}\,\Delta t \qquad . \qquad (5\text{-}5c)$$

If it is assumed that initiation of crazes occurs finally within say 100 seconds of application of the final tensile stress, it is only necessary to use the above scheme for evolution of porosity during the relaxation of residual stresses where such relaxation is substantial. This is because the applied tension is constant and the relaxation of the residual stresses is only significant over much longer spans of time than 100 seconds. Therefore, stress relaxation need not be considered for this final time step. This is not true in the case of the PB particle, however, where the matrix will craze immediately after application of tension. Since the stress will be considered constant after tension is applied, the porosity rate will also be constant $\dot{\beta}_{AT}$ (AT=After Tension) over this final step, and the additional porosity from this time increment will simply be

$$\Delta\beta_{AT} = \dot{\beta}_{AT}\,\Delta t \qquad . \qquad (5\text{-}6)$$

To summarize, the formation of a porosity level:

1. During relaxation of residual stresses, before tension (BT)

$$\beta_{BT} = \int_0^{t_T} \dot{\beta}_0 \exp\left[-\Delta G(\sigma_e)/\kappa T \right] dt$$

where the integral is determined with the updating scheme to account for relaxing and t_T = time at which tension is applied.

2. After Tension (AT)

$$\Delta\beta_{AT} = \dot{\beta}_{AT}\, \Delta t$$

where $\Delta t = t_{cI} - t_T$; t_{cI} = estimated time at which crazes are expected to initiate.

The total porosity is therefore

$$\beta = \beta_{BT} + \Delta\beta_{AT} \quad . \tag{5-7}$$

To determine if crazes will now form, equation (5-3) for plastic pore expansion is used. Basically, this equation answers the question: Given a certain porosity from (5-7) and a certain final stress state with a deviatoric component of σ_e, and a negative pressure component of σ, is this stress state large enough to plastically expand the pores? For this evaluation, Q is obtained from known loci for σ, for given β and σ_e. If equation (5-3) is not satisfied, it indicates that the level of micro-porosity is insufficient to initiate a craze by plastic cavity expansion under the given combination of β and σ_e. To determine at what time crazes will initiate, one can modify t_{cI} (assuming t_T is a known time) which in turn will modify β which in turn will modify Q, etc. One then checks to see if (5-3) is satisfied, if not the iteration can continue until the time at which a craze is initiated, if indeed such is the case.

5.3. Results

The method outlined in Section 5.2 was used to determine whether craze initiation occurs for the four particles of interest. The porosity level and the total stress state existing at the assumed time of craze initiation were determined for each particle. Whether or not crazes subsequently initiate was determined by using this information in the equation for plastic pore expansion (5-3).

The porosity levels in the matrix at the equatorial particle border are listed in Table 6. The porosity before tension is applied, β_{gr}, was calculated during the relaxation of the thermal residual stresses(see Appendix 3). A time span of approximately 8 days($7(10^5)$ seconds) is allowed for the porosity development for the three real particles: CS PB/PS, CS LMWPB/PS, and Homogenized. This is a realistic time span for a laboratory experiment, because it is not unusual for a typical sample to be "on the shelf" for several days before being used. The stresses in the material containing the idealized PB particle relaxed at a very high rate. The porosity level before tension in this particle was taken at just $4.6(10^4)$ seconds because only a negligible amount of porosity will develop after this time span. After tension is applied, crazes generally appear within 100 seconds and, thus, a time of 100 seconds was allowed for porosity development after tension. These two levels were summed to give the total porosity at the time of craze initiation.

As Table 6 shows, very little porosity is developed in the materials with the real particles. Of these three particles, the CS LMWPB/PS particle has developed a

TABLE 6.
POROSITY LEVEL IN MATRIX
AT EQUATORIAL PARTICLE/MATRIX INTERFACE

PARTICLE	PB	HOMOGENIZED	CS PB/PS	CS LMWPB/PS
TIME(SEC)	$4.6(10^{4})$	$7.0(10^{5})$	$7.0(10^{5})$	$7.0(10^{5})$
β (BT)	$2.0(10^{-1})$	0.0	$6.8(10^{-23})$	$1.7(10^{-11})$
TIME(SEC)	$1(10^{2})$	$1(10^{2})$	$1(10^{2})$	$1(10^{2})$
$\Delta\beta$ (AT)	$1.9(10^{-11})$	$4.3(10^{-8})$	$3.6(10^{-25})$	$2.1(10^{-21})$
β (TOTAL)	$2.0(10^{-1})$	$4.3(10^{-8})$	$6.8(10^{-23})$	$1.7(10^{-11})$

porosity level several orders of magnitude larger than the other particles during the period of thermal stress relaxation. However, the Homogenized particle exceeds this level once tension is applied because its far-field tensile stress is 30 MPa versus 10 MPa for the other particles. The idealized PB particle develops a porosity level far in excess of the three real particles because of its much greater thermal mismatch. Unfortunately, the porosity levels computed for the three real particls are far too low to aid in the initiation of crazes indicating that the stress relaxation history is not crucial in early pore development but only in governing the final level of stress. This will be discussed further below.

The complete stress state in the matrix at the equatorial border at the assumed time of craze initiation is shown in Table 7. These stresses are determined by taking the thermal residual stresses remaining after the allotted relaxation period and superposing them with those stresses that occur once tension is applied. The negative pressure, σ, for the particles ranges from 7 MPa to 13 MPa. However, the deviatoric stress varies greatly amongst the particles ranging from 15 MPa for the CS PB/PS particle to 41 MPa for the idealized PB particle. Since the porosity rate is exponentially dependent upon the deviatoric stress as shown in equation (5-2), this value is extremely important in the craze initiation process. The results for $\Delta\beta_{AT}$ in Table 6 show that the deviatoric stress, σ_e, from Table 7 was not high enough for the three real particles to result in any substantial porosity development as stated above.

In order to determine whether or not the craze initiation criterion is satisfied, the factor, Q, giving the reduction of the required negative pressure, must be

TABLE 7.

COMPLETE EQUATORIAL STRESS STATE
IN MATRIX AT PARTICLE/MATRIX INTERFACE

PARTICLE	PB	HOMOGENIZED	CS PB/PS	CS LMWPB/PS
σ_r(MPa)	32.0	9.26	9.81	15.1
σ_θ(MPa)	21.7	31.3	13.3	15.8
σ_ϕ(MPa)	3.29	-3.28	-3.09	-1.36
σ_e(MPa)	25.2	30.3	14.9	16.8
σ (MPA)	19.0	12.4	6.66	9.84

determined. Subsequently, knowing Q, , and for each particle, equation (5-3) is used to determine craze initiation. Since Q is a function of the equivalent stress, σ_e, and the porosity, β, as shown in Figure 42, Q was found to be 1.00 for the three real particles and 0.68 for the idealized PB particle. This is because of the combination of a very low porosity level and a small deviatoric stress for the real particles and corresponding higher values for the PB particle. Given the values for Q, σ, and β, the craze initiation criterion is not quantitatively satisfied for any of these particles as shown in Table 8. In other words, theoretically, the materials containing these particles will not craze under the given stress histories according to this model unless another source of stress is found or a physical condition is discovered to aid nucleation. These theoretical results, although apparently thorough, do not agree quantitatively with the experiments of Gebizlioglu, et. al. (1983) on such materials. Gebizlioglu has tested the three real materials and found them to craze, each to a different extent. This will be discussed in the next section.

TABLE 8.

CRAZE INITIATION CRITERION APPLICATION RESULTS

PARTICLE	Q	$Q(2Y/3)\ln(1/\beta)$ (MPa)	σ (MPA)	CRAZE INITIATION?
PB	0.80	60.	11.6	NO, $11.6 < 60.$
HOMOGENIZED	1.00	792.	12.4	NO, $12.4 < 792.$
CS PB/PS	1.00	2382.	6.66	NO, $6.66 < 2382.$
CS LMWPB/PS	1.00	1157.	9.84	NO, $9.84 < 1157.$

6. Discussion

The complete stress history of a heterogeneous "rubber" particle in a homogeneous PS matrix and its effect on the initiation of crazes in that matrix has been discussed. The importance of both the elastic and the thermal misfits have been examined and quantitatively determined for the four particles of interest -- the idealized PB particle, the Homogenized particle, the CS PB/PS particle, and the CS LMWPB/PS particle. The role of the elastic misfit between an isotropic particle and an isotropic matrix has long been recognized (Goodier, 1933). Here, this analysis has been extended to a composite particle in an isotropic matrix with the aid of finite elements. The importance of the thermal mismatch between rubber particles and polymer matrices has not been quantitatively determined before, although there does exist some diffuse awareness of its role among some manufacturers of high impact polymers and is even briefly mentioned in Bucknall's book (1). Comparing the results of Section 2 and Section 4, one can see that the magnitudes of the thermal residual stresses at room temperature (Table 2) are in the same range as the magnitudes of the tensile induced stresses(Table 3). Even though the thermal residual stresses surrounding a particle in an infinite matrix do not produce a negative pressure, they do produce a substantial deviatoric stress. As was discussed in Section 5, it is this deviatoric component which is essential to the development of microporosity. Therefore, the thermal residual stresses play a vital role in the process of craze initiation and cannot be neglected in a thorough analysis.

Although the theoretical analysis does not predict the initiation of crazes which is observed in experiments,

it does predict the correct trend for the three particles. Gebizlioglu observes crazing in materials with the Homogenized particle at a tensile stress of 30 MPa and in the CS LMWPB/PS particle at a tensile stress of 10 MPa. The theoretical analysis showed zero porosity development for the Homogenized particle and a small amount of porosity development for the CS LMWPB/PS particle during thermal residual stress relaxation. However, after tension is applied, the magnitude of the applied stress on the material containing the Homogenized particle is large enough for its total porosity level to match that of the CS LMWPB/PS. The tensile stress applied to the CS LMWPB/PS material is small enough to add a negligible amount of porosity as compared to the porosity developed during relaxation. The application of a tensile stress also creates a negative pressure at the equator of the order of 10 MPa for both particles. Therefore, these two materials are at approximately the same stage when crazing is observed (even though according to theoretical analysis crazing does not occur). The CS PB/PS particle does not craze as readily under the 10 MPa tensile load. Our theoretical results also match this trend because the total porosity formed is several orders of magnitude below that of the CS LMWPB/PS and the negative pressure is also lower. Therefore, even though the theoretical predictions do not correspond exactly with the experiments, they do follow the correct trend.

There exist several factors which may account for the discrepancy between the theoretical and experimental results, a few of which we have been able to discard. The possibility of any inadequacy in the Argon-Hannoosh Craze Initiation Criterion can be ruled out as they have demonstrated that this criterion accurately accounts for craze nucleation in PS material possessing a controlled

surface roughness as well as PS pellets which were free of stress concentrations (1977). This criterion has also been independently verified by Kawagoe and Kitagawa to predict both air and environmental crazing (1981). The possibility of thermal anisotropy within the shells of the concentric sphere particles was considered and found to have little effect on the stress state in the matrix. Mechanical anisotropy within the particles may also exist, however this should not be able to raise the stress state and/or porosity to the level necessary for craze initiation. The presence of additional stresses has also been considered. There may exist an osmotic pressure in the CS LMWPB/PS particle due to the movement of the low molecular weight PB through the skeletal high molecular weight PB. However, this stress is thought to be self-equilibrated. The strongest possibility which may account for the discrepancy is the hypothesis that craze nucleation in these materials is not a homogeneous process but, indeed, a heterogeneous process. It may be heterogeneous in the sense that a catalyst exists in the form of a perturbation in the interface between the particle and the matrix, or there may even exist a new phase in this region. In a parallel problem, the craze growth has been demonstrated by Argon and Salama (1977) to be one of heterogeneously convoluting the polymer-air interface and not by homogeneously nucleating cavities ahead of the craze tip. This hypothesis that an interface containing perturbations may reduce the high stress and porosity levels required to initiate crazes could account for the discrepancy between the theoretical and experimental results for the material containing the CS LMWPB/PS particle. It would not account for the Homogenized particle because its interface with the matrix is very well-defined. To verify this theory, a much more detailed analysis of the nature and behavior of the

PB-PS interface will have to be conducted. Such very detailed information on the nature of block copolymer interfaces is only now developing.

In the material containing the Homogenized particle, crazes are not seen to originate from the particles themselves, but from the surface. Therefore, the discrepancy between theoretical and experimental results may be due to the neglect of tensile stress concentrations due to surface roughness which may be higher than those around the particle. This is feasible because the tensile stress concentration factor for this particle was only 1.16, and, also, the stress concentration due to the thermal mismatch between the particle and the matrix does not lend itself to porosity development.

Although the theoretical model did not match the experimental results and predict the initiation of crazes, it did predict the correct trend among the three particles. The critical steps in the stress history of the materials have been identified and quantitatively examined. These include the development of thermal residual stresses, the non-linear relaxation of these stresses, and the application of a tensile stress. The effect of the development of a local micro-porosity during the stress relaxation stage and subsequent tensile stress stage has also been examined. These results indicated a shared role between the thermal residual stresses and the tensile stresses in setting up a stress concentration around the particles. It has been suggested that the discrepancy between the experimental and the theoretical results may be due to a perturbated interface between the matrix and the particle which would make the craze initiation process a heterogeneous process rather than a homogeneous one as I have treated it. These perturbations may reduce the stress

and porosity levels found necessary for the initiation of crazes. An analysis of the nature and the behavior of the particle/matrix interface could determine if this is true and is suggested for future research. The behavior of the low molecular weight PB within the high molecular weight PB skeleton while under loading is also suggested for future research. These ideas, when investigated, may further determine the role of "rubber" particles in polymers in the initiation of crazes.

APPENDICES

1. COMPUTATION OF HOMOGENIZED MATERIAL PROPERTIES

2. RELAXATION OF THERMAL RESIDUAL STRESSES DUE TO CREEP OF POLYSTYRENE MATRIX

3. COMPUTATION OF STRESS RELAXATION AND POROSITY DEVELOPMENT

4. STRESS FIELD SURROUNDING A SPHERICAL PARTICLE DUE TO A UNIFORM TENSILE STRESS AT INFINITY

5. FINITE ELEMENT ANALYSIS

APPENDIX 1

COMPUTATION OF HOMOGENIZED MATERIAL PROPERTIES

Chow(1978) has generalized the work of Eshelby to include the effect of surrounding particles on a particle in a composite matrix in order to obtain equations which yield the average properties of the composite material as a whole. When the particles are spherical, the equations are as follows:

Parameters:

$$\alpha = \frac{1}{3}\frac{(1+\nu_m)}{(1-\nu_m)} \quad ; \quad \beta = \frac{2}{15}\frac{(4-5\nu_m)}{(1-\nu_m)} \quad ;$$

$$k = 1 + (K_p/K_m - 1)(1-\phi)\alpha \quad ;$$

$$G = 1 + (\mu_p/\mu_m - 1)(1-\phi)\beta \quad ;$$

$$\phi =$$

Bulk Modulus:

$$K_c = \left\{ \left[\frac{K_p/K_m - 1}{k} \right] \phi + 1 \right\} K_m$$

Young's Modulus:

$$E_c = \left\{ 1 + \left[\frac{(K_p/K_m - 1)G + 2(\mu_p/\mu_m - 1)k}{3kG} \right] \phi \right\} E_m$$

Coefficient of Thermal Expansion:

$$\gamma_c = \gamma_m + \frac{K_p}{K_m} \frac{(\gamma_p - \gamma_m)\phi}{1 + (K_p/K_m - 1)[(1-\phi)\alpha + \phi]}$$

For the Homogenized spherical particle of randomly

wavy rods, the above equations yield (with $\phi = 0.23$):

$$K_c = 2.88(10^3)\ \text{MPa} ;$$
$$E_c = 2.40(10^3)\ \text{MPa} ;$$
$$\nu_c = 0.361 ;$$
$$\mu_c = 0.882(10^3)\ \text{MPa};$$
$$\gamma_c = 3.074(10^{-4})\ ^\circ C^{-1}.$$

For the reference H2 particle used for comparative purposes with the CS PB/PS particle, $\phi = 0.25$. This yields:

$$K_c = 2.85(10^3)\ \text{MPa} ;$$
$$E_c = 2.34(10^3)\ \text{MPa} ;$$
$$\nu_c = 0.363 ;$$
$$\mu_c = 0.856(10^3)\ \text{MPa};$$
$$\gamma_c = 3.172(10^{-4})\ ^\circ C^{-1}.$$

It is interesting to compare these results with an upper bound approximation using Voigt's method where

$$\mu_v = \sum_i \phi_i \mu_i \quad ; \quad K_v = \sum_i \phi_i K_i \quad ,$$

for the Homogenized particle one would obtain

$$\mu_v = 0.938(10^3)\ \text{MPa},$$
$$K_v = 2.933(10^3)\ \text{MPa}.$$

Conducting a lower bound approximation using the Reuss method

$$\mu_R = \left[\sum_i \phi_i / \mu_i \right]^{-1} \quad ; \quad K_R = \left[\sum_i \phi_i / K_i \right]^{-1}$$

gives for the Homogenized particle:

$\mu_R = 2.476$ MPa,
$K_R = 2.788(10^3)$ MPa.

Comparing Chow's results with the upper and lower bounds, one sees they are closer to an upper bound. However, for the Bulk modulus (and, therefore, also for the coefficient of thermal expansion which is related to the Bulk modulus) the difference between upper and lower bounds is not very significant. Therefore the thermal stress analysis can be considered accurate as it depends upon the Bulk modulus and the thermal expansion coefficient; and the more widely differing shear responses of PB and PS are not effective in this case. The stresses found due to the applied tension may be slightly higher because the effective shear modulus may be lower than that calculated here.

APPENDIX 2

RELAXATION OF THERMAL RESIDUAL STRESSES DUE TO CREEP OF PS MATRIX

The creep stress relaxation is of interest for the case of two concentric spheres of different isotropic materials which contain spherically symmetric thermal residual stresses. The inner sphere of radius a is an elastic material and the outer shell is also elastic however, it is subject to creep under sustained loading such as an initially imposed residual stress due to a thermal expansion misfit. The expression which describes this creep behavior, for polystyrene, is (Argon and Bessonov, 1972):

$$\dot{\epsilon}_c = \frac{\gamma}{\sqrt{3}} \exp\left[-56.8\left(1-\left(\frac{T}{\sqrt{3}\,t}\right)^{5/6}\right)\right] \qquad \text{(A2-1)}$$

The problem is to determine how this creep behavior of the outer shell (matrix) affects the stresses in this shell and the inner sphere (particle).

Basic kinematics will first be considered. The total strain can be expressed as the sum of the elastic, thermal, and creep strains. The thermal strains are initially imposed and constant with time. They prescribe the initial spherically symmetric elastic misfit. Therefore, for $t>0$,

$$\begin{aligned} \epsilon_r &= \epsilon_r^e + \epsilon_r^c \,, \\ \epsilon_\theta &= \epsilon_\theta^e + \epsilon_\theta^c \,, \\ \epsilon_\phi &= \epsilon_\theta \,. \end{aligned} \qquad \text{(A2-2)}$$

Introducing the elastic stress-strain relation, the total strains may be written as

$$\epsilon_r = \frac{1}{E}\left[\sigma_r - 2\nu\sigma_\theta\right] + \epsilon_r^c \,,$$

$$\epsilon_\theta = \frac{1}{E}\left[(1-\nu)\sigma_\theta - \nu\sigma_r\right] + \epsilon_\theta^c \,. \qquad \text{(A2-3)}$$

This can be rewritten to give an expression for the stresses as a function of the total strain and the creep strain:

$$\sigma_r = \frac{E}{(1-2\nu)(1+\nu)}\left[(1-\nu)(\epsilon_r - \epsilon_r^c) + 2\nu(\epsilon_\theta - \epsilon_\theta^c)\right] ; \qquad \text{(A2-4)}$$

$$\sigma_\theta = \frac{E}{(1-2\nu)(1+\nu)}\left[(\epsilon_\theta - \epsilon_\theta^c) + \nu(\epsilon_r - \epsilon_r^c)\right] .$$

We currently have as unknowns the components of stress, total strain and creep strain. In order to obtain an expression for the creep strain rate components in terms of the effective creep strain which is known, equation (A2-1), we employ the assumption of material incompressibility during creep flow:

$$\dot{\epsilon}_r^c + 2\dot{\epsilon}_\theta^c = 0 \,;$$

$$\dot{\epsilon}_r^c = -2\dot{\epsilon}_\theta^c \,.$$

The definition of effective strain rate relates the effective creep rate to its components:

$$\dot{\epsilon}_c \equiv \left[\frac{2}{3}\epsilon_{ij}\epsilon_{ij}\right]^{1/2} \qquad \text{(A2-5)}$$

$$\epsilon = \pm\dot{\epsilon}_r^c = \mp 2\dot{\epsilon}_\theta^c$$

The appropriate signs are determined by the deviatoric stress state. In this case, the initial radial deviatoric stress state is positive, and the initial tangential deviatoric stresses are negative. This results in:

$$\dot{\epsilon}_c = \dot{\epsilon}_r^c = -2\dot{\epsilon}_\theta^c \,. \qquad \text{(A2-6)}$$

Writing equations (A2-4) in rate form and substituting in equation (A2-6), expressions in terms of total strain rates

(unknowns) and effective creep rates (known) are obtained for the stress rates:

$$\dot{\sigma}_r = \frac{E}{(1-2\nu)(1+\nu)}\left[(1-\nu)\dot{\epsilon}_r + 2\nu\dot{\epsilon}_\theta - (1-2\nu)\dot{\epsilon}^c\right] ; \qquad \text{(A2-7)}$$

$$\sigma = \frac{E}{(1-2\nu)(1+\nu)}\left[\dot{\epsilon}_\theta + \nu\dot{\epsilon}_r + \frac{1}{2}(1-2\nu)\dot{\epsilon}^c\right] .$$

The total strain rates are to be found from the equilibrium equations. Since this problem is spherically symmetric, the equilibrium equations reduce to one:

$$\frac{d\dot{\sigma}_r}{dr} + \frac{2(\dot{\sigma}_r - \dot{\sigma}_\theta)}{r} = 0 \qquad \text{(A2-8)}$$

This can be rewritten in terms of the total strain rates and the creep strain rates by employing the relations (A2-7) which gives:

$$(1-\nu)\frac{d\dot{\epsilon}_r}{dr} + 2\nu\frac{d\dot{\epsilon}_\theta}{dr} + \frac{2(1-2\nu)(\dot{\epsilon}_r - \dot{\epsilon}_\theta)}{r} = (1-2\nu)\frac{d\dot{\epsilon}_c}{dr} + 3(1-2\nu)\frac{\dot{\epsilon}^c}{r} .$$

A relation between the total radial strain and the total tangential strain may be found by beginning with their strain-displacement relations:

$$\dot{\epsilon}_\theta = \dot{u}/r \quad ; \quad \dot{\epsilon}_r = d\dot{u}/dr \quad ; \qquad \text{(A2-9)}$$

and differentiating to obtain:

$$\dot{\epsilon}_r = \dot{\epsilon}_\theta + r\frac{d\dot{\epsilon}_\theta}{dr} \quad ;$$

$$\frac{d\dot{\epsilon}_r}{dr} = r\frac{d^2\dot{\epsilon}_\theta}{dr^2} + 2\frac{d\dot{\epsilon}_\theta}{dr} .$$

Therefore, the equilibrium equations may be written in terms of the total tangential strain rate (unknown) and the creep strain rate (known):

$$4\frac{d\dot{\epsilon}_\theta}{dr} + r\frac{d^2\dot{\epsilon}_\theta}{dr^2} = \frac{1-2\nu}{1-\nu}\left[\frac{d\dot{\epsilon}_c}{dr} + 3\frac{\dot{\epsilon}_c}{r}\right]$$

multiplying by r^3 and rearranging yields:

$$\frac{d}{dr}\left[r^4\frac{d\dot{\epsilon}_\theta}{dr}\right] = \frac{(1-2\nu)}{(1-\nu)}\frac{d}{dr}\left[r^3\dot{\epsilon}^c\right] . \qquad \text{(A2-10)}$$

This can be integrated twice to obtain an expression for

$$\dot{\epsilon}_\theta = \frac{1-2\nu}{1-\nu}\left[\int_a^r \frac{1}{r}\dot{\epsilon}^c dr - a^3\dot{\epsilon}^c(a)\left[\frac{1}{3a^3} - \frac{1}{3r^3}\right]\right] + a^4\frac{d\dot{\epsilon}_\theta}{dr}\Big|_a\left[\frac{1}{3a^3} - \frac{1}{3r^3}\right] + \dot{\epsilon}_\theta(a) \qquad \text{(A2-11)}$$

By collecting unknown constant coefficients and assigning symbols to known expressions for simplicity,

$$C_1 = a^4\frac{d\dot{\epsilon}_\theta}{dr}\Big|_a \; ; \quad C_2 = \frac{a}{3}\frac{d\dot{\epsilon}_\theta}{dr}\Big|_a + \dot{\epsilon}_\theta(a) \; ; \qquad \text{(A2-12)}$$

$$A = \dot{\epsilon}_c(a) \; ; \quad I(r) = \int_a^r \frac{1}{r}\dot{\epsilon}^c(r)dr \; . \qquad \text{(A2-13)}$$

the total strain rates can be written as:

$$\dot{\epsilon}_\theta = \frac{1-2\nu}{1-\nu}\left[I(r) - \frac{A}{3}\left(1 - \frac{a^3}{r^3}\right)\right] - \frac{C_1}{3r^3} + C_2 \; ; \qquad \text{(A2-14)}$$

$$\dot{\epsilon}_r = \frac{1-2\nu}{1-\nu}\left[I(r) + \dot{\epsilon}^c - \frac{A}{3}\left(1 + 2\frac{a^3}{r^3}\right)\right] + \frac{2C_1}{3r^3} + C_2 \; .$$

Case 1. Particle in an Infinite Matrix

For the particle in an infinite body, application of the following boundary conditions will yield the appropriate expressions for C_1 and C_2:

$$\begin{aligned} &1.\ @\ r=a\ ,\ \dot{\sigma}_r=\dot{\sigma}_p\ ; \\ &2.\ @\ r=a\ ,\ \dot{u}_r=\dot{u}_p\ ; \\ &3.\ @\ r\to\infty\ ,\ \dot{\sigma}_r=\dot{\epsilon}_\theta=\dot{u}_r=0. \end{aligned} \tag{A2-15}$$

Boundary condition 1 yields:

$$\dot{\sigma}_p=\hat{E}\left[(1-\nu)\dot{\epsilon}_r+2\nu\dot{\epsilon}_\theta-(1-2\nu)\dot{\epsilon}_c\right]\ ;$$

$$\dot{\sigma}_p=\hat{E}\left[(1+\nu)\dot{\epsilon}_\theta(a)+a(1-\nu)\left.\frac{d\dot{\epsilon}_\theta}{dr}\right|_a-(1-2\nu)\dot{\epsilon}_c(a)\right]\ ; \tag{A2-16}$$

where $\hat{E} = E/((1-2\nu)(1+\nu))$.

Boundary condition 2 yields:

$$\begin{aligned} &u_p=\alpha_p\Delta T a+\frac{\sigma_p}{3K_p}a\ ; \\ &\dot{u}_p=\frac{\dot{\sigma}_p}{3K_p}a\ ; \\ &\dot{\sigma}_p=3K_p\dot{\epsilon}_\theta(a)\ . \end{aligned} \tag{A2-17}$$

By equating equations A2-16 and A2-17, we obtain an expression for $\dot{\epsilon}_\theta(a)$:

$$3K_p\dot{\epsilon}_\theta(a)=\hat{E}\left[(1+\nu)\dot{\epsilon}_\theta(a)+a(1-\nu)\left.\frac{d\dot{\epsilon}_\theta}{dr}\right|_a-(1-2\nu)\dot{\epsilon}^c(a)\right]\ ;$$

$$\dot{\epsilon}_\theta(a)=\frac{\hat{E}}{3(K_p-K_m)}\left[a(1-\nu)\left.\frac{d\dot{\epsilon}_\theta}{dr}\right|_a-(1-2\nu)\dot{\epsilon}^c(a)\right]\ . \tag{A2-18}$$

Applying boundary condition 3 yields an expression for C_2:

$$C_2=\frac{1-2\nu}{1-\nu}\left[\frac{A}{3}-I(\infty)\right]\ . \tag{A2-19}$$

Rewriting equation A2-12 for C_2 in terms of C_1 and $\dot{\epsilon}_\theta$ yields:

$$C_2 = \frac{C_1}{3a^3} + \dot{\epsilon}_a(a) \quad . \qquad \text{(A2-20)}$$

Substituting equations A2-19 and A2-18 into A2-20 results in an expression for C_1:

$$\frac{1-2\nu}{1-\nu}\left[\frac{A}{3} - I(\infty)\right] = \frac{C_1}{3a^3} + \frac{\hat{E}}{3(K_p-K_m)}\left[(1-\nu)\frac{C_1}{a^3} - (1-2\nu)\dot{\epsilon}_c(a)\right] ;$$

$$C_1 = \frac{1-2\nu}{1-\nu} 3a^3 \left[\frac{A}{3} - \frac{K_a - K_m}{K_p - K_m + \hat{E}(1-\nu)} I(\infty)\right] \qquad \text{(A2-21)}$$

Therefore, by substituting equations A2-20 and A2-21 into equations A2-14 and, subsequently, A2-14 into A2-7, the complete solution for the stress rates are found.

Case 2. Particle in a Finite Matrix

For the particle in a finite body, application of the following boundary conditions will yield the appropriate expressions for C_1 and C_2:

$$\begin{aligned} &1.\quad \omega\, r=a\,,\ \dot{\sigma}_r=\dot{\sigma}_p\,,\\ &2.\quad \omega\, r=a\,,\ \dot{u}_r=\dot{u}_p=\dot{\sigma}_p a/3K_p\,,\\ &3.\quad \omega\, r=b\,,\ \dot{\sigma}_r=0\,. \end{aligned} \tag{A2-22}$$

Applying boundary condition 1 yields:

$$\frac{\dot{\sigma}_p}{E}=\left[\frac{2}{3a^3(1+\nu)}C_1+\frac{C_2}{1-2\nu}-\frac{A}{1+\nu}\right] \tag{A2-23}$$

where $\hat{E} = E/((1-2\nu)(1+\nu))$.
Applying boundary condition 2 yields:

$$\frac{\dot{\sigma}_p}{E}=\frac{R}{1-2\nu_p}\left[-\frac{C_1}{3a^3}+C_2\right] \tag{A2-24}$$

where R is the ratio of the particle Young's modulus to the matrix Young's modulus, $R = E_p/E$. By equating equations A2-23 and A2-24, an expression for C_2 in terms of C_1 is obtained:

$$\frac{R}{1-2\nu_p}\left[-\frac{C_1}{3a^3}+C_2\right]=\frac{2}{3a^3(1+\nu)}C_1+\frac{C_2}{1-2\nu}-\frac{A}{1+\nu}\,;$$

$$C_2=\frac{(1-2\nu_p)(1-2\nu)}{R(1-2\nu)-(1-2\nu_p)}\left[C_1\frac{2(1-2\nu_p)+R(1+\nu)}{3a^3(1-2\nu_p)(1+\nu)}-\frac{A}{1+\nu}\right]. \tag{A2-25}$$

Applying boundary condition 3 yields an expression for C_1 in terms of C_2 :

$$0 = \hat{E}\left[(1-\nu)\left[\frac{1-2\nu}{1-\nu}\left(I(b)-\frac{A}{3}(1-2c)\right)\right]+\frac{2C_1(1-\nu)}{3b^3}+C_2(1-\nu)\right.$$
$$\left.+2\nu\left[\frac{1-2\nu}{1-\nu}\left(I(b)-\frac{A}{3}(1-c)\right)\right]-\frac{2\nu C_1}{3b^3}+2\nu C_2\right] \; ; \; c=(a/b)^3 \; ;$$

$$C_1=\frac{3b^3}{2}\left[-I(b)\frac{1+\nu}{1-\nu}+\frac{A}{3(1-\nu)}\left[1+\nu+2\nu(1-c)\right]-C_2\frac{1+\nu}{1-2\nu}\right] . \quad \text{(A2-26)}$$

Substituting equation A2-25 into A2-26 results in:

$$C_1=\frac{3b^3}{2}\left[-I(b)\frac{1+\nu}{1-\nu}+\frac{A}{3(1-\nu)}\left(1+\nu+2\nu(1-c)\right)\right.$$
$$\left.-\frac{(1+\nu)(1-2\nu_p)}{R(1-2\nu)-(1-2\nu_p)}\left[C_1\frac{2(1-2\nu_0)+R(1+\nu)}{3a^3(1-2\nu_p)(1+\nu)}-\frac{A}{1+\nu}\right]\right] . \quad \text{(A2-27)}$$

By grouping constant terms together,

$$Q = R(1-2\nu)-(1-2\nu_p) , \quad \text{(A2-28)}$$
$$M = 2(1-2\nu_p)+R(1+\nu)$$
$$F = 1+\nu+2c(1-2\nu)$$

the unknown C_1 can be found to be:

$$C_1=\frac{3Qa^3}{2cQ+M}\left[-I(b)\frac{1+\nu}{1-\nu}+A\left[\frac{F}{3(1-\nu)}+\frac{1-2\nu_p}{Q}\right]\right] \quad ; \quad \text{(A2-29)}$$

and the unknown C_2 :

$$C_2=\frac{(1-2\nu_p)(1-2\nu)}{Q}\left[C_1\frac{M}{3a^3(1-2\nu_p)(1+\nu)}-\frac{A}{1+\nu}\right] . \quad \text{(A2-30)}$$

Therefore, by substituting A2-28 into A2-29 and A2-29 into A2-30, the unknown constants in the total strain rate expression A2-14 are found. By substituting equations A2-14 into the stress rate expressions A2-7, we have the solution for the stress rate due to creep of the matrix.

Finally, in order to obtain the stress as a function of time, the stress rate must be integrated over time. This is shown in Appendix 3.

APPENDIX 3

COMPUTATION OF STRESS RELAXATION AND POROSITY DEVELOPMENT

A relatively short FORTRAN program RELAX has been written to compute the relaxation of the thermal residual stresses in the matrix surrounding an isotropic particle and the development of microporosity in this same region during this same time interval. The program is basically self-explanatory through its numerous comment cards. The basic steps are as follows:

1. Read in material property data, time increment data, radial position data, and initial elastic strains at particle/matrix interface;
2. Calculate constants, based on given data, which are frequently used;
3. Calculate initial radial distribution of strain and stress from the initial thermal expansion misfit;
4. Calculate creep rate and porosity rate for this iteration;
5. Calculate radial and tangential strain rates for this iteration;
6. Determine time increment to assure stability of solution for that increment;
7. Calculate elastic strains, creep strains, stresses, and porosity for this increment;
8. Update the time;
9. Repeat steps 4 through 8 NTM times;
10. Print results.

The radial postions necessary are determined by the initial radial variation of deviatoric stress. The positions are chosen such that

$$I(r) = \int_a^r \frac{1}{r} \dot{\varepsilon}_c(r)\, dr$$

may be accurately evaluated with trapezoidal integration. The time increment is chosen such that the maximum creep strain increment does not exceed a certain percentage (PCT) of the elastic strain:

$$\Delta t \leq (PCT)\, \varepsilon^e / \dot{\varepsilon}_c$$

This increment is then used in a forward Euler time integration:

$$\text{e.g.} \quad {}^{t+\Delta t}\sigma_r = {}^{t}\sigma_r + {}^{t}\dot{\sigma}_r \Delta t$$

A listing of the program, extensively commented, follows.

```
      PROGRAM RELAX
C THIS PROGRAM CALCULATES THE STRESSES IN THE MATRIX SURROUNDING
C AN INCLUSION AS THEY RELAX DUE TO CREEP; IT ALSO CALCULATES THE
C POROSITY  AS IT DEVELOPS WHILE THE STRESSES RELAX
C
C R=RADIAL POSITION; ER=RADIAL STRAIN; ETH=TANGENTIAL STRAIN;
C SR=RADIAL STRESS; STH=TANGENTIAL STRESS; SE=EQUIVALENT STRESS;
C SM=MEAN STRESS; EC=CREEP STRAIN; EPC=CREEP STRAIN RATE;
C XI1=INTEGRAL OF CREEP RATE/RADIUS TAKEN OVER RADIUS; POR=POROSITY;
C PORP=POROSITY RATE; ERD=RADIAL STRAIN RATE; ETHD=TANGENTIAL RATE
C
      DIMENSION R(25),ER(25),ETH(25),SR(25),STH(25),SE(25),SM(25),
     C EC(25),EPC(25),XI1(25),ERD(25),ETHD(25),POR(25),PORP(25)
C ASSIGN INITIATION CRITERION CONSTANTS
      DATA POR1,POR2/1.66E7,-1157.2697/
C READ MATERIAL PROPERTIES
C YM=YOUNGS MODULUS; PR=POISSON RATIO; PRP=PARTICLE POISSON RATIO;
C A1=EXP(56.8); A2=(PREEXP COEF)*EXP(-56.8);
C RATIO=2(1-2*PRP)+(1+PR)*YMP/YM
      READ(5,*) YM,PR,RATIO,PRP,A1,A2
C READ NUMBER OF TIME INCREMENTS,
C PERCENT SUCH THAT TIME INC.=PCT*ELASTIC STRAIN/CREEP STRAIN
      READ(5,*) NTM,PCT
C READ NUMBER OF RADIAL POINTS,LOCATION OF RADIAL POINTS
      READ(5,*) NPT,(R(I),I=1,NPT)
C READ INITIAL(ELASTIC) STRAINS
      READ(5,*) ER1,ETH1
C CALCULATE CONSTANTS WHICH ARE REPEATEDLY USED
      PR22=PR*2.
      PR11=1.+PR
      PR2=1.-PR22
      PR1=1.-PR
      PPR=PR2/PR1
      YMP=YM/PR2/PR11
```

```
      R3=R(1)**3
      R33=3.*R3
      PR2P=1.-2.*PRP
      B3=R(NPT)**3
      C=R3/B3
      P211=PR2/PR11
      PR2H=0.5*PR2
      RP=PR11/PR1
      SR(1)=0.
      Z1=RATIO*PR2-PR2P
      Z2=2*PR2P+RATIO*PR11
      Z3=PR11+2.*C*PR2
      Z4=2.*C*Z1/(2.*C*Z1+Z2)
      Z5=Z3/3./PR1+PR2P/Z1
      BZ=Z4*1.5*B3
      CZ1=PR2P*PR2/Z1
      Z7=3.*R3*PR2P*PR11
      CZ2=Z2/Z7
          DO 5 JK=8,NPT
    5 PORP(JK)=0.
C CALCULATE ER,ETH,SR,STH,SE,SM INITIALLY, GIVEN ER AND ETH AT INTER
          DO 10 I=1,NPT
      AR=R3/R(I)**3
      EX=C/(1.-C)*SR(1)/YM*PR2
      ER(I)=(ER1+EX)*AR-EX
      ETH(I)=(ETH1+EX)*AR-EX
      SR(I)=YMP*(PR1*ER(I)+PR22*ETH(I))
      STH(I)=YMP*(ETH(I)+PR*ER(I))
      SE(I)=ABS(SR(I)-STH(I))
      SM(I)=(SR(I)+2.*STH(I))/3.
      EC(I)=0.
      POR(1)=0.
   10 CONTINUE
      T=0.
C ITERATE OVER NTM TIME INCREMENTS OF DT
```

```
      DO 100 J=1,NTM
     WRITE(6,500) J,T
C CALCULATE THE CREEP RATE FOR THIS TIME
      DO 20 I=1,NPT
     XL=SE(I)/238.
     XLL=XL**0.8333
     EPC(I)=A1*A2**XLL
  20 CONTINUE
C CALCULATE THE POROSITY RATE FOR THIS TIME STEP
      DO 21 I=1,7
  21 PORP(I)=POR1*EXP(POR2/SE(I))
C
C CALCULATE INTEGRAL I1 WITH TRAPEZOIDAL INTEGRATION
C
      XI1(1)=0.
      T2=EPC(1)/R(1)
        DO 25 II=2,NPT
      K=II-1
      T1=T2
      T2=EPC(II)/R(II)
      RR=R(II)-R(K)
      XI1(II)=XI1(K)+(T1+T2)*RR/2.
  25 CONTINUE
C
C
C  CALCULATE "CONSTANTS" C1D,C2D
      X1=XI1(NPT)*RP
      C1D=BZ*(-X1+EPC(1)*Z5)
      C2D=CZ1*(C1D*CZ2-EPC(1)/PR11)
      DO 30 I=1,NPT
      RR3=R(I)**3
C CALCULATE RADIAL AND TANGENTIAL STRAIN RATES
      ETHD(I)=PPR*(XI1(I)-EPC(1)/3.*(1.-R3/RR3))-C1D/3./RR3+C2D
      ERD(I)=PPR*(XI1(I)+EPC(I)-EPC(1)/3.*(1.+2.*R3/RR3))+
     1 2.*C1D/3./RR3+C2D
```

```
      WRITE(6,501) R(I),ER(I),ETH(I),EC(I),SR(I),STH(I),SE(I),
     1 SM(I),ERD(I),ETHD(I),EPC(I),POR(I)
C
C DETERMINE TIME STEP
C
      DER=ABS(ER(1)-EC(1))
      DETH=ABS(ETH(1)-EC(1))
      DE=DER
      IF(DETH.LT.DER) DE=DETH
      PO=DE/EPC(1)*PCT
      M=0
   26 PO=PO/10.
      M=M+1
      IF(PO.GT.10.0) GO TO 26
      DT=INT(PO)*10.**M
      IF(DT.LT.10.0) DT=10.
C
C CALCULATE ER,ETH,EC,SR,STH,SE,SM FOR NEXT INCREMENT
      ER(I)=ER(I)+ERD(I)*DT
      ETH(I)=ETH(I)+ETHD(I)*DT
      EC(I)=EC(I)+EPC(I)*DT
      POR(I)=POR(I)+PORP(I)*DT
      SR(I)=YMP*(PR1*ER(I) + PR22*ETH(I) -PR2*EC(I))
      STH(I)=YMP*(ETH(I) + PR*ER(I)+PR2H*EC(I))
      SE(I)=ABS(SR(I)-STH(I))
      SM(I)=(SR(I)+2.*STH(I))/3.
   30 CONTINUE
C INCREMENT TIME
      T=T+DT
  100 CONTINUE
C FORMAT STATEMENTS
  500 FORMAT(1H1,//,5X,'INCREMENT: ',I3,2X,'TIME: ',F11.2,' SEC',
     1 //,T2,'RADIUS',T22,'STRAINS',T61,'STRESSES',T97,'STRAIN RATES'
     2 /,T12,'RADIAL',T22,'TANGENT',T34,'CREEP',T45,'RADIAL',T55,
     3 'TANGENT',T67,'MISES',T79,'MEAN',T89,'RADIAL',T99,'TANGENT',
```

```
   4 T111,'CREEP',T122,'POROSITY',//)
501 FORMAT(1X,F6.3,1X,11(E10.3,1X),/)
    STOP
    END
```

APPENDIX 4

STRESS FIELD SURROUNDING A SPHERICAL PARTICLE DUE TO A UNIFORM TENSILE STRESS AT INFINITY

A uniform stress field in a material due to a stress applied at infinity is disturbed by the presence of a particle. In 1933, Goodier determined the effect of a spherical or cylindrical elastic inclusion on a uniform stress state. Referring to Figure A4, his solution for the effect of a spherical inclusion on the matrix stress state due to a tensile stress applied at infinity follows (subscript 1 indicates matrix; 2 indicates particle):

T = applied tensile stress in r direction, $\theta = 0$;

$$u_r = -\frac{A}{r^2} - \frac{3B}{r^4} + \left[\frac{5-4\nu}{1-2\nu}\frac{C}{r^2} - \frac{9B}{r^4}\right]\cos 2\theta \;;$$

$$u_\theta = -\left[\frac{2C}{r^2} + \frac{6B}{r^4}\right]\sin 2\theta \;;$$

$$\sigma_{rr} = 2\mu\left[\frac{2A}{r^3} - \frac{2\nu}{1-2\nu}\frac{C}{r^3} + \frac{12B}{r^5} + \left(-2\frac{5-\nu}{1-2\nu}\frac{C}{r^3} + \frac{36B}{r^5}\right)\cos 2\theta\right] \;;$$

$$\sigma_{\theta\theta} = 2\mu\left[-\frac{A}{r^3} - \frac{2\nu}{1-\nu}\frac{C}{r^3} - \frac{3B}{r^5} + \left(\frac{C}{r^3} - 21\frac{B}{r^5}\right)\cos 2\theta\right] \;;$$

$$\sigma_{\gamma\gamma} = 2\mu\left[\frac{A}{r^3} - \frac{2(1-\nu)}{1-2\nu}\frac{C}{r^3} - 9\frac{B}{r^5} + \left(\frac{3C}{r^3} - 15\frac{B}{r^5}\right)\cos 2\theta\right] \;;$$

$$\sigma_{r\theta} = 2\mu\left[-\frac{2(1+\nu)}{1-2\nu}\frac{C}{r^3} + 24\frac{B}{r^5}\right]\sin 2\theta$$

where

$$A = \frac{Ta^3}{4\mu_1 F}\left[-\frac{1}{2}\frac{(\mu_1-\mu_2)}{D}\left((1-2\nu_2)(6-5\nu_1)2\mu_1 + (3+19\nu_2-20\nu_1\nu_2)\mu_2\right) + \left((1-\nu_1)\frac{1+\nu_2}{1+\nu_1} - \nu_2\right)\mu_2 - (1-2\nu_2)\mu_1\right]$$

$$B = \frac{Ta^5}{8\mu_1}\frac{(\mu_1-\mu_2)}{D} \;;$$

$$C = \frac{T a^5}{8\mu_1} \frac{5(1-2\nu_1)(\mu_1-\mu_2)}{D}$$

$$D = (7-5\nu_1)\mu_1 + (8-10\nu_1)\mu_2$$

$$F = (1-2\nu_2)2\mu_1 + (1+\nu_2)\mu_2$$

The complete stress state is obtained by superposing the above stress state on the uniform tension.

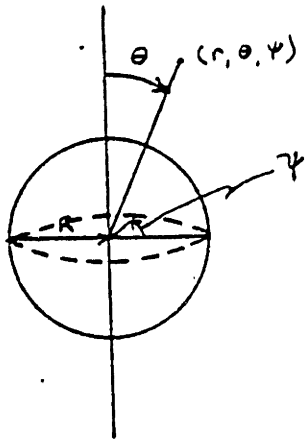

Figure A4.

TABLE A.

COMPARISON OF FINITE ELEMENT ANALYSIS SOLUTION
WITH ELASTICITY ANALYSIS SOLUTION

PARTICLE	Thermal Stress, (MPa)		Tensile Stress Concentration Factor, k	
	Finite Element Analysis	Elasticity Analysis	Finite Element Analysis	Elasticity Analysis
PB	---	34.5	1.92	1.88
HOMOGENIZED	7.93	7.95	1.17	1.16
PB(c=0.20)	28.7	28.7	---	---

APPENDIX 5

FINITE ELEMENT ANALYSIS

Finite element analyses were conducted using the general purpose finite element program ABAQUS. A finite element analysis was conducted to obtain the solution to the following problems:

1. Thermal Residual Stresses for Concentric Sphere Particles;
2. Relaxation of Residual Stresses for Concentric Sphere Particles;
3. Uniform Applied Tensile Stress for Concentric Sphere Particles;
4. Uniform Applied Tensile Stress for all particles in a finite matrix.

The finite element analysis of each problem is similar in the respect that the same type of element and same order of integration can be used in the modelling. They differ because the symmetry, loading, and (for problem 2) material behavior requirements differ. For these reasons, the finite element mesh and boundary conditions are identical for problems 1 and 2; and problems 3 and 4 have similar meshes with different boundary conditions. The accuracy of the model for each of the first three problems is determined by comparing the solution from the finite element analysis of an isotropic particle with the corresponding closed form solution.

All of the problems are axially symmetric with respect to the z-axis (Figure A5-1) in geometry, loading, and boundary conditions. Therefore, axisymmetric elements

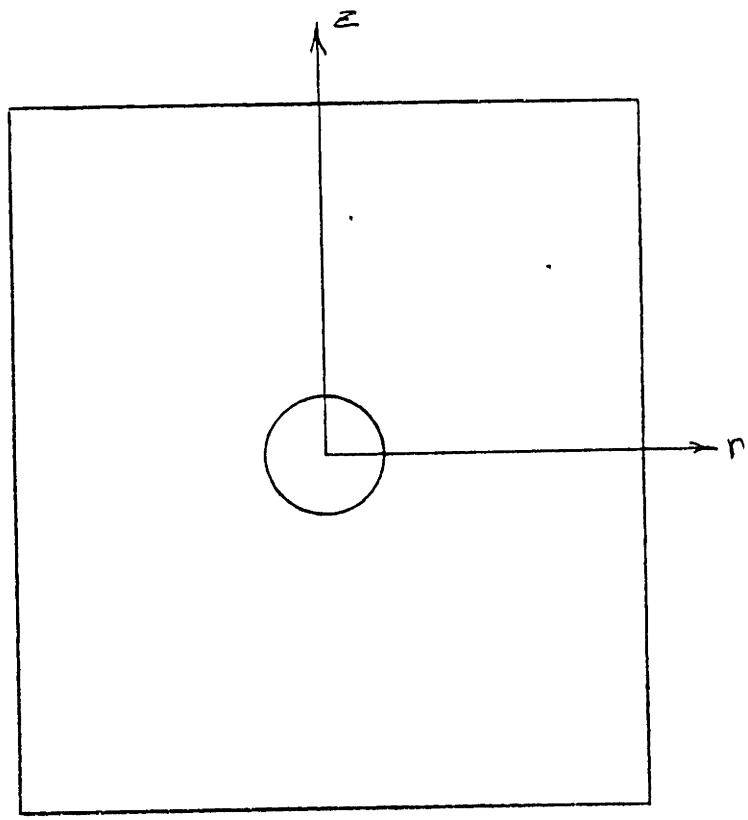

Figure A5-1. Schematic of a particle in a matrix. All problems are axially symmetric in geometry, loading, and boundary conditions with respect to the z axis.

may be used and a "2-D" model is all that is necessary. Also, all of the problems contain an "incompressible" material, rubber, which has a Poisson ratio of 0.499. In order to prevent the locking problem of finite elements with such characteristics, reduced integration is used in the analysis. Therefore, axisymmetric elements with reduced integration are used in the finite element analysis of each of the four problems.

As mentioned above, the same mesh and boundary conditions are used for problems 1 and 2. This is because the problems are both spherically symmetric. The mesh consists of a "fan" of axisymmetric elements which are permitted to displace radially only. This is pictured in Figure A5-2. To determine the thermal residual stresses requires an elastic analysis and thus problem 1 only requires the elastic material properties. Since problem 2 consists of creeping of the PS matrix, the creep law, equation 3-1, must be defined in an ABAQUS subroutine.

The mesh for problems 3 and 4 is a bit more complicated because these problems are axially symmetric about the z-axis with reflective symmetry about the y-axis. The mesh and boundary conditions for problem 3 are shown in Figure A5-3. Additional boundary conditions along the top edge and free side of the mesh must be prescribed to reproduce the effects of a finite matrix. The top edge is conditioned to displace uniformly in the z direction, and the free side displaces uniformly in the y direction. This condition is shown in Figure A5-4.

A comparison of the finite element solution for an isotropic particle with the elasticity or creep solution for each problem was used to determine the size of mesh to use. The resulting meshes produced very small errors. For

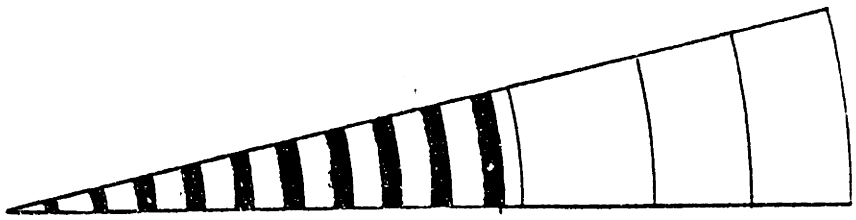

Figure A5-2. "Fan" model used for the spherically symmetric problems. Example shown is for a particle/matrix volume ratio of 0.20.

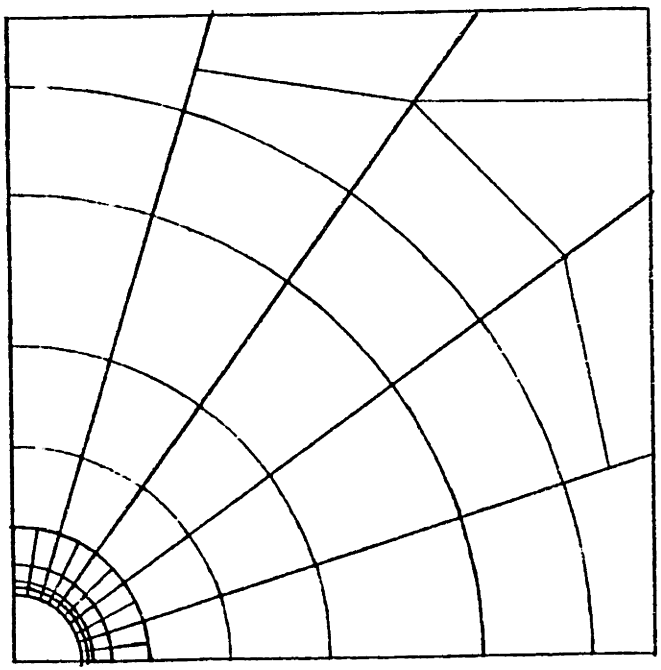

(a) matrix mesh

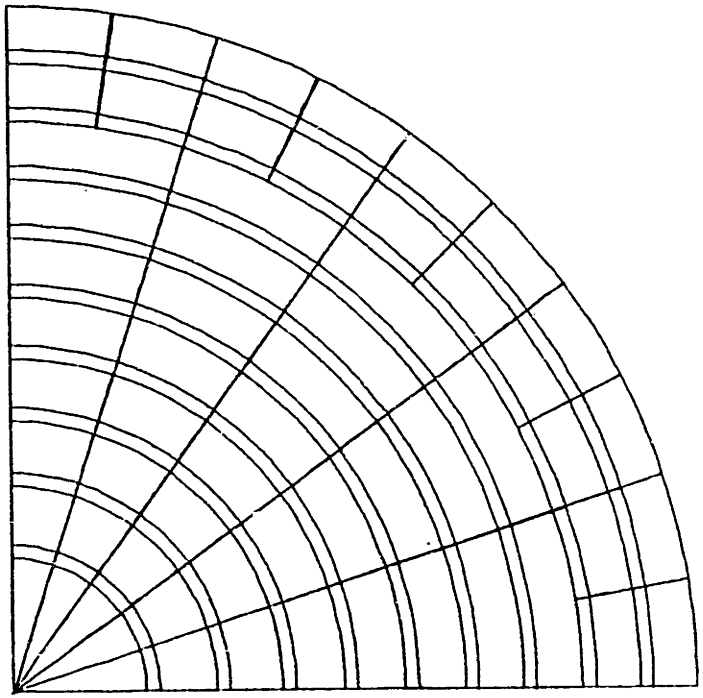

(b) enlarged particle mesh

Figure A5-3. Mesh for the particle in an "infinite" body subjected to a tensile stress.

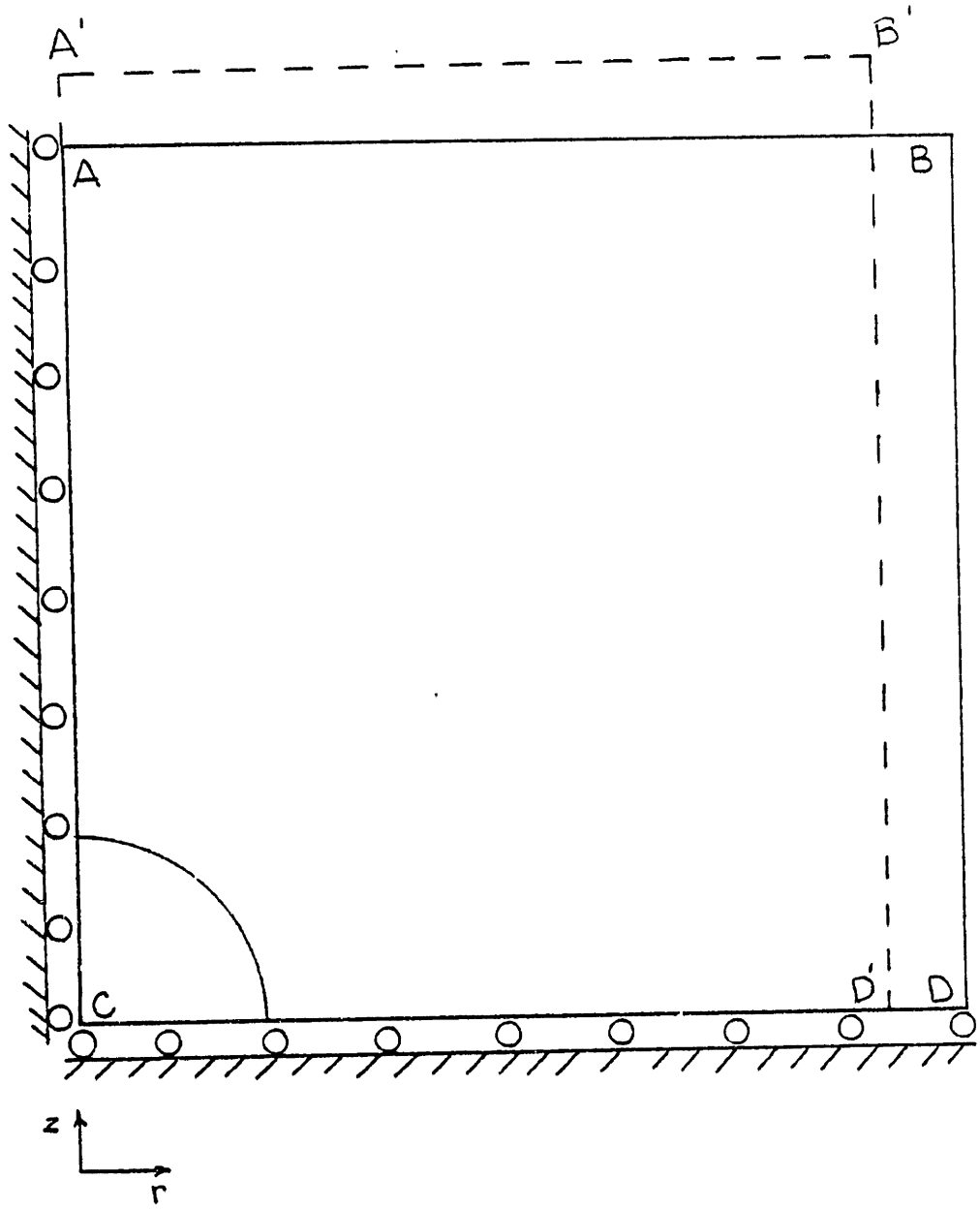

Figure A5-4. Schematic showing additional boundary conditions imposed on a mesh similar to Figure A5-3 to model finite matrix effects.

problem 1, the error was less than 1% as shown in Table A which compares the radial stress obtained from the finite element analysis and elasticity analysis for the PB and Homogenized particles. For problem 2, the error was also very small. Figure A5-5 depicts the relaxation behavior from the creep analysis as a smooth curve; the discrete points were obtained from the finite element analysis. The points are seen to lie right along the curve. The applied tensile stress comparison is also listed in Table A for the PB and Homogenized particles. This indicated less than 3% error. The very small error for each of the problems indicates that the finite element modelling and analysis has been correctly and accurately executed.

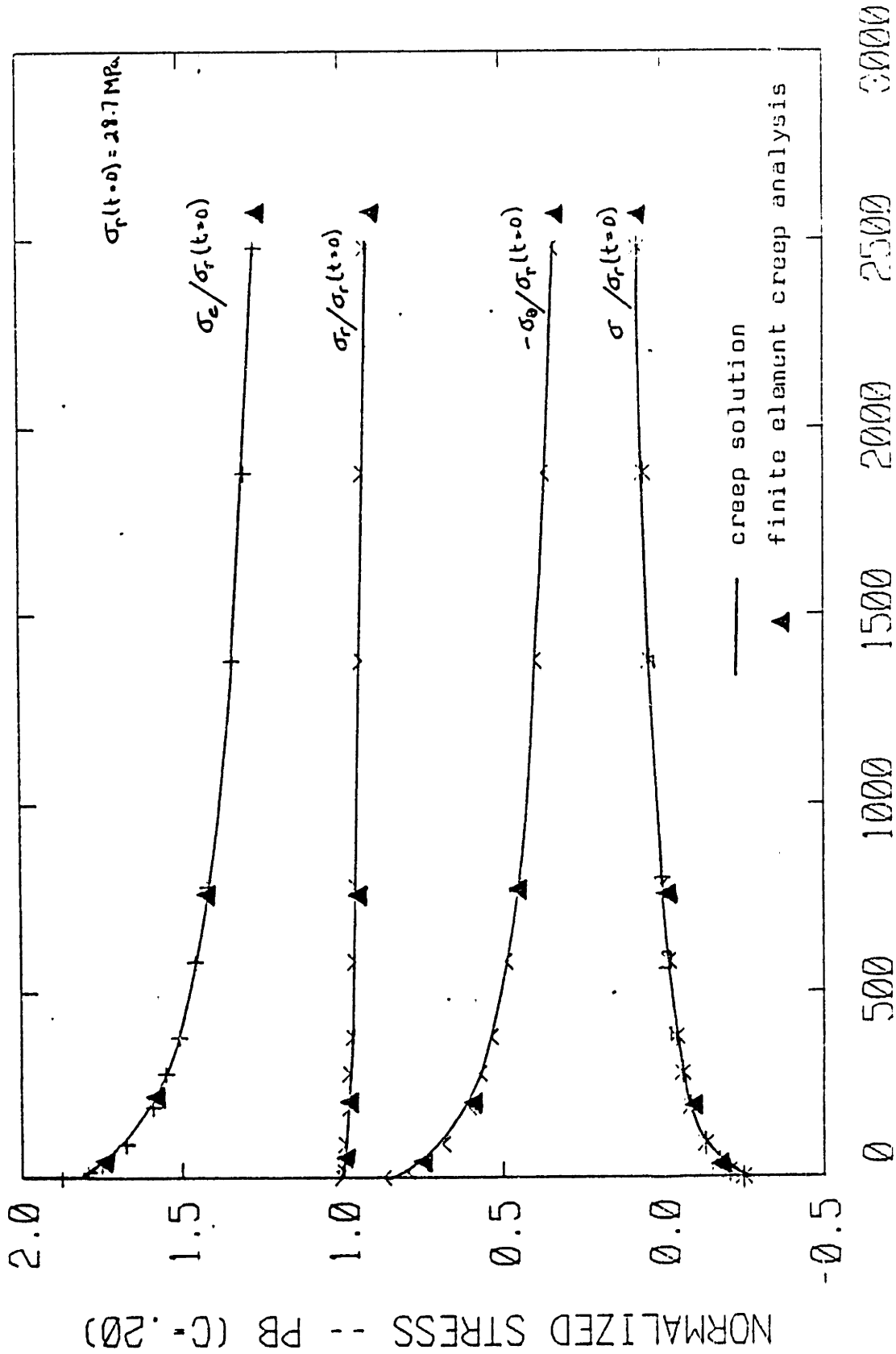

Figure A5-5. Comparison of stress relaxation as cmputed by finite elements with that computed with the creep analysis of Sectin 3.2.

REFERENCES

1. Bucknall, C. B., TOUGHENED PLASTICS, Applied Science, London,1977.

2. Maxwell, B. and Rahm, L. F., J. Soc. Plastics Eng., 6, 1950, 7.

3. Bucknall, C. B. and Smith, R. R., Polymer, 6, 1965, 437.

4. Sternstein, S. S. and Ongchin, L., Polymer Preprints, 10(2), 1969, 117.

5. Oxborough, R. J. and Bowden, P. B., Phil. Mag., 30, 1974, 171.

6. Argon, A. S. and Hannoosh, J. G., Phil. Mag., 36, 1977, 1195.

7. Kawagoe, M. and Kitagawa, M., J. Polymer Sci.-Physics, 19, 1981, 1423.

8. Chow, T. S., J. Polymer Sci.-Physics, 16, 1978, 959.

9. Chow, T. S., J. Polymer Sci.-Physics, 16, 1978, 967.

10. Hibbitt, Karlson, and Sorenson, ABAQUS, 1981.

11. Argon, A. S. and Bessonov, M. I., Phil. Mag., 35, 1977, 917.

12. Goodier, J. N., ASME Trans., 55, 1933, 39.

13. Broutman, J. J. and Panizza, G., Int. J. Poly. Mat., 1, 1971, 95.

14. Argon, A. S., Pure Appl. Chem., 43, 1975, 247.

15. McClintock, F. A. and Stowers, I. F., Research Memorandum No. 159, Fatigue and Plasticity Laboratory, M.E. Dept., M.I.T., Cambridge, MA, 1970.

16. Gurson, A. L., ASME J. Eng. Matls. Techn., 99, 1977, 2.

17. Gebizlioglu, O. S., et. al., 1983, to be published.

18. Argon, A. S. and Salama, M. M., Phil. Mag., 36, 1977, 1217.